

LIBRARY Michigan State University

This is to certify that the dissertation entitled

OPTICAL AND ELECTROCHEMICAL CHARACTERIZATION OF BIOMACROMOLECULAR INTERACTIONS AT FLUID-LIKE INTERFACES

presented by

LAVANYA PARTHASARATHY

has been accepted towards fulfillment of the requirements for the

DOCTORAL degree in CHEMICAL ENGINEERING

Majour Professor's Signature

08/05/15

Date

MSU is an Affirmative Action/Equal Opportunity Institution

PLACE IN RETURN BOX to remove this checkout from your record.

TO AVOID FINES return on or before date due.

MAY BE RECALLED with earlier due date if requested.

DATE DUE	DATE DUE	DATE DUE
AUG 0 3 2008		
050410		

2/05 c:/CIRC/DateDue.indd-p.15

OPTICAL AND ELECTROCHEMICAL CHARACTERIZATION OF BIOMACROMOLECULAR INTERACTIONS AT FLUID-LIKE INTERFACES

Ву

LAVANYA PARTHASARATHY

A DISSERTATION

Submitted to
Michigan State University
In partial fulfillment of the requirements
for the degree of

DOCTOR OF PHILOSOPHY

DEPARTMENT OF CHEMICAL ENGINEERING AND MATERIALS SCIENCE

2005

ABSTRACT

OPTICAL AND ELECTROCHEMICAL CHARACTERIZATION OF BIOMACROMOLECULAR INTERACTIONS AT FLUID-LIKE INTERFACES

By

LAVANYA PARTHASARATHY

This thesis comprises three different studies, each aimed at understanding biomacromolecular interactions at fluid-like interfaces. The first study is on sequential and competitive adsorption and interactions of nisin and selected proteins at a model oilwater interface, using total internal reflection fluorescence microscopy (TIRFM). Experimental results showed strong evidence of significantly enhanced adsorption of some proteins in the presence of nisin. Apparent interfacial concentrations of β -casein were three times higher in the presence of nisin than when the pure protein adsorbed by itself under identical conditions. Enhanced adsorption was also observed for lysozyme and bovine serum albumin (BSA) in the presence of nisin, compared to adsorption of each protein by itself. Very little enhanced adsorption was observed for fibronectin in the presence of nisin. The exact mechanism for adsorption enhancement by nisin is not clear at this time. However, the experimental evidence suggests strongly that molecular weight, size of the adsorbing protein, and bulk protein concentration are all important factors.

The second study concerned the development of a flow cell to enable simultaneous optical and electrochemical characterization of biomimetic interfaces. Modifications were made to our existing optical flow cell to incorporate the capability to conduct cyclic voltammetry (CV) measurements using a three-electrode system. The



feasibility of the simultaneous optical-electrochemical set-up was tested using the dye resorufin. On potential scans towards increasingly negative voltages, the fluorescent resorufin was reversibly reduced to non-fluorescent dihydroresorufin, coincident with a decrease in fluorescence emission intensity. Similarly, upon scanning towards increasingly positive voltages, the dihydroresorufin was reversibly oxidized to resorufin, resulting in an increase in fluorescence emission.

The third study outlines the process involved in the development and characterization of a fructose dehydrogenase (FDH) biosensor based on indirect bioelectrocatalysis, using coenzyme Q6 as the mediator. FDH, a naturally membranebound enzyme, was incorporated along with Q6 into a bilayer lipid membrane (BLM) deposited on indium tin oxide (ITO). The sensor was evaluated by using CV to monitor the change in anodic current upon addition of D-fructose. However, this FDH biosensor exhibited poor sensitivity, because electron tunneling through the BLM was very low. To improve electron tunneling, octyltrimethoxysilane was used to form an 8-carbon monolayer on ITO, and liposomes containing FDH and Q6 were deposited to form the outer leaflet of a biomimetic layer. This sensor demonstrated a clear dependence of the anodic current on D-fructose concentration, with a linear dependence over D-fructose concentrations of 0.056mM to 1.98mM, and a plateau at higher D-fructose concentrations. The bilayer was characterized optically using fluorescence recovery after pattern photobleaching (FRAPP). The diffusion coefficient of the upper leaflet of the biomimetic layer was 4.4 x 10⁻¹⁰ cm²/sec, with a membrane fluidity of 0.59. These values are characteristic of what have been reported in the technical literature.

Dedicated to my parents and my brother

ACKNOWLEDGEMENTS

I would like to begin with thanking my advisor, Dr. Robert Y. Ofoli. I am fortunate to have worked with him over the past six years. Our interaction began when he first recruited me. It has been a great pleasure working with him, and I sincerely thank him for providing me with this opportunity. His hands-off approach and open door-policy have taught me to be an independent thinker, and this is the most valuable attribute I will carry forward. I would like to especially thank him for being patient with me while reviewing my Ph.D. thesis and encouraging me all along the way – I hope I leave here a better writer than when I joined!

I would like to thank Dr. Mark Worden for his helpful suggestions and for serving on my committee, and also for the collaborations, and the free use of his laboratory facilities (specifically the CV). It has been a pleasure having Dr. Gary Blanchard on my committee. I enjoyed taking his classes and appreciate his help with the quantum yield experiments and for pointing me in the right direction to obtain the green laser – Thank you. I would like to thank Dr. Christina Chan for serving on my committee and her encouragement after my first defense.

I would like to thank Nancy, JoAnn, Jackie and Kim for always being helpful with a bright smile. I appreciate all the things they did for me.

The completion of this dissertation would have been difficult without the support of my friends, colleagues and family. Their constant support and encouragement during the rough patches, and friendship, guidance and companionship during other times made to their continued association. I would like to begin with thanking Sachin Vaidya. "Navigating the TIRFM waters" as he calls it, would have been next to impossible if we had not worked together. The two of us started our experiments together in the lab and he has been a great colleague and a wonderful friend. I shall always cherish the years that I worked with him. I would like to thank Arun, Kiran, Bhaskar and Prerna for always being there for me. I would also like to thank Neeraj, Brian, Prajakt, Amit, Sunder, Tejas, Soumya, Giri and Mukta.

Another group of people that I am indebted to is my family here in Michigan. My parents sent me here with the confidence and the assurance in their hearts that I would be taken care of. I would like to begin by thanking Rengan Chithappa, Mali Chithi, Ramesh, Subhashini, Aisha and Vijay – I cannot imagine what I would have done without them and that they will always have a special place in my life. I would like to thank another group of my family here (Cheen, Kannan, Kinna, Sridhar mama, Sudha, Jayshree, Robbi, Jyothi, Preetha, Varshini, Netra, Keshav and Smriti) for supporting me and providing me with enriching memories that I will treasure.

I would like to thank my family in India (Suja Chithi, Vardarajan Chithappa, Balaji Mama, Amudha Manni, Srivathsan, Supraja, Vidya, Myla Athai and Sampath Athimber) who always encouraged me and loved me unconditionally. I will always remember and miss my grandparents and I wish my grandfather were here to share this moment with me – he always encouraged me and took great pride even in my smallest

achievements. I thank my grandmother Andalu Patty for her belief and pride in me.

Finally, I would like to acknowledge the people who were always there by my side, without whom I cannot even remotely imagine coming this far in life – my parents and my brother. It has been tough being far away from them, but they have ALWAYS been there – taking pride in my accomplishments, encouraging me to achieve more, always having faith in me and for all the sacrifices they have made. My mother has been the beacon in my life. I thank my father for the unshakable faith he has always vested in me. I end, knowing that all that I have achieved would not have been possible without God's grace.

TABLE OF CONTENTS

1	INTRODUCTION	1
1.1 1.2	Enhanced adsorption of proteins in the presence of the polypeptide nisin Development of a protocol for simultaneous optical and electroc characterization of biomacromolecules in TIR geometry	hemical
1.3	Development and optical-electrochemical characterization of a biosensor b D- fructose dehydrogenase (FDH)	ased on
2	ENHANCED ADSORPTION OF PROTEINS IN THE PRESENCE OF POLYPEPTIDE NISIN	
2.1	ABSTRACT	
2.2		
	2.1 Nisin	
	2.2 Total Internal Reflection Fluorescence Microscopy (TIRFM)	
	2.3 The Liquid-liquid Interface	
	MATERIALS AND METHODS	
	3.1 Preparation of protein solutions	
	3.2 Experimental Setup	
2.4 2.5		
3	DEVELOPMENT OF A PROTOCOL FOR SIMULTANEOUS OPTICA ELECTROCHEMICAL CHARACTERIZATION BIOMACROMOLECULES IN TIR GEOMETRY	OF
3.1	ABSTRACT	44
3.2	INTRODUCTION	45
3.	2.1 Optical characterization	
	3.2.1.1 Total Internal Reflection Fluorescence Microscopy (TIRFM)	
3.	.2.2 Electrochemical characterization	
	3.2.2.1 Cyclic voltammetry (CV)	
	EXPERIMENTAL SET-UP	
	.3.1 TIRFM flow cell	
3.	3.2 Modifications to TIRFM set-up to conduct optical and electroc	
	experiments (first generation)	
2	3.3.2.1 Materials and Methods: Ferricyanide Experiments	
	.3.3 Results and Discussion: Ferricyanide Experiments	
٥.	.3.4 Problems with first generation optical – electrochemical set-up and r modifications (second generation experimental set-up)	
	3.3.4.1 Problems encountered with the second generation experimental set	
	3.3.4.2 Proof-of-concept of optical/electrochemical set-up	-
3.	.3.5 Introduction to resazurin	

	3.3.5.1 Materials and methods: Resazurin Experiments	64
3.	3.6 Experimental details: Resazurin Experiments	. 64
3.	3.7 Results and Discussion: Resazurin Experiments	. 65
3.4	CONCLUSION	. 68
3.5	FUTURE WORK	. 69
4	DEVELOPMENT AND OPTICAL-ELECTROCHEMIC	
	CHARACTERIZATION OF A BIOSENSOR BASED ON D-FRUCTO	
	DEHYDROGENASE (FDH)	. 88
4.1	ABSTRACT	88
4.2	INTRODUCTION	
4.3		
	3.1 Introduction to FDH	
	3.2 Theory	
	3.3 Introduction to FRAPP	
	EXPERIMENTAL SECTION	
	4.1 Materials	
4.	4.2 Preparation of the proteoliposome solution	
4.	4.3 Adsorption of proteoliposome solution onto ITO-coated glass slides	. 99
4.	4.4 Preparation of hydrophobic silane monolayers on ITO-coated glass slides	
4.	4.5 Adsorption of proteoliposomes onto silanized ITO slides	
4.	4.6 Cyclic Voltammetry Experiments	
4.	4.7 Set-up for FRAPP Experiments	101
	4.4.7.1 Optical set-up for FRAPP experiments	101
	4.4.7.2 Experimental cell used for FRAPP experiments to study FDH system . :	103
	4.4.7.3 Preparation of biomimetic layer for FRAPP experiments	104
4.5	RESULTS AND DISCUSSION	
4.	5.1 Incorporation of FDH in a biomimetic layer	
	4.5.1.1 Optical characterization	109
	4.5.1.2 Electrochemical characterization	110
4.6	CONCLUSIONS	111
4.7	FUTURE WORK	112
_		
5	APPENDICES	125
5.1	APPENDIX A:	125
	1.1 MATLAB program used for filtering analog measurements to remove d	
٦.	current measurements obtained during the phases when the chopper bloc	
	the laser beam.	
5	1.2 MATLAB program used for averaging data	
	1.3 Labview Program for collecting fluorescence data in the analog mode	
	1.4 Labview Program for collecting fluorescence data in the digital (pho	
٥.		129

			_
REFERENCES	·	132	2

LIST OF TABLES

Table	3-1. Input parameters used to obtain cyclic voltammetry measurements for the ferricyanide experiments
Table	3-2. Input parameters used to obtain cyclic voltammetry measurements for the resazurin and resorufin experiments
Table	3-3. Electrochemical properties of the dyes resazurin and resorufin (Maeda et al. 2000; Maeda et al. 2001)
Table	3-4. Optical properties of the dyes resazurin and resorufin (Maeda et al. 2000; Maeda et al. 2001)
Table	4-1. Input parameters used to conduct cyclic voltammetry measurements for the D-Fructose dehydrogenase system
Table	4-2. Summary of regression values obtained by fitting experimental FRAPP data to the single species model [Equation (4.8) (Wright et al. 1988; Starr and Thompson 2002)

LIST OF FIGURES

Figure 2-1. Experimental set-up for TIRFM experiments
Figure 2-2. Equilibrium adsorption of β-casein followed by introduction of nisin 29
Figure 2-3. Adsorption of nisin followed by introduction of β-casein
Figure 2-4. Assessment of β-casein adsorption reversibility
Figure 2-5. Enhanced adsorption of β-casein in the presence of nisin
Figure 2-6. Enhanced adsorption of β-casein in the presence of nisin
Figure 2-7. Control experiment for β-casein.
Figure 2-8. Interaction of BSA and nisin
Figure 2-9. Proposed scheme of the interaction between β-casein and nisin
Figure 2-10. Interaction of lysozyme and nisin
Figure 2-11. Control Experiment for Lysozyme
Figure 2-12. Lysozyme adsorption.
Figure 2-13. Interaction of fibronectin and nisin
Figure 2-14. Interaction of lysozyme (at a lower concentration) and nisin
Figure 2-15. Interaction of BSA (at a lower concentration) with nisin
Figure 2-16. Interaction between Fibronectin (at a lower concentration) and nisin 43
Figure 3-1. A typical cyclic voltammogram
Figure 3-2. Diagram of flow cell used for TIRFM characterization experiments 75
Figure 3-3. Diagram of flow cell for optical and electrochemical experiments (first generation design)
Figure 3-4. Cyclic Voltammogram obtained in the first generation TIRFM-CV flow cell
Figure 3-5. Cyclic voltammogram obtained in a conventional three-electrode set-up fo comparison
Figure 3-6. Comparison of cyclic voltammograms obtained in our modified firs

generation TIRFM-CV set-up, and in a conventional three-electrode set-up 79
Figure 3-7. Diagram of second generation optical – electrochemical flow cell 80
Figure 3-8. Reaction "a" is an irreversible reaction that converts resazurin to fluorescent resorufin; reaction "b" is a reversible reaction that converts resorufin to non-fluorescent dihydroresorufin
Figure 3-9. Cyclic Voltammogram of 0.02mM resazurin in PBS buffer
Figure 3-10. Fluorescence data obtained in the TIRFM-CV flow cell containing 0.02mM resazurin
Figure 3-11. Combined plot of fluorescence vs. time and applied potential vs. time for 0.02mM resazurin
Figure 3-12. Cyclic Voltammogram of 0.002mM resorufin in PBS buffer 85
Figure 3-13. Fluorescence data obtained in the TIRFM-CV flow cell for 0.002mM resorufin
Figure 3-14. Combined plot of fluorescence versus time and applied potential versus time for 0.002mM resorufin
Figure 4-1. Surface chemistry used to form an 8-carbon monolayer on ITO-coated glass surface using trimethoxyoctylsilane as the linker molecule
Figure 4-2. Experimental set-up for fluorescence recovery after pattern photobleaching (FRAPP) experiments in the epi-illumination mode
Figure 4-3. Fringe pattern in illuminated region obtained by using 100 lines per inch ronchi ruling. b) The observation area is restricted by placing an aperture in the camera/PMT image plane, to ensure that fluorescence recovery is restricted to fluorophores in the fringes.
Figure 4-4. CV curves obtained for a BLM-based FDH sensor
Figure 4-5. Expanded view of relevant portion of data
Figure 4-6. Catalytic response of an immobilized FDH biosensor
Figure 4-7. Expanded view of the relevant portion of data
Figure 4-8. Calibration curve of current density versus D-fructose concentration 122
Figure 4-9. Linear part of calibration curve at 800mV
Figure 4-10. (a) Typical FRAPP curve obtained with FDH and the coenzyme

	immobilized in the biomimetic layer. The solid line represents fit to the data, using a model that describes a population containing a single mobile and immobile fraction (Smith and McConnell 1978; Wright et al. 1988; Starr and Thompson 2002). (b) Plot of residual versus time showing excellent goodness of fit
Figure	5-1. Labview flowsheet for collecting fluorescence data in the analog mode (left hand side) (Figure 5.1 continued on next page)
Figure	5-2contd. Labview flowsheet for collecting fluorescence data in the analog mode (Right hand side of Figure 5.1)
Figure	5-3. Labview flowsheet for collecting fluorescence data in the digital (photon counting) mode (Figure 5-3 continued on next two pages)
Figure	5-4contd. Labview flowsheet for collecting fluorescence data in the digital (photon counting) mode (Figure 5-3 continued on next page)
Figure	5-5contd. Labview flowsheet for collecting fluorescence data in the digital (photon counting) mode

ABBREVIATIONS

 θ angle of incidence of laser beam

 θ_c critical angle

 λ_0 wavelength of the incident laser light

a transfer coefficient

v scan rate

A electrode area

Ag/AgCl silver/silver chloride

a.u. arbitrary units

BSA bovine serum albumin

BLM bilayer lipid membrane

C concentration

Co coatings

CV cyclic voltammetry

D diffusion coefficient

 d_p penetration depth of the evanescent wave

E external applied potential

 $E^{o'}$ formal reduction potential

 E_{pa} anodic peak potential

 E_{pc} cathodic peak potential

 ΔE_p separation of the anodic and cathodic peak potential

F faraday's constant

F1, F2 optical flats

FDH fructose dehydrogenase

FITC fluorescein iso-thiocyanate

FPR fluorescence photobleaching recovery

FRAPP fluorescence recovery after pattern photobleaching

i_p peak current

i_{pa} anodic peak current

i_{pc} cathodic peak current

ITO indium tin oxide

k° standard homogenous electron-transfer rate constant

K₃Fe(CN)₆ potassium ferricyanide

KNO₃ potassium nitrate

m monitoring beam

M1, M2 mirrors

number of electrons

NAD nicotinamide adenine dinucleotide

NADH reduced form of nicotinamide adenine dinulecotide

NDF neutral density filter

 n_1 refractive index of the denser medium

 n_2 refractive index of the rarer medium

[O] concentration of oxidized species

pb photobleaching beam

PBS phosphate buffered saline

[R] concentration of reduced species

R universal gas constant

RBS detergent solution

sADH secondary alcohol dehydrogenase

SCE saturated calomel electrode

Sh shutter

T temperature

TIR total internal reflection

TIRFM total internal reflection fluorescence microscopy

1 INTRODUCTION

The adsorption of proteins at interfaces and their behavior in the adsorbed state are critical in controlling the function of many biological systems. For example, protein adsorption at oil-water interfaces is important in stabilization of emulsions in food products and cosmetics (Dickinson 1977; Dickinson 1994). Protein adsorption also plays an important role in biosensors and in biomedical applications such as rapid diagnostic assays and development of biocompatible devices. Protein adsorption is the first step that occurs when a body reacts to an implanted biomaterial (Andrade 1985), and its adsorption to biomaterials is important in modulating cell adhesion (Hynes 1992; Sanocki 2004). Understanding of competitive interactions between proteins adsorbed at interfaces is also important in biological systems, because most processes involve adsorption of proteins from complex media such as blood or serum which contain a variety of species.

Though each chapter of this thesis addresses a unique problem, the common theme is that they are all geared towards understanding biomacromolecular interactions at fluid-like interfaces. Chapter 2 presents work on the characterization of the adsorption and interaction of the polypeptide nisin and selected proteins at the oil-water interface. Chapter 3 outlines the process of developing an experimental protocol that enables simultaneous optical and electrochemical characterization of biomacromolecules in total internal reflection (TIR) geometry, along with proof-of-concept experiments to demonstrate the feasibility of the set-up, using the dye resorufin. Following this demonstration, the experimental tool was utilized for optical and electrochemical

characterization of a biosensor based on D-fructose dehydrogenase (FDH). Details of this study are presented in Chapter 4. Each of these studies is briefly discussed below.

1.1 Enhanced adsorption of proteins in the presence of the polypeptide nisin

Understanding conformational changes and the behavior of proteins upon adsorption to interfaces is important in a variety of pharmaceutical and biomedical applications, including rapid diagnostic assays, development of scaffolds for tissue engineering, and drug delivery. Drugs have to be delivered to intracellular sites for effective therapeutic applications. The hydrophobic nature of the membrane does not allow the drug to translocate across the membrane by itself. Therefore, one of the major challenges facing drug delivery is achieving drug transport across cell membranes.

Lantibiotics possess a unique physical structure which makes them highly surface active. They are also amphiphilic, thus enhancing their potential for use as emulsifiers in drug formulations. One of the lantibiotics of interest is nisin, which has a unique property in its ability to translocate across the cell membrane. Its small size, surface activity and ability to translocate across the membrane makes it a good candidate for transporting therapeutic compounds across the membrane (Bower et al. 2001). In particular, the potential for transporting drugs such as insulin in nisin-formulated emulsions through the mucosal membrane in the nasal passage is very promising, and was a primary motivation for this study. As part of the preliminary experiments towards achieving this goal, we characterized the adsorption and interactions of nisin at the oilwater interface, generally considered a crude but effective approximation of a biological

membrane (Volkov 1998). For example, the oil-water interface has been used to model drug transport across cellular membranes, as a gauge of pharmacological activity (Arai et al. 1993). In Chapter 2 of this thesis, we present results of a study investigating the adsorption and interactions of nisin with selected labeled proteins at the oil-water interface, and report observations of enhanced interfacial adsorption of certain proteins in the presence of nisin.

1.2 Development of a protocol for simultaneous optical and electrochemical characterization of biomacromolecules in TIR geometry

Analytical devices such as biosensors are characterized by complex interactions at their biomimetic interfaces. However, most characterization techniques use one protocol at a time. We believe the ability to characterize interactions using more than one technique simultaneously would be very useful in providing additional information to aid in understanding and interpreting phenomena in these complex systems. As a result, we have incorporated the ability to conduct electrochemical measurements in our existing optical flow cell, to provide an important tool for situations when optical and electrochemical characterization can be used together to corroborate occurrence of the same event on one sample. For example, in enzyme-based biosensors which utilize nicotinamide adenine dinucleotide (NAD), the reversible conversion of NAD to NADH can be monitored optically by the emission of fluorescence at 450nm. The conversion between the two redox forms NAD and NADH can also be tracked electrochemically using cyclic voltammetry (CV).

Alternatively, this tool would also be useful in situations when optical and electrochemical measurements can give two independent pieces of information about a single sample. For example, in enzymatic sensors based on bilayer lipid membrane (BLM), optical measurements can be used to confirm the formation and integrity of the lipid bilayer, and electrochemical measurements can be used to study redox reactions catalyzed by enzymes at the same biomimetic interface.

To this end, we have modified the flow cell used in our total internal reflection fluorescence microscopy (TIRFM) apparatus to incorporate the capability to also conduct electrochemical measurements. The details of this work are given in chapter 3. The functionality of the modified set-up was tested and confirmed by monitoring the reversible redox conversion of resorufin to dihydroresorufin. When the potential was scanned to reduce resorufin to dihydroresorufin, a decrease in fluorescence was observed. Similarly, when the potential was scanned to oxidize dihydroresorufin to resorufin, an increase in fluorescence emission was observed. In addition to allowing the estimation of interfacial concentrations, the resulting data could potentially be used to understand the kinetics of the reaction.

1.3 Development and optical-electrochemical characterization of a biosensor based on D- fructose dehydrogenase (FDH)

During the past decade, there has been widespread interest in the development of biosensors for applications in areas such as food technology, agriculture, environmental monitoring, and biomedical devices (Castillo et al. 2004; Mehrvar and Abdi 2004).

Biosensors are being increasingly used due to their ease of miniaturization, high specificity and sensitivity, short response times, and the fact that analyte detection does not require prior separation of the sample (Castillo et al. 2004). A biosensor is an analytical device that detects biochemical and physiological changes. It comprises a receptor (biological recognition element) and a transducer in close proximity to each other. It converts a specific recognition event between the receptor and the target analyte into a measurable signal. There are two main classes of biosensors – catalytic or bioaffinity. Catalytic biosensors enable measurement of the steady-state concentration of analytes formed and/or consumed during a biocatalytic reaction. Bioaffinity biosensors, on the other hand, are used to detect specific interactions between a receptor molecule and a target analyte (antibody-antigen interactions).

Some common modes of transduction in biosensors are electrochemical (potentiometric, amperometric, conductometric) (Chaubey and Malhotra 2002; Dzyadevych et al. 2002; Gerard et al. 2002), optical (absorbance, fluorescence, luminescence, light scattering, refractive index) (Cush et al. 1993; DiazGarcia and ValenciaGonzalez 1995; Barak et al. 1997; Karlsson and Falt 1997; Lin et al. 1997; Mehrvar et al. 2000), mechanical (Raiteri et al. 2001), thermal (Abel et al. 1996; Ivnitski et al. 1999; Ramanathan and Danielsson 2001), piezoelectric (Muramatsu et al. 1987; Davis and Leary 1989; Saini et al. 1991), and magnetic (Baselt et al. 1998). The preferred transduction modes are usually electrochemical for catalytic biosensors, and optical for bioaffinity biosensors. The most widely used catalytic biosensors are enzyme-based electrochemical sensors, which are of special interest because of the high

specificity, selectivity and efficiency of the enzyme towards the target analyte.

We have developed an electrochemical catalytic biosensor based on the enzyme fructose dehydrogenase (FDH) for the detection of D-fructose, and have characterized it both optically and electrochemically (Chapter 4). FDH, a membrane-bound enzyme was immobilized in a lipid bilayer membrane with the mediator coenzyme Q₆, also incorporated into the bilayer. The biomimetic layer was deposited on transparent indium tin oxide (ITO)-coated glass, allowing us to characterize the biosensor both optically and electrochemically. The formation of the lipid bilayer on the ITO-coated slide was confirmed optically, using fluorescence recovery after pattern photobleaching (FRAPP). The functionality of the biosensor was confirmed electrochemically, based on increased catalytic current upon addition of D-fructose to the flow cell.

2 ENHANCED ADSORPTION OF PROTEINS IN THE PRESENCE OF THE POLYPEPTIDE NISIN

2.1 ABSTRACT

We present sequential and competitive adsorption experiments on interactions between nisin and selected proteins at a model oil-water interface. We used total internal reflection fluorescence microscopy (TIRFM) with an evanescent wave configured to a depth of 85 nm, to confine the area of observation to the interface and its immediate vicinity. All proteins except nisin were labeled with fluorescein isothiocyanate (FITC).

Experimental results showed strong evidence of significantly enhanced adsorption of some proteins in the presence of nisin. Apparent interfacial concentrations of β -casein were nearly three times higher in the presence of nisin than when the pure protein adsorbed by itself under identical conditions. Enhanced adsorption was also observed for lysozyme and bovine serum albumin (BSA) in the presence of nisin, in comparison to adsorption of each protein by itself. Very little enhanced adsorption was observed for fibronectin in the presence of nisin.

The exact mechanism for adsorption enhancement by nisin is not fully clear. However, the experimental data suggest strongly that molecular weight, size of the adsorbing protein, and bulk protein concentration are all important factors.

2.2 INTRODUCTION

2.2.1 Nisin

Nisin is a small (3.5 kDa) positively charged amphipathic polypeptide, produced by *Lactococcus lactis*. It contains dehydrated residues and lanthionine or thioether rings, has antimicrobial activity against a large variety of gram-positive bacteria, and has been widely used as a food preservative in the dairy industry (Hurst 1981). Its antimicrobial activity stems primarily from permeabilization/pore formation of the cytoplasmic membrane of target organisms (Breukink et al. 1998; Van Kraaij et al. 1998; Breukink and de Kruijff 1999; Breukink et al. 1999; Enserink 1999; Van heusden et al. 2002). The peptide initially binds to the membrane with its C-terminus through electrostatic interactions; after that the N-terminus is inserted into the lipid phase of the membrane. Lipid-II, a cell wall precursor, binds to nisin, resulting in a transmembrane orientation of the polypeptide; subsequent oligomerization of nisin and lipid-II leads to pore formation.

Because of its antimicrobial properties, there is interest in using nisin in formulations that could effectively transfer drugs across the cellular membrane (Bower et al. 2001). To realize this promise, it is necessary to understand the interactions of nisin at fluid-like interfaces. Thus, the goal of this study was to characterize the adsorption dynamics and interactions of nisin at a model oil-water interface, and to assess its potential for use in pharmaceutical formulations.

The primary tool for characterizing protein adsorption and interactions in our

laboratory is total internal reflection fluorescence microscopy (TIRFM), which requires proteins to be labeled with fluorophores. However, nisin was not labeled in this work because a previous study in our laboratory had demonstrated that fluorescent labels can markedly affect both protein diffusion and interfacial dynamics (Gajraj and Ofoli 2000b). Due to its small size (3.5 kDa) in relation to the fluorophore we commonly use to label proteins in our laboratory (FITC, ~0.350 kDa), attaching this label to nisin had the potential of significantly affecting its interfacial dynamics. To avoid this, we decided to track nisin's interfacial dynamics through its competitive interactions with selected labeled proteins at the interface. This decision was based in part on several studies that had reported that nisin adsorbs strongly at the hydrophobic/hydrophilic interface (Bower 1995; Giffard et al. 1996; Lakamraju et al. 1996; Bani-Jaber et al. 2000; Lee et al. 2000). We hypothesized that the combination of its high interfacial activity and small size (which usually translates into high diffusivity) (Dickinson 1977) would enable nisin to relatively easily displace other proteins from the interface. This would enable us to monitor its interfacial behavior by measuring the dynamics of displacement of labeled proteins from the interface.

This interfacial characterization was done in sequential and competitive adsorption experiments, using a diverse group of labeled proteins of varying characteristics. We measured interactions of nisin with two fibrous proteins [β-casein (24 kDa) and fibronectin (440 kDa)] and two globular proteins [lysozyme (14.3 kDa) and bovine serum albumin (66 kDa)]. This group of proteins was selected to provide a range of hydrodynamic size, molecular weight, and structure. In addition, the interfacial

behavior of each of these proteins has been characterized in our laboratory (Gajraj and Ofoli 2000b; Vaidya and Ofoli 2005), so their adsorption characteristics were well understood.

2.2.2 Total Internal Reflection Fluorescence Microscopy (TIRFM)

Protein adsorption was measured using total internal reflection fluorescence microscopy (TIRFM), an optical technique that enables molecular level investigations of macromolecular adsorption and interactions at a variety of interfaces. It provides the ability to selectively illuminate macromolecules within tens of nanometers of the interface and is a non-intrusive, in situ technique. TIRFM has been used at the liquidliquid interface to study protein dynamics (Tupy et al. 1998; Gajraj and Ofoli 2000a; Gajraj and Ofoli 2000b; Vaidya and Ofoli 2005), and at the solid-liquid interface to study receptor-ligand interactions (Asanov et al. 1998), living cells and single molecules, adsorption and relaxation kinetics of proteins (Wertz and Santore 1999; Wertz and Santore 2001; Wertz and Santore 2002; Wertz and Santore 2002), diffusion, adsorption kinetics and lateral mobility of proteins (Giffard et al. 1996; Yuan et al. 2003, Thompson et al. 1981, Gajraj and Ofoli 2000b; Vaidya and Ofoli 2005), and formation and morphology of lipid bilayers (Wagner and Tamm 2000). We present here only a brief introduction to TIRFM. Further detail can be obtained from Axelrod et al. 1983; Axelrod 1989; Axelrod 1992; Gajraj 1999; Gajraj and Ofoli 2000a.

When a beam of light traveling in a medium of higher refractive index (n_I) strikes a medium of lower refractive index (n_2) at an angle (θ) greater than the critical angle (θ_c) ,

the beam is totally internally reflected. The critical angle is given by

$$\theta_c = \sin^{-1}\left(\frac{n_2}{n_1}\right), \quad n_2 < n_1$$
 (2.1)

Upon total internal reflection, an electromagnetic field or evanescent wave is induced in the rarer medium at the interface. The amplitude of the evanescent wave decays exponentially with depth into the rarer medium, with a penetration depth (d_p) that depends on the refractive indices of the two media, the angle of incidence (θ) and the wavelength of the incident light (λ_{θ}) :

$$d_{p} = \frac{\lambda_{0}}{4\pi n_{1} \sqrt{\sin^{2} \theta - \left(\frac{n_{2}}{n_{1}}\right)^{2}}}$$
 (2.2)

The penetration depth is usually on the order of 80nm with the setup in our laboratory, thus making this a truly surface-selective technique.

2.2.3 The Liquid-liquid Interface

Liquid-liquid interfaces are of considerable importance in biological systems, particularly in pharmacology, food processing, biomedical engineering and biotechnology. For example, the distribution of proteins and surfactants at the liquid-liquid interface influences the properties of food systems such as emulsions and microemulsions (Dickinson 1998). Liquid-liquid interfaces also provide a simple approximation to cellular interfaces where many important biological processes such as

receptor-ligand interactions, electron transfer, enzymatic reactions and drug delivery occur (Arai et al. 1993).

Thus, the study of protein adsorption and interactions at fluid-like interfaces is relevant in understanding the complex processes taking place in biological systems. In particular, the oil-water interface serves as a crude approximation of a biological membrane (Volkov 1998).

2.3 MATERIALS AND METHODS

2.3.1 Preparation of protein solutions

Pure nisin was provided as a generous gift from Dr. Joseph McGuire, Department of Food Science and Technology, Oregon State University, Corvallis, OR. Bovine β-casein was purchased from the Hannah Research Institute (Lot No. B/6/6, Ayr, Scotland) at 95% purity. Bovine serum albumin (A-7511) and lysozyme (L-2879) were obtained from the Sigma Chemical Co. (St. Louis, MO), and fibronectin (FC010) was obtained from Chemicon International (Temecula, CA). All proteins were used as received, without further modification. Sodium phosphate monobasic and sodium phosphate dibasic, which were used in the preparation of the buffers, were purchased from the Sigma Chemical Company (St. Louis, MO).

Nisin was dissolved in sodium phosphate monobasic (pH 4.5, 0.05M) to ensure complete solubilization. Sodium phosphate dibasic (pH 9.1, 0.05M) was added to the nisin solution to bring the pH up to 7.4 (Lee et al. 2000). All proteins except nisin were

labeled with fluoroscein-5-isothiocyanate (FITC, F-1907, Molecular Probes, Eugene, OR), using the protocol given by Brinkley (Brinkley 1992). In brief, the labeling reaction for each protein was carried out at room temperature in carbonate buffer (pH 9.1, 0.05M) for periods of four to six hours in the dark. The protein solution was then dialysed against phosphate buffer (pH 7.40, 0.05M) to remove any unreacted dye. Dialysis was carried out over a period of 24 to 36 hours, in a 4-6 stage continuously stirred operation with a regenerated cellulose porous membrane (Spectra/Por 1, 132655, molecular weight cutoff of 6000 to 8000, Spectrum Laboratories, Rancho Dominguez, CA). The solutions of labeled proteins were initially frozen in aliquots, and thawed and diluted to the required concentration before each experiment. Absorbance spectroscopy measurements were carried out on a diode array spectrophotometer (Model 8452A, Hewlett-Packard, Brielle, NJ) to determine the concentrations of proteins and the labeling ratios. A labeling ratio (dye to protein) less than unity was usually used for all experiments, to avoid potential problems with concentration quenching.

2.3.2 Experimental Setup

Our experimental set-up (Figure 2-1) has been described in detail in an earlier paper (Gajraj and Ofoli 2000a). An important modification to the original setup is that we have added a photon counter to detect very low fluorescence emission intensities at the interface. Experiments at high concentrations (concentrations higher than 10⁻⁵M) were conducted in stop-flow mode, where the protein solution continuously flowed into the sample cell for a period of about 30 minutes, after which flow into the cell was

terminated. Experiments at lower concentrations (particularly below 10⁻⁷M) were carried out in continuous flow mode, to avoid the possibility of bulk depletion of proteins during the experiment.

Solutions were simultaneously infused and withdrawn from the flow cell at a rate of 0.047 ml/min (shear rate of 0.43s⁻¹), using a Harvard Apparatus infusion/withdrawal syringe pump (Model 551382, Harvard Apparatus, South Natick, MA). Fluorescence emission was measured with a photomultiplier tube (R4632, Hamamatsu, Bridgewater, NJ) for protein solutions at high concentrations, and the analog measurements were filtered to remove dark current during periods where the chopper blocked the laser beam. Data filtering was carried out using a program written in MATLAB (Mathworks inc., Natick, MA) (see Appendix A). Fluorescence measurements for the low concentration experiments were collected using the same photomultiplier tube, with the signal amplified by a SR445 pre-amplifier (Stanford Research Systems, Sunnyvale, CA). The output of the pre-amplifier was sent to a photon counter (SR400 Dual Channel Gated Photon Counter, Stanford Research Systems, Sunnyvale, CA), which was used to accurately track both adsorption and desorption, even at bulk protein concentrations as low as 10-8 M. Labview 6.0 (National Instruments, Austin, TX) served as the computerized data acquisition software (Figure 5-1 and Figure 5-3 in Appendix A). Some images in this dissertation have been presented in color.

Since many of the experiments were conducted over long periods of time (durations of several hours sometimes), we took precautions to prevent unintended photobleaching of the fluorophore by the monitoring beam. First, a beam chopper (SR540, Stanford Research Systems, Sunnyvale, CA) was continuously used during all experiments. In addition, the photon counter was triggered by the chopper and gated such that data were collected only when the flow cell was illuminated by the laser beam. Secondly, the monitoring beam was blocked during long experiments, to provide additional protection against photobleaching; the beam was allowed to illuminate the interface only during periods of fluorescence emission measurements. Finally, the monitoring beam was configured to a low intensity of 2-3µW, as measured by a Newport power meter (818-SL, Newport, Irvine, CA).

All experiments were conducted at the oil-water interface, using a flow cell described in an earlier paper (Gajraj and Ofoli 2000a). For this study, the oil-water interface was formed by bringing a 20-60µm layer of oil in contact with an 800µm layer of water. The bottom slide was coated with polyethylene oxide (PEO, Sigma Chemical Co., St. Louis, MO) to eliminate protein adsorption on that surface (Jeon and Andrade 1991; Andrade et al. 1996). Readings acquired at different locations at the oil-water interface were reproducible during a given experiment; data acquired on the same batch of labeled proteins were also reproducible.

2.4 RESULTS AND DISCUSSION

We conducted competitive and sequential adsorption experiments using unlabeled nisin and FITC-labeled β -casein. We chose to work with β -casein because its adsorption characteristics have been well-characterized in several studies (Graham and Phillips

1979; Hunter et al. 1991; Dickinson et al. 1993; Russev et al. 2000). To minimize shear at the interface, very low flow rates of approximately 0.045ml/min (shear rates of 0.43s⁻¹) were used to introduce protein solutions into the flow cell. The time for protein adsorption to approach pseudo-steady state behavior in our flow cell (as indicated by the fluorescence emission intensity profile) varied between 30 and 50 minutes. This is much faster than the characteristic time of adsorption at interfaces of normal depth (which can be as long as a few hours). The reduced time of adsorption is the result of the thinness of the oil-water assembly, which is on the order of 800μm.

In initial experiments, labeled β -casein at a bulk concentration of $10^{-5}M$ was introduced into the flow cell and allowed to adsorb at the interface in a continuous flow format. When the fluorescence emission intensity level approached a pseudo-steady state value after about 35 minutes, nisin (at a bulk concentration of $10^{-5}M$) was introduced into the flow cell (Figure 2-2). As expected, we observed a continuous drop in fluorescence emission intensity upon introduction of nisin. This behavior appeared to confirm our initial hypothesis that nisin, being smaller and more surface-active, was displacing adsorbed β -casein from the interface. However, there are at least two other plausible explanations for the behavior observed in Figure 2-2. The first is that β -casein was removed from the interface as a result of the shear induced by the continuous flow of nisin into the flow cell as the experiment proceeded. This is unlikely, because earlier experiments conducted in our laboratory had demonstrated that the liquid-liquid interface remains stable at flow rates of up to 0.05ml/min. The second plausible explanation is

that, since the nisin solution contained no β -casein, the adsorbed β -casein is removed from the interface by mass transfer resulting from the concentration gradient induced by the depletion of proteins in the bulk. That is, the bulk concentration of β -casein continuously decreased as the nisin solution flowed into the sample cell.

To investigate this further, we ran the reverse experiment where nisin at the same bulk concentration (10^{-5} M) was adsorbed at the interface for a period of about 30 minutes, followed by the introduction of β -casein (also at a bulk concentration of 10^{-5} M) into the flow cell. Upon introduction of β -casein, we observed an increase in the fluorescence emission intensity, indicating that β -casein was adsorbing at the oil-water interface, even in the presence of pre-adsorbed nisin (Figure 2-3). This was an unexpected result, because the presence of nisin at the interface clearly did not preclude or even significantly hinder β -casein adsorption. In fact, this result appeared to provide evidence that nisin is less surface-active than β -casein. However, another plausible explanation was that, at the low bulk concentrations at which the experiments were conducted, the interface was never saturated, allowing both nisin and β -casein to adsorb and coexist with essentially no effective interfacial competition.

To evaluate this possibility, we conducted an experiment where we allowed for equilibrium adsorption of β -casein (10⁻⁵M) at the oil-water interface, after which a protein-free buffer solution was introduced into the flow cell. Upon introduction of the buffer solution, a significant drop in the fluorescence emission level was observed, indicating desorption of β -casein from the interface (Figure 2-4). The extent of apparent

 β -casein desorption from the interface was comparable to what was observed earlier upon interaction of β -casein with nisin (Figure 2-2). This indicated that β -casein was removed because it is reversibly (loosely) adsorbed at the interface, not because nisin has superior interfacial activity by comparison.

Follow-up experiments were modified to help determine if concentration gradients play a role in the desorption of β -casein from the interface. Similar to the first set of experiments, we allowed β-casein (10⁻⁵M) to adsorb at the oil-water interface until the fluorescence signal approached pseudo-equilibrium. We then introduced a mixture of nisin and β-casein (each at identical concentrations of 10⁻⁵M) into the flow cell. The infusion of both β-casein and nisin was done to maintain the β-casein bulk concentration at a fixed level, to prevent bulk depletion of the protein. Upon introduction of the mixture, we observed a significant increase in fluorescence emission intensity, indicating that \(\beta\)-casein was adsorbing in substantially larger quantities than was observed when it adsorbed alone at the interface (Figure 2-5). The level of fluorescence emission intensity represents an increase of about 3 times the level initially observed, which qualitatively indicates that approximately three times more β-casein was adsorbing at the interface in the presence of nisin, in comparison to β-casein adsorbing alone. In addition, the slope of the initial adsorption profiles for β-casein adsorbing alone was essentially identical to that for the adsorption of β-casein in the presence of nisin (Figure 2-5). The profiles also clearly show two distinct approaches to equilibrium – one with β-casein adsorbing by itself and a second with β-casein adsorbing in the presence of nisin. The same result was

observed when the concentration of β -casein was lowered by a factor of ten (from 10^{-5} M to 10^{-6} M), with the bulk concentration of nisin maintained at 10^{-5} M. In that case, an increase of more than 8 times the initial fluorescence emission level was observed, with the signal not reaching an apparent steady value during the time of the experiment (Figure 2-6).

To evaluate whether this effect is due to factors other than the presence of nisin, we conducted a control experiment where we allowed β -casein to adsorb at a bulk concentration of 10^{-5} M until a pseudo-steady state fluorescence emission level was attained. At that time, a solution of β -casein at the same concentration was introduced into the flow cell, to assess the extent of additional protein adsorption. While a small change in fluorescence emission intensity was observed, the increase was negligible in comparison to that observed in the presence of nisin (Figure 2-7). These results suggest strongly that there is increased or "enhanced" adsorption of β -casein in the presence of nisin.

To investigate this further, we studied the adsorption and interactions of nisin with three other proteins: bovine serum albumin (BSA), lysozyme and fibronectin. This particular group of proteins was chosen because of their diverse size, structure and adsorption characteristics. The experimental protocol was similar to the one used in the experiments conducted with β -casein and nisin. After pseudo-stabilization of the BSA adsorption profile, a solution containing BSA and nisin, each at a bulk concentration of 10^{-5} M, was introduced into the flow cell. We observed little or no change in the

fluorescence emission level, even after 60 minutes of interaction (Figure 2-8). Therefore, while the adsorption of β -casein (a fibrous protein of molecular weight 24 kDa) was enhanced in the presence of nisin, there was no apparent enhancement in the adsorption of BSA (a globular protein of molecular weight 66 kDa).

To the best of our knowledge, this level of "enhanced" adsorption of one protein in the presence of another has not been previously reported. We should, however, present the kinetic modeling work of Fang and Szleifer on the adsorption of an equimolar solution containing a small and a large protein (Fang and Szleifer 2001). They showed that the two proteins initially adsorb together but, after a short time, the rate of adsorption of the smaller protein decreases and that of the larger protein increases, because the surface-protein interaction is stronger for the larger protein. Fang and Szleifer's kinetic modeling studies were conducted at a bare interface while, in the present study, the mixture of nisin and the competing protein arrived at an interface that already had a preadsorbed layer of the larger protein. It is reasonable to expect that the interaction between a protein and a bare (clean) surface would be much stronger than that between the same protein and a pre-adsorbed protein layer.

While we do not know the exact mechanism for its occurrence, there are several plausible explanations for the observation. First, nisin is a pore forming protein capable of penetrating cellular membranes (Van Kraaij et al. 1998; Bower et al. 2001; Van heusden et al. 2002). Therefore, one possible explanation is that, as the original protein (β-casein, for example) adsorbs towards its equilibrium concentration at the interface, it

forms a film that may mimic a cellular membrane. When nisin is introduced into the flow cell, its interaction with the adsorbed protein film "stretches" the interface, thus creating additional adsorption sites for the interacting proteins to adsorb. We speculate that this "stretching" may actually be more of a type of "corrugation" of the linear adsorbed film at the interface, which results in the creation of a larger surface area over the same linear horizontal dimension.

Another possible explanation is that nisin causes the adsorbed protein to reorient itself at the interface, resulting in more efficient packing (Figure 2-9). For example, some studies have reported a reorientation of lysozyme upon initial adsorption and interaction with the surface, following which space is created for additional proteins to adsorb at the interface (Robeson and Tilton 1996; Daly et al. 2003). Nisin apparently accentuates this effect, because the increases in adsorption reported by these earlier studies were not as large as the enhanced adsorption observed in our experiments.

Other factors that could influence adsorption enhancement include protein size and/or molecular weight, and protein type (globular versus random coil). For example, physical protein size and/or molecular weight would be a factor in adsorption enhancement if it is assumed that nisin creates identical pore sizes in each adsorbed layer. Then, the smaller β -casein protein molecules would be better able to pack into the pores than larger proteins such as BSA. In that case, we would observe more significant enhanced adsorption for β -casein than for BSA. One could also speculate that, if the structure and the resulting adsorbed layer influence the process, then nisin may be better

able to create space in the adsorbed β -case layer (which likely adsorbs in more of a condensed layer at the oil-water interface), than in the adsorbed albumin layer (which adsorbs in more of an expanded or spread-out configuration at the oil-water interface) (Graham and Phillips 1979).

To evaluate these factors, we conducted similar experiments with lysozyme in the presence of nisin. Lysozyme is a globular protein like BSA, but smaller in size (14.3 kDa) than both BSA and β-casein. As was done in the previous experiments, a solution containing both lysozyme and nisin (each at 10⁻⁵M) was introduced into the flow cell after lysozyme adsorption had reached pseudo-equilibrium. Upon introduction of this solution, we observed a slight increase in fluorescence emission intensity (Figure 2-10). Since this increase was not as large as what was observed for β -casein, a control experiment similar to what was done with β-casein was conducted by introducing additional lysozyme into the flow cell after pseudo-equilibrium adsorption was achieved. As was the case for β -casein, the slight increase observed in the control experiment is clearly less significant than was observed in the presence of nisin (Figure 2-11). Hence, there is an indication of "enhanced" adsorption of lysozyme in the presence of nisin (Figure 2-10), although not as significant as that observed for β -casein. This is also evident in an additional experiment conducted in the presence of nisin as shown in Figure 2-12.

There is evidence in the literature to suggest that lysozyme achieves a higher surface coverage than β-casein at the same bulk molar concentration (Hunter et al. 1991).

Therefore, a possible consequence of the higher surface coverage is that lysozyme may form a thicker film at the interface than β -casein. Ordinarily, one would expect the thicker film to promote formation of more stable pores, which could lead to enhanced adsorption. However, lysozyme is also known to form a more expanded layer at the oilwater interface than β -casein, which forms a condensed layer (Graham and Phillips 1979). As discussed above, this may tend to reduce the possibility of enhanced adsorption.

To further evaluate the effect of nisin on adsorbed fibrous proteins, we conducted experiments on interactions of nisin and fibronectin, a much larger fibrous protein at 440 kDa. The results showed a fairly small enhanced fibronectin adsorption in the presence of nisin (Figure 2-13), in comparison to the protein adsorbing by itself. In all cases examined, no "enhanced" adsorption was observed for proteins that were larger in molecular weight than β -casein. This would tend to support the speculation that smaller proteins are better able to adsorb effectively into nisin-induced pores than larger ones.

To assess the effect of bulk protein concentration, we conducted experiments on lysozyme at a concentration of 10⁻⁷M, 100 times lower than in the earlier experiments, with the bulk concentration of nisin maintained at 10⁻⁵M. The experimental protocol was the same as that for the earlier experiments. Upon introduction of the lysozyme-nisin mixture, we observed very pronounced enhanced adsorption. Just as significant was the fact that the adsorption curve for lysozyme during the initial enhanced adsorption phase was 2.6, which is identical to the initial slope of the adsorption curve in the absence of

nisin (Figure 2-14).

These data on lysozyme at lower concentrations would indicate that, along with size, bulk protein concentration may be an important factor in the mechanism for adsorption enhancement and may, perhaps, be even more important than the structure of the protein. To evaluate this factor, we repeated the BSA and fibronectin experiments at much lower concentrations. The BSA experiments were run at a bulk concentration of 8x10⁻⁷M, with the nisin concentration remaining at 10⁻⁵M. At this much lower BSA concentration, diffusion became an important factor because it took a long time to attain pseudo-steady adsorption in a reasonable amount of time. Therefore, we introduced the mixture of nisin and BSA into the flow cell before pseudo-equilibrium BSA adsorption was achieved. We then compared different segments of the adsorption profile on the basis of the initial adsorption slopes before and after introducing the mixture of proteins into the flow cell.

An examination of the data (Figure 2-15) shows clearly that the slope of the adsorption profile increases significantly upon introduction of BSA and nisin (0.59), in comparison to the profile of BSA adsorbing in the absence of nisin (0.21). Thus, there is a slight increase in the rate of adsorption in the presence of nisin, although it is not as large as that observed with β -casein or lysozyme at the lower concentrations. While there is clear evidence of enhanced BSA adsorption at lower concentrations in the presence of nisin, we observed only minor adsorption enhancement in fibronectin experiments conducted at much lower concentrations (Figure 2-16). Collectively, these

experiments appear to indicate that the important factors in adsorption enhancement in the presence of nisin are the size, molecular weight and bulk concentration of the adsorbing protein. Another factor we have not yet investigated is the possibility of ordered multilayer formation in the presence of nisin.

Increases in fluorescence emission intensities can be attributed to a) an increase in the amount of fluorescently tagged molecules at the interface and/or b) a change in the fluorophore quantum yield. To evaluate the quantum yield issue, we measured the absorption and emission spectra of both pure β -casein and a mixture of β -casein and nisin at the same concentrations. No significant differences were observed between the two samples. In addition, lifetime studies conducted in collaboration with Dr. Gary Blanchard of the MSU Chemistry Department using time correlated single photon counting spectroscopy have shown that the quantum yield is the same for surface-associated proteins as for proteins in the bulk (Vaidya 2005). Thus, the increased adsorption is most likely due to nisin-induced interfacial interactions, rather than a change in the quantum yield of the fluorophores.

As discussed earlier, the theory offered by Fang and Szleifer (Fang and Szleifer 2001) is also plausible. However, we believe that the interfacial energetics are very different for the two situations. In addition, similar experiments conducted in our laboratory on the interaction between human serum albumin (66 kDa) and fibronectin (440 kDa) did not show any evidence of enhanced adsorption of fibronectin (Vaidya and Ofoli 2005). This appears to provide confirmation that the increased adsorption is

specific to nisin (and perhaps other lantibiotics), rather than the result of an interaction between a large and a small molecular weight protein as observed by Fang and Szleifer (Fang and Szleifer 2001).

2.5 CONCLUSIONS

We have used total internal reflection fluorescence microscopy (TIRFM) to characterize the interfacial behavior of nisin, an antimicrobial pore-forming polypeptide. Sequential and competitive adsorption experiments on nisin and several labeled proteins (β-casein, bovine serum albumin, lysozyme and fibronectin) were conducted at the oilwater interface. This group of proteins were chosen because of significant variations in molecular weight, hydrodynamic size, and structure. A key finding was the observation of enhanced levels of adsorption of certain proteins at the oil-water interface in the presence of nisin. The apparent surface coverage of β-casein (at a bulk concentration of 10⁻⁵M) in the presence of nisin was nearly three times the value observed for the protein when it adsorbed by itself at the interface. Enhanced adsorption was also observed for lysozyme at the same bulk molar concentration. Experiments conducted at lower bulk concentrations resulted in even more pronounced enhanced adsorption for β-casein, bovine serum albumin and lysozyme. We also observed adsorption enhancement for the interaction of fibronectin and nisin, although this was not significant at any concentration.

Based on the experimental results, we propose that the significant factors influencing enhanced adsorption in the presence of nisin are molecular weight, size of the adsorbing protein, and the bulk concentration of proteins. While the exact reason(s)

and/or mechanisms for this phenomenon are still being investigated, we can reasonably conclude that the adsorption enhancement is an effect specific to nisin and perhaps other lantibiotics, because of the ability to form pores in membranes.

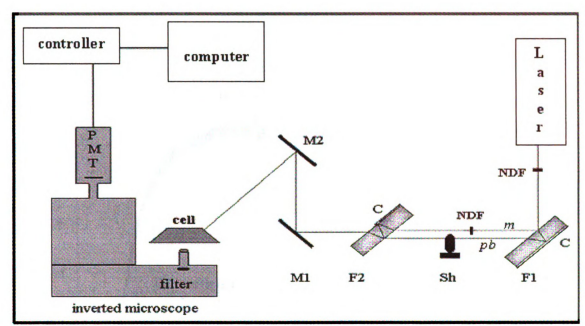


Figure 2-1a

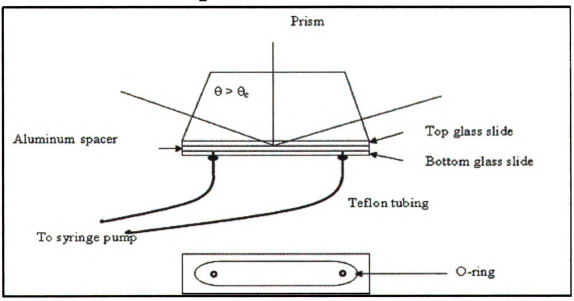


Figure 2-1b

Figure 2-1. Experimental set-up for TIRFM experiments

a) Optical train: PMT – photomultiplier tube; M2, M1 – mirror; F1,F2 – optical flats; C – coatings; Sh – shutter; NDF – neutral density filters; m – monitoring beam; pb – photobleaching beam. b) Flow cell showing holes for sample infusion and withdrawal.

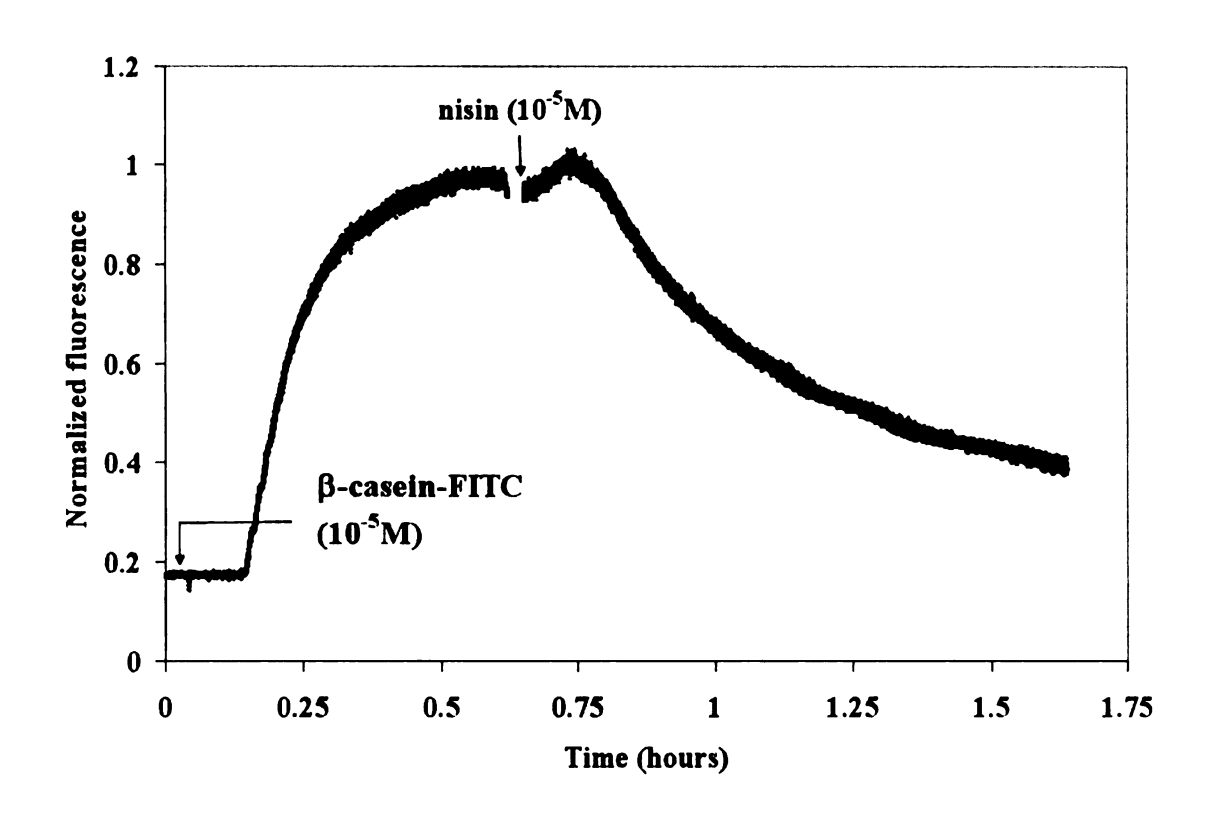


Figure 2-2. Equilibrium adsorption of β -casein followed by introduction of nisin.

The initial adsorption profile shows equilibrium adsorption of β -casein-FITC (10⁻⁵M) at an oil-water interface. Upon pseudo-stabilization of the fluorescence emission signal, unlabeled nisin (10⁻⁵M) was introduced into the flow cell. The fluorescence level decreased upon introduction of unlabeled nisin, indicating apparent β -casein desorption from the interface. All solutions were introduced at a shear rate of 0.43 s⁻¹.

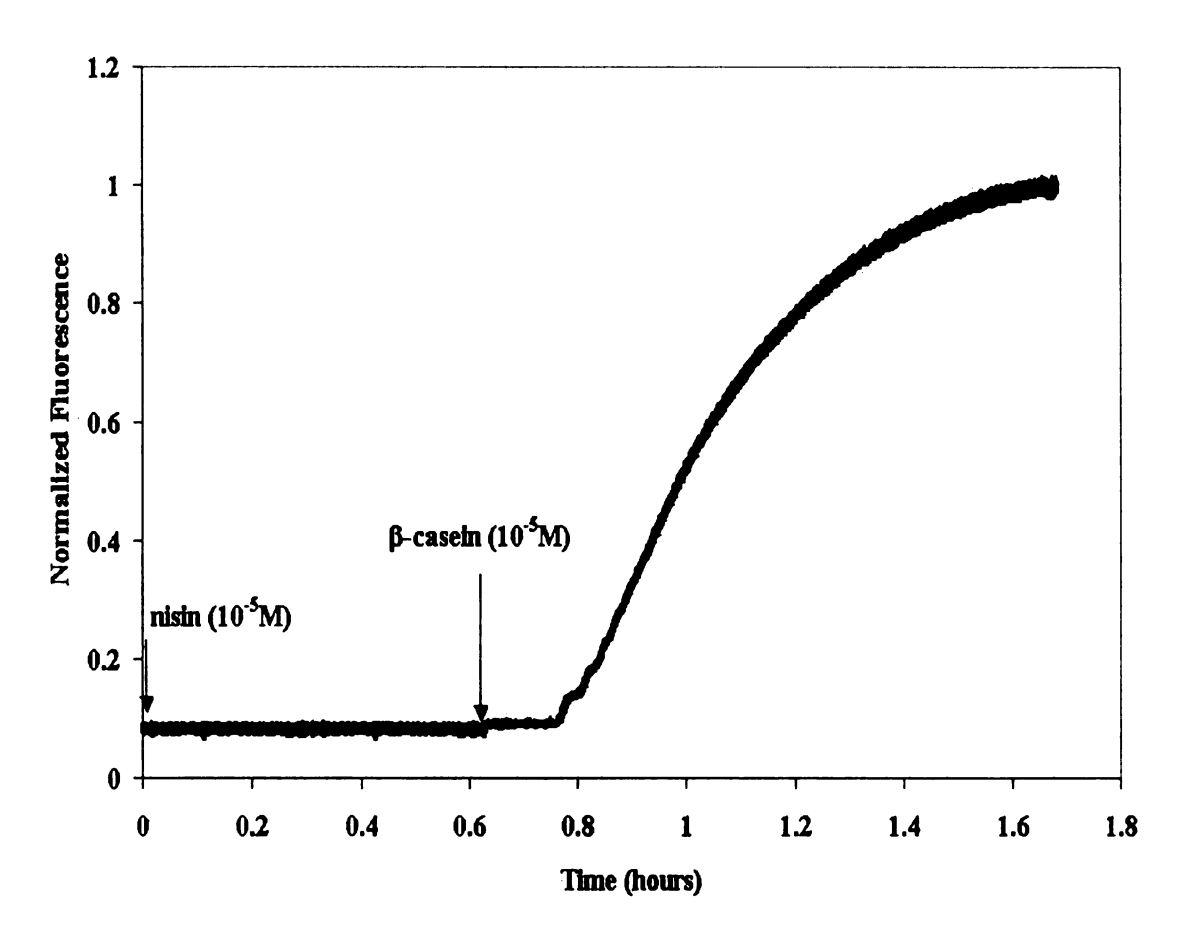


Figure 2-3. Adsorption of nisin followed by introduction of β-casein.

Following adsorption of unlabeled nisin (10^{-5} M) at the oil-water interface (for a period of about 30 minutes), β -casein-FITC (10^{-5} M) was introduced into the flow cell. Clearly, the prior adsorption of nisin at the interface did not preclude β -casein adsorption. All solutions were introduced at a shear rate of 0.43 s⁻¹.

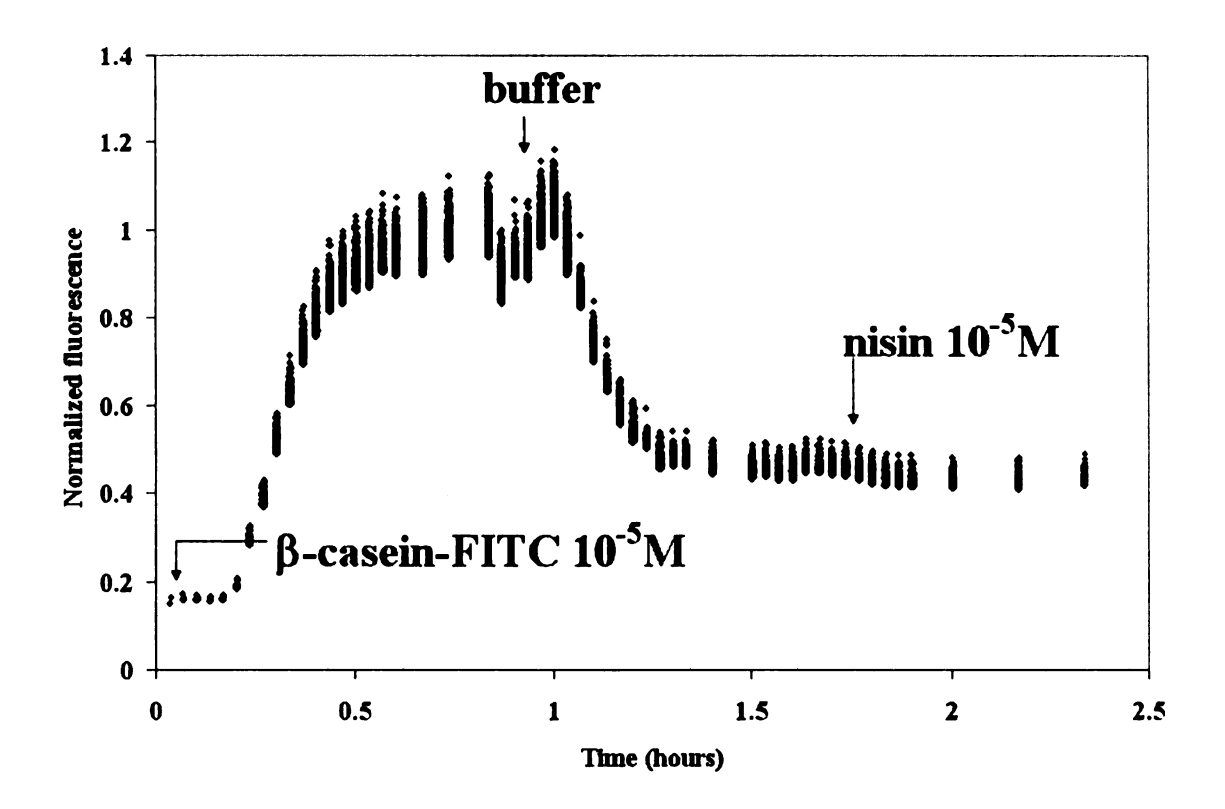


Figure 2-4. Assessment of β -casein adsorption reversibility.

The initial adsorption profile shows equilibrium adsorption of β -casein-FITC ($10^{-5}M$) at the oil-water interface. After the fluorescence level stabilized, a phosphate buffered saline solution (PBS) was introduced into the flow cell. The resulting drop in fluorescence emission is an indication of β -casein desorption from the interface. Following stabilization of the signal, unlabeled nisin ($10^{-5}M$) was introduced into the flow cell to check if nisin would induce further desorption of β -casein from the interface. However, very little additional desorption was observed. All solutions were introduced at a shear rate of $0.43 \, \text{s}^{-1}$.

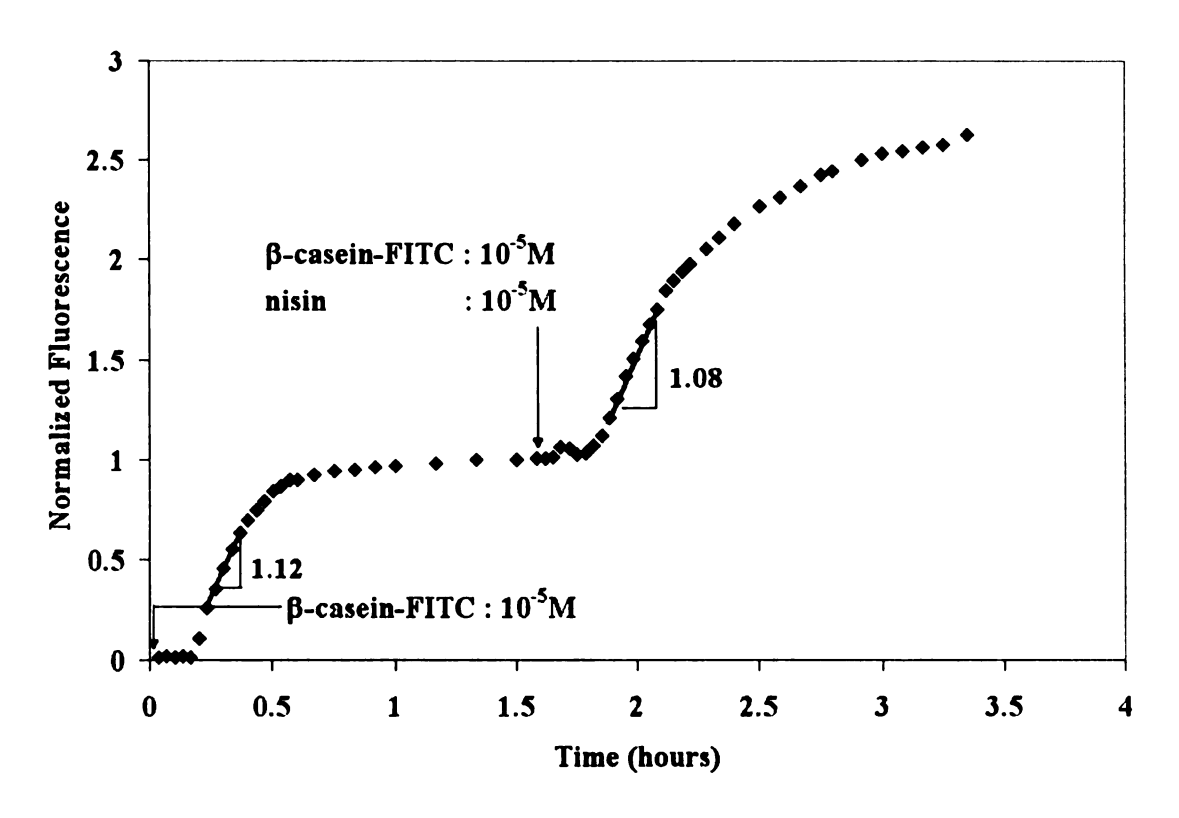


Figure 2-5. Enhanced adsorption of β -casein in the presence of nisin.

The initial profile is for the adsorption of labeled β -casein (10⁻⁵M) at the oil-water interface. Upon pseudo-stabilization of the fluorescence emission level, a mixture of labeled β -casein and unlabeled nisin, each at 10⁻⁵M, was introduced into the flow cell. The fluorescence emission intensity increased nearly three-fold, indicating very significant additional adsorption of β -casein ("enhanced adsorption") at the interface. All solutions were introduced at a shear rate of 0.43 s⁻¹.

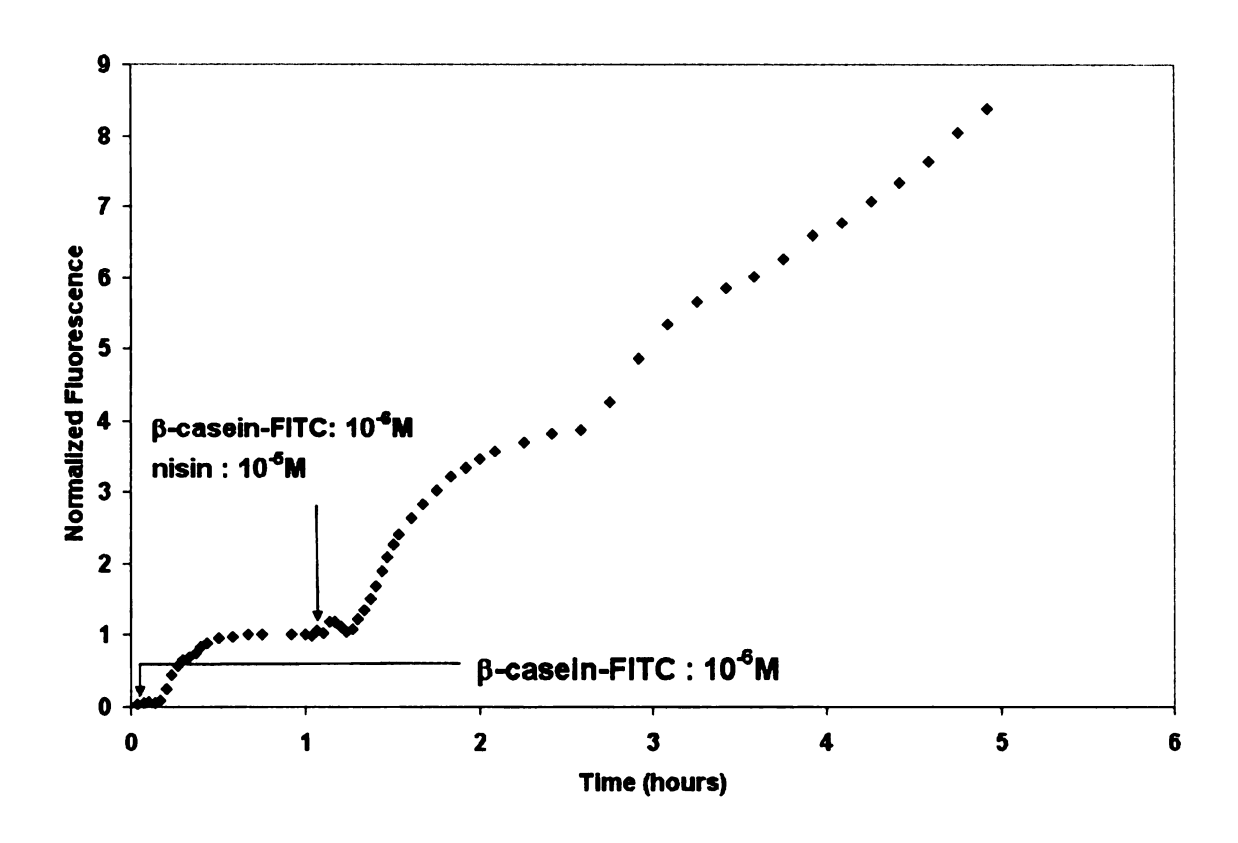


Figure 2-6. Enhanced adsorption of β-casein in the presence of nisin.

The initial profile is for the adsorption of labeled β -casein (10^{-6} M) at the oil-water interface. Upon pseudo-stabilization of the fluorescence signal, a mixture of labeled β -casein (at a concentration of 10^{-6} M) and unlabeled nisin (10^{-5} M) was introduced into the flow cell. The fluorescence emission increased several-fold, and did not attain a steady state value during the experiment. This is an indication of very significant enhanced adsorption of β -casein in the presence of nisin. All solutions were introduced at a shear rate of 0.43 s^{-1} .

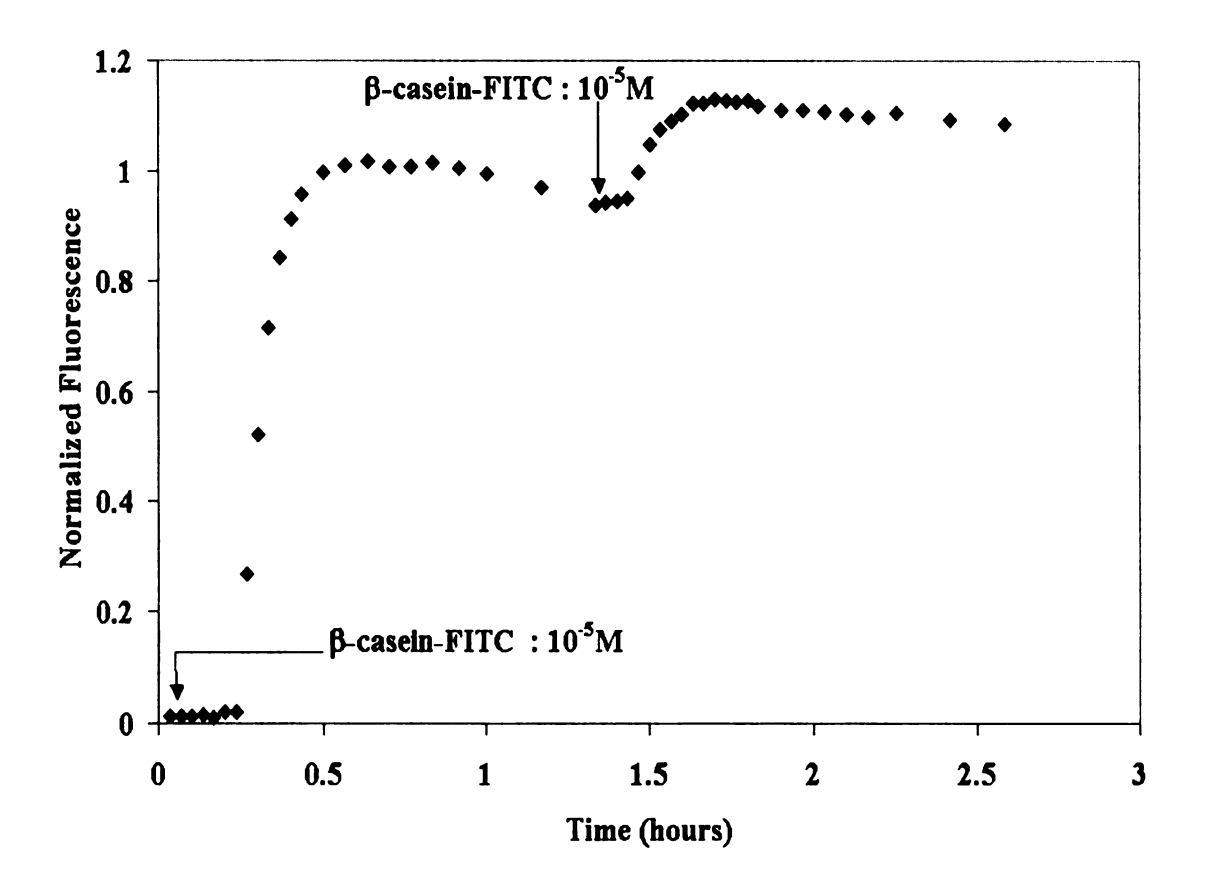


Figure 2-7. Control experiment for β -casein.

β-casein-FITC (10^{-5} M) was initially adsorbed at the oil-water interface. Following stabilization of the fluorescence signal, additional β-casein-FITC (10^{-5} M) was introduced into the flow cell. Clearly, the increased fluorescence emission is not as significant as that observed in the presence of nisin, indicating that adsorption enhancement is due solely to the interaction with the polypeptide nisin. All solutions were introduced at a shear rate of 0.43 s⁻¹.

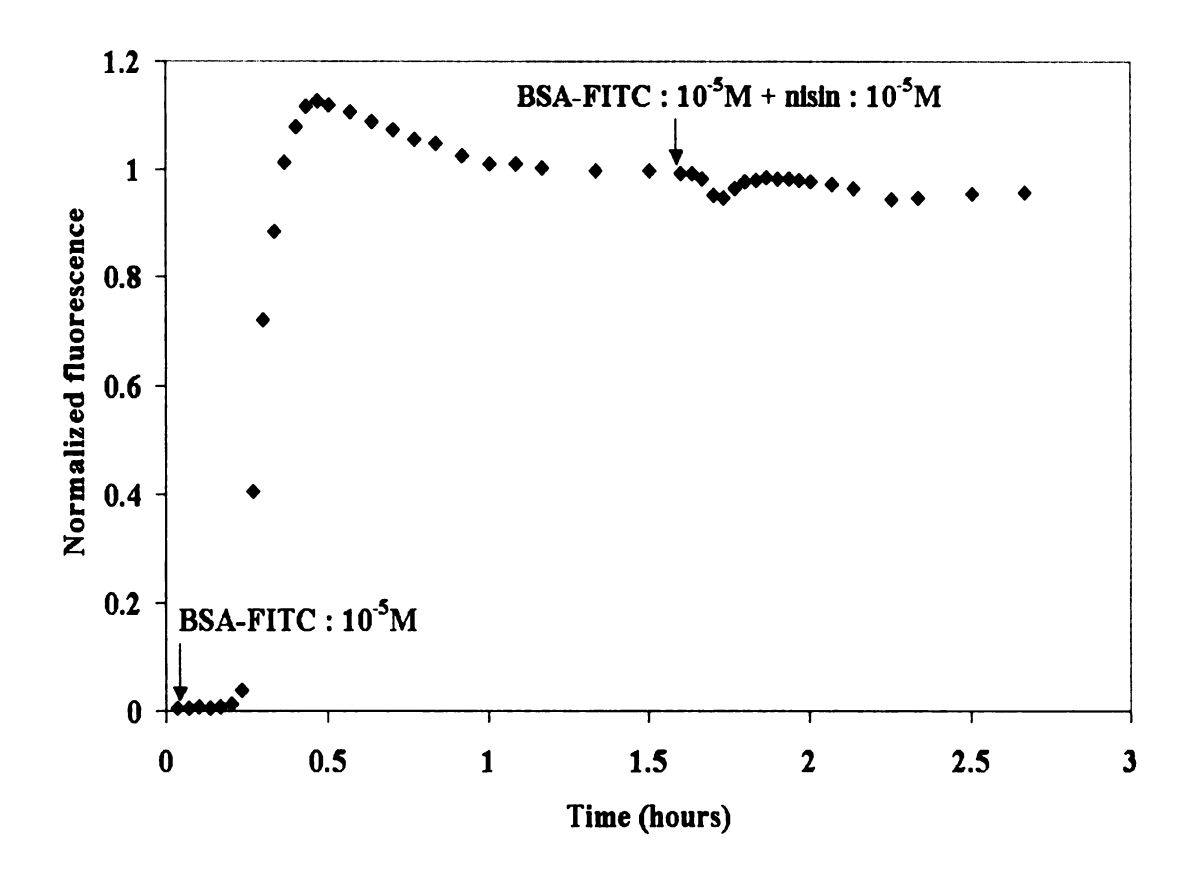


Figure 2-8. Interaction of BSA and nisin.

The initial profile shows the pseudo-equilibrium adsorption of BSA-FITC (10⁻⁵M) at the oil-water interface. A mixture of BSA-FITC and unlabeled nisin, each at 10⁻⁵M, was introduced into the flow cell upon stabilization of the fluorescence level. No change in the fluorescence emission was observed, indicating negligible adsorption enhancement for BSA at this bulk concentration. We should note the initial overshoot in the adsorption profile prior to adding the binary protein mixture. This type of behavior has been attributed to orientational changes within the adsorbed layer (for example, from an end-on to side-on configuration) by which a kinetically favored orientation is replaced by a more stable orientation that requires more surface area per protein molecule (Wertz and Santore 2002). All solutions were introduced at a shear rate of 0.43 s⁻¹.

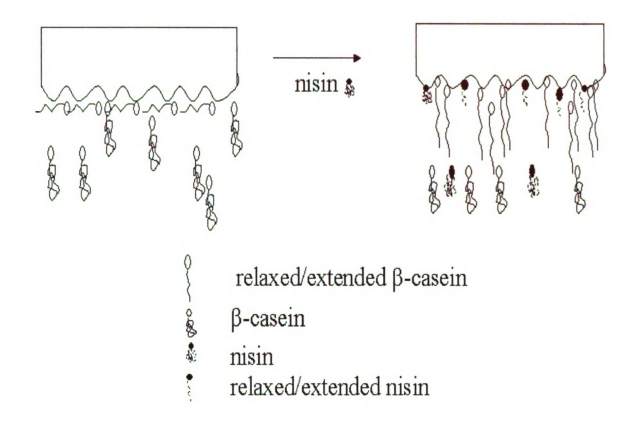


Figure 2-9. Proposed scheme of the interaction between β-casein and nisin.

The figure on the left shows a film of β -casein formed at the interface after pseudo-equilibrium adsorption. We hypothesize that, when the β -casein is adsorbed at the interface, the protein initially spreads out to occupy more surface area per molecule. We propose that, upon introduction of nisin, the polypeptide interacts with the adsorbed β -casein molecules to cause reorientation of the protein molecules. This reorientation results in more efficient packing, and creates more room for additional proteins to adsorb.

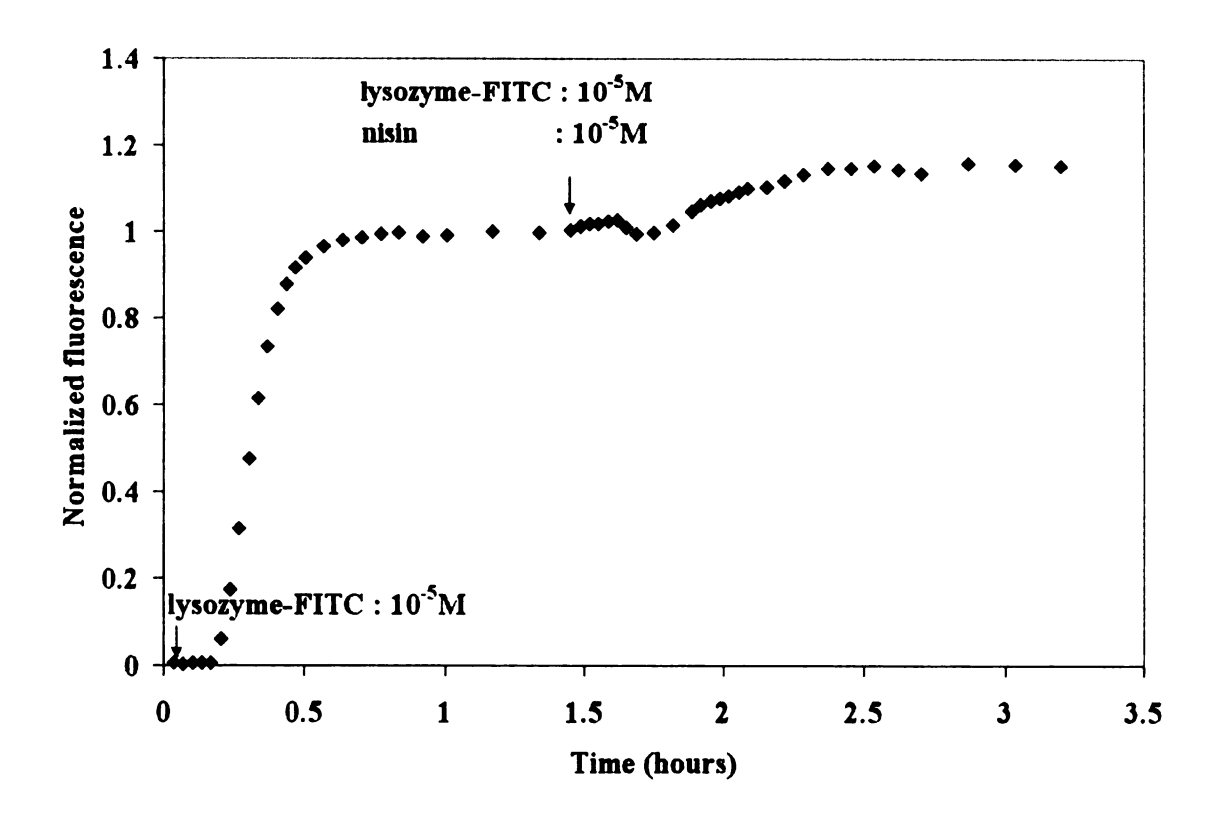


Figure 2-10. Interaction of lysozyme and nisin.

Lysozyme-FITC (10⁻⁵M) was initially adsorbed at the oil-water interface till apparent equilibrium. Then a mixture of labeled lysozyme and unlabeled nisin, each at 10⁻⁵M, was introduced into the flow cell. Following this, a small increase in fluorescence emission intensity was observed, indicating some degree of adsorption enhancement. All solutions were introduced at a shear rate of 0.43 s⁻¹.

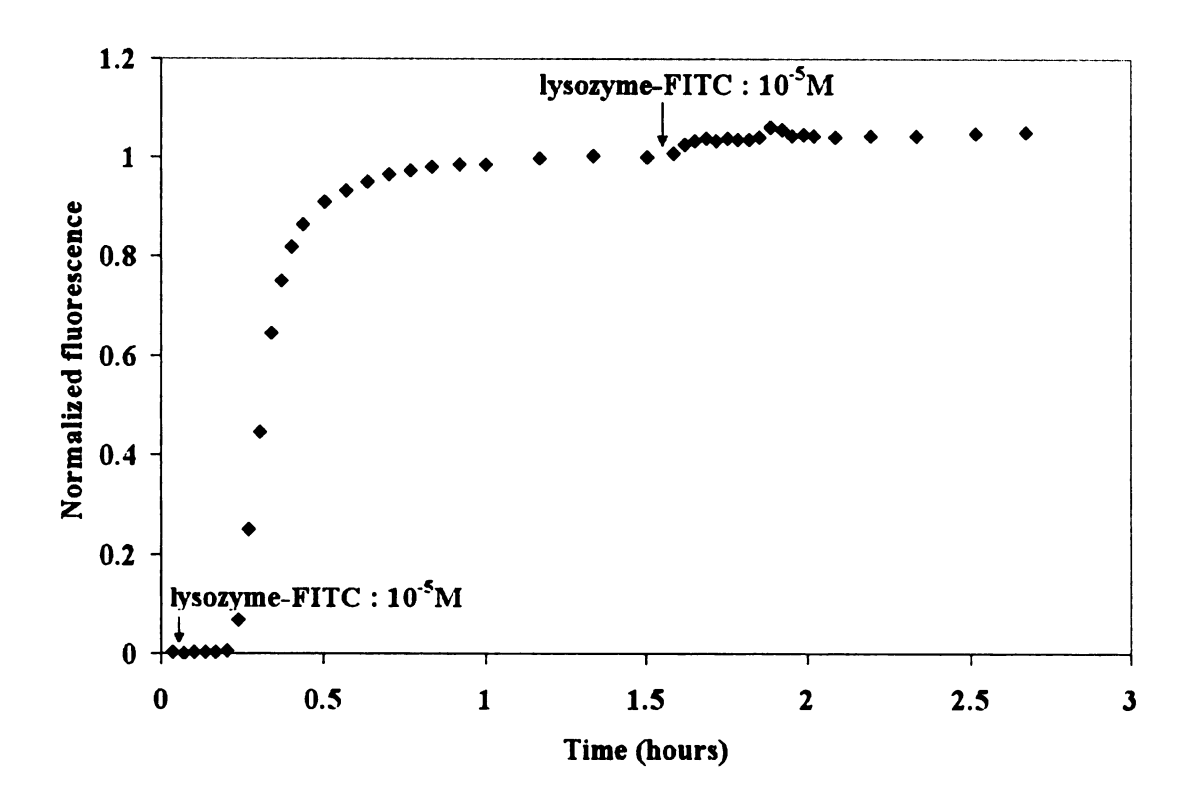


Figure 2-11. Control Experiment for Lysozyme.

The initial adsorption of lysozyme-FITC (10⁻⁵M) to apparent equilibrium was followed by re-introduction of the same solution (at the same concentration) into the flow cell. This resulted in a very small increase in fluorescence emission intensity. All solutions were introduced at a shear rate of 0.43 s⁻¹.

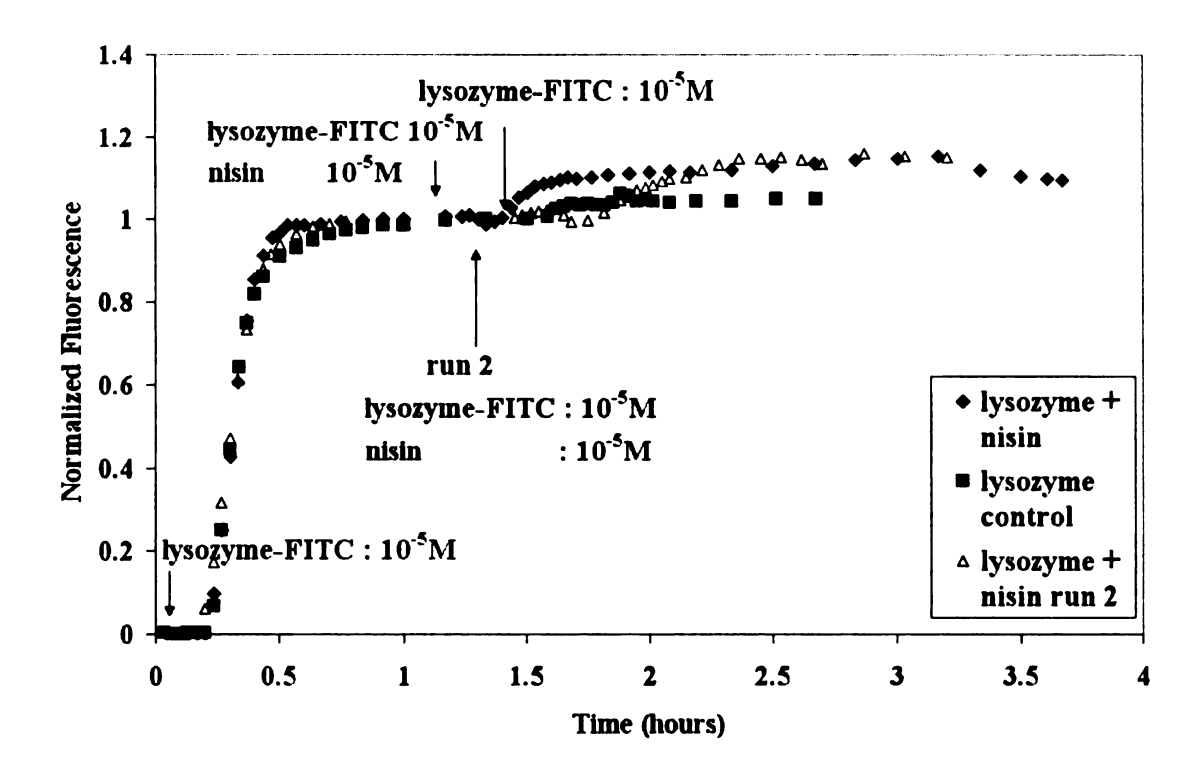


Figure 2-12. Lysozyme adsorption.

This figure shows three lysozyme adsorption profiles from separate experiments. The data show a larger increase in fluorescence emission in the two experiments where nisin is present, compared to the one experiment of lysozyme adsorbing alone. The fluorescence data have been normalized by the initial pseudo-stabilization level in each experiment. All solutions were introduced at a shear rate of 0.43 s⁻¹.

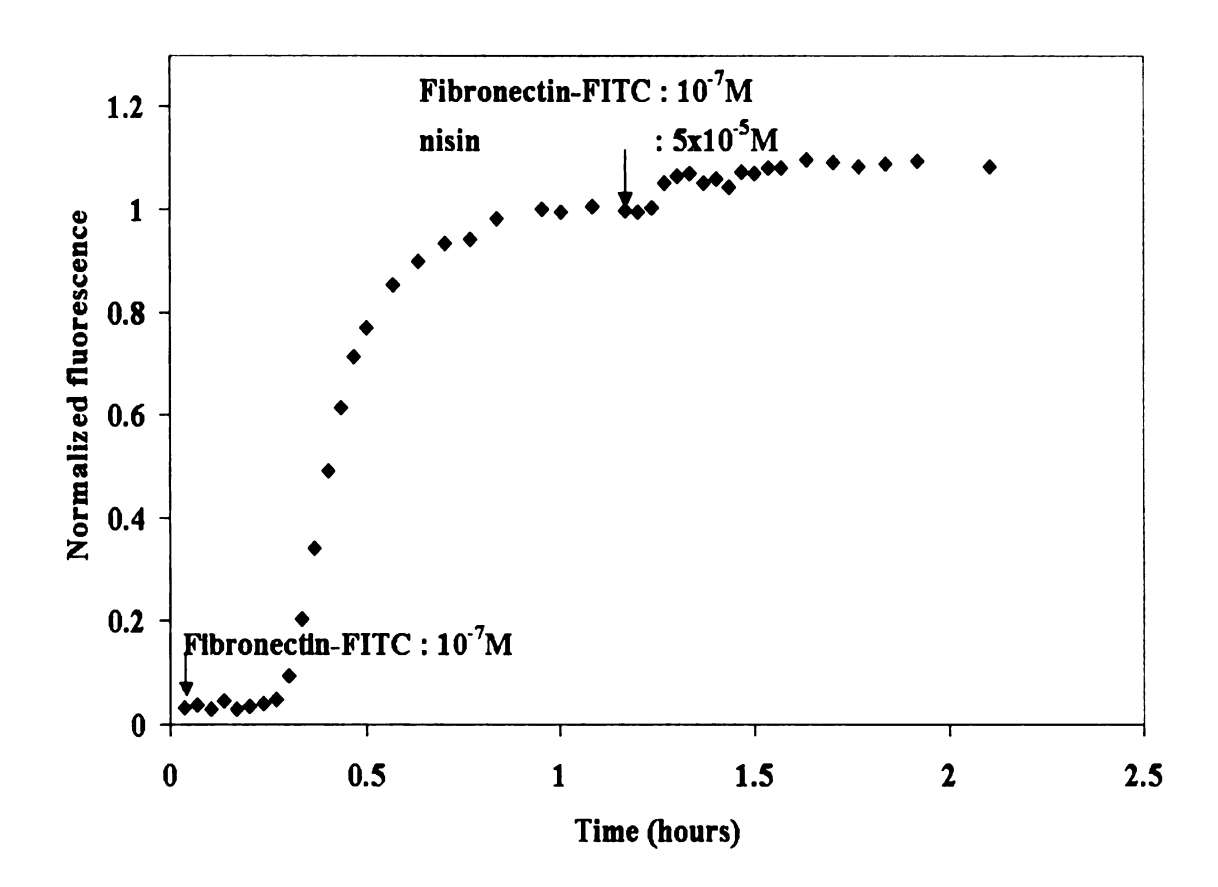


Figure 2-13. Interaction of fibronectin and nisin.

Pseudo-equilibrium adsorption of fibronectin-FITC (10⁻⁷M) is achieved in about an hour at the oil-water interface. Upon introduction of a mixture of fibronectin-FITC (10⁻⁷M) and nisin (10⁻⁵M), a slight increase in fluorescence emission was observed. All solutions were introduced at a shear rate of 0.43 s⁻¹.

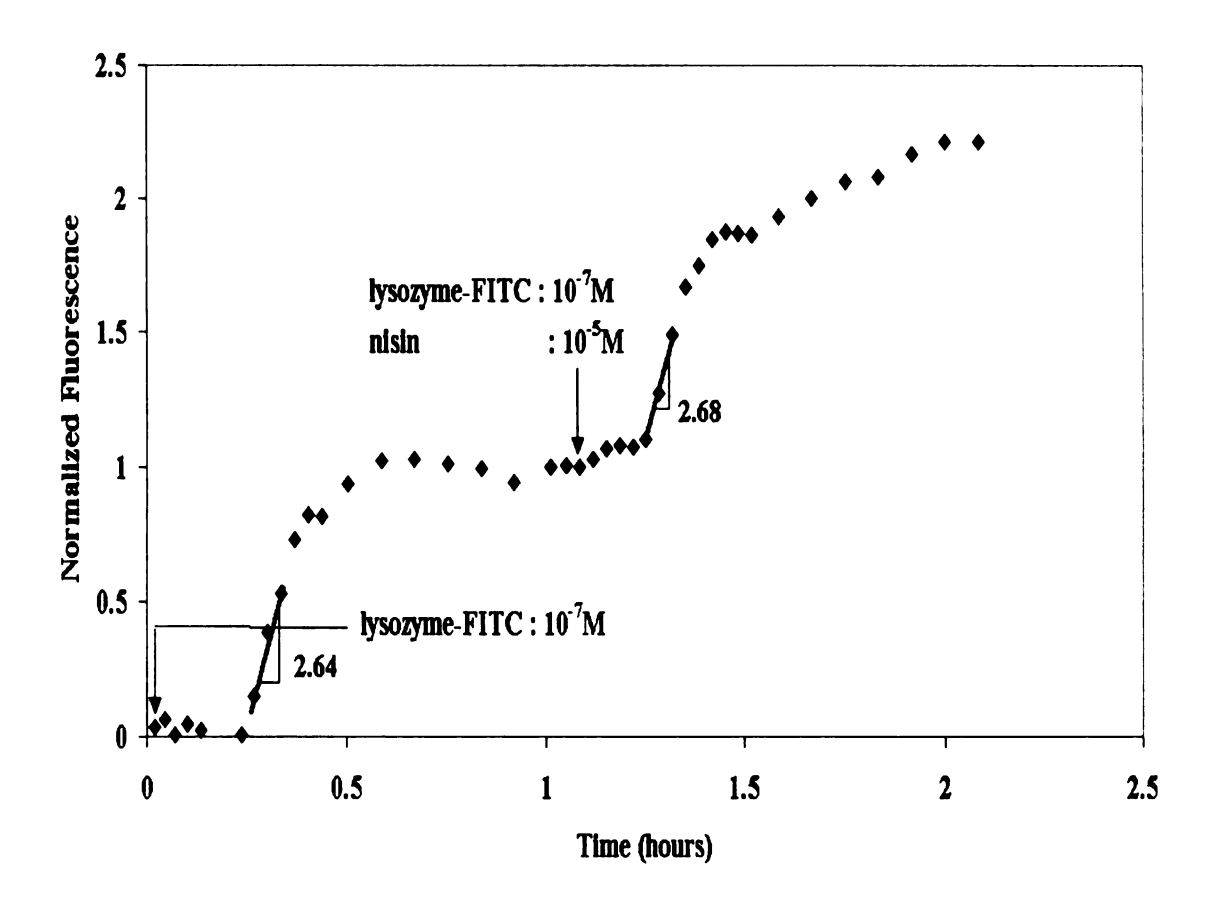


Figure 2-14. Interaction of lysozyme (at a lower concentration) and nisin.

This experiment is similar to the lysozyme adsorption experiment presented earlier, except at a lower bulk concentration. After introduction of the mixture of lysozyme-FITC ($10^{-7}M$) and nisin ($10^{-5}M$), greater than a two-fold increase in fluorescence emission intensity was observed. This trend is very similar to what was observed at higher molar concentrations for β -casein adsorbing in the presence of nisin. All solutions were introduced at a shear rate of $0.43 \, \text{s}^{-1}$.

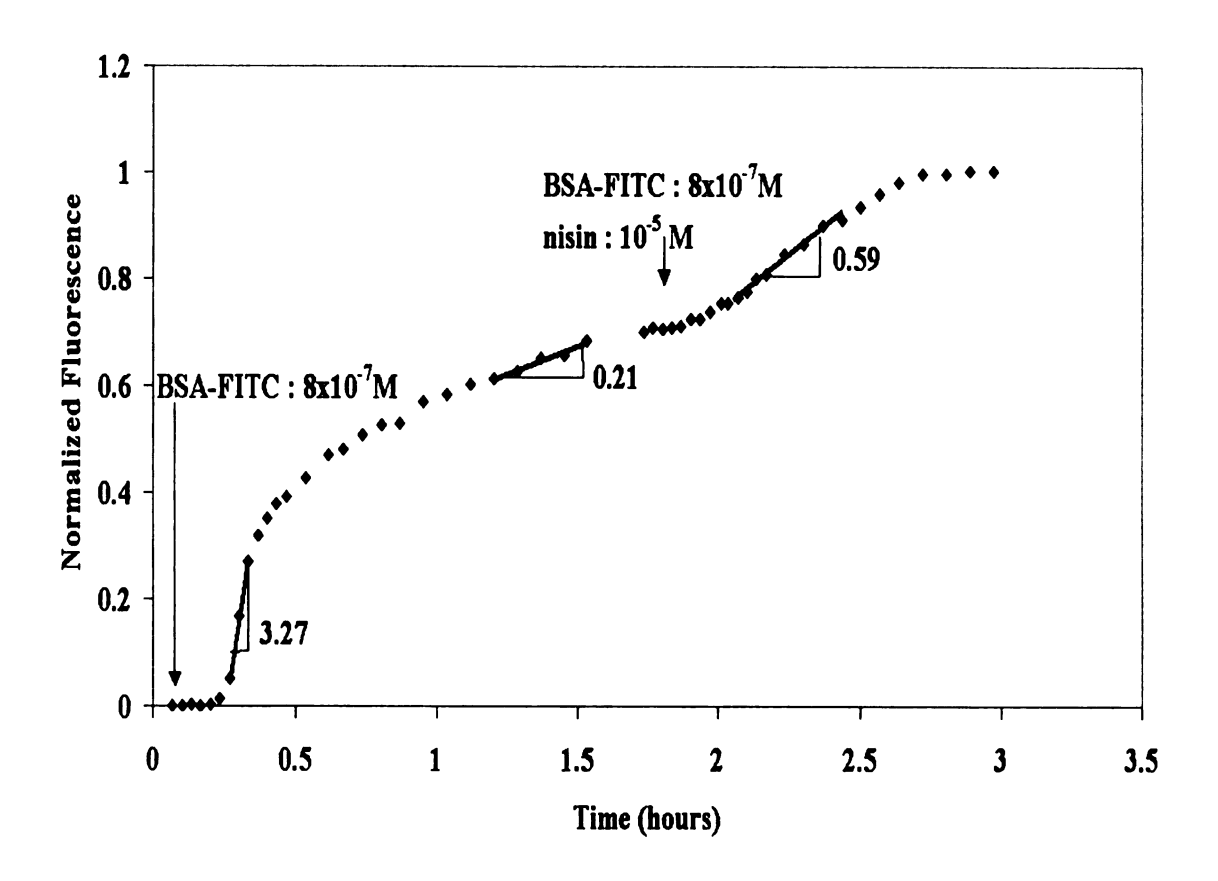


Figure 2-15. Interaction of BSA (at a lower concentration) with nisin.

A solution of BSA-FITC (8x10⁻⁷M) was allowed to adsorb to the oil-water interface. Since the fluorescence emission level did not stabilize even after 90 min, we introduced the mixture of BSA-FITC (8x10⁻⁷M) and nisin (10⁻⁵M), and observed the adsorption slopes (indicative of the rates of adsorption) before and after introduction of the mixture. The slope of the profile (0.59) after introduction of the binary mixture of nisin and BSA-FITC was significantly larger than the prior slope (0.21) for BSA-FITC adsorbing by itself. All solutions were introduced at a shear rate of 0.43 s⁻¹.

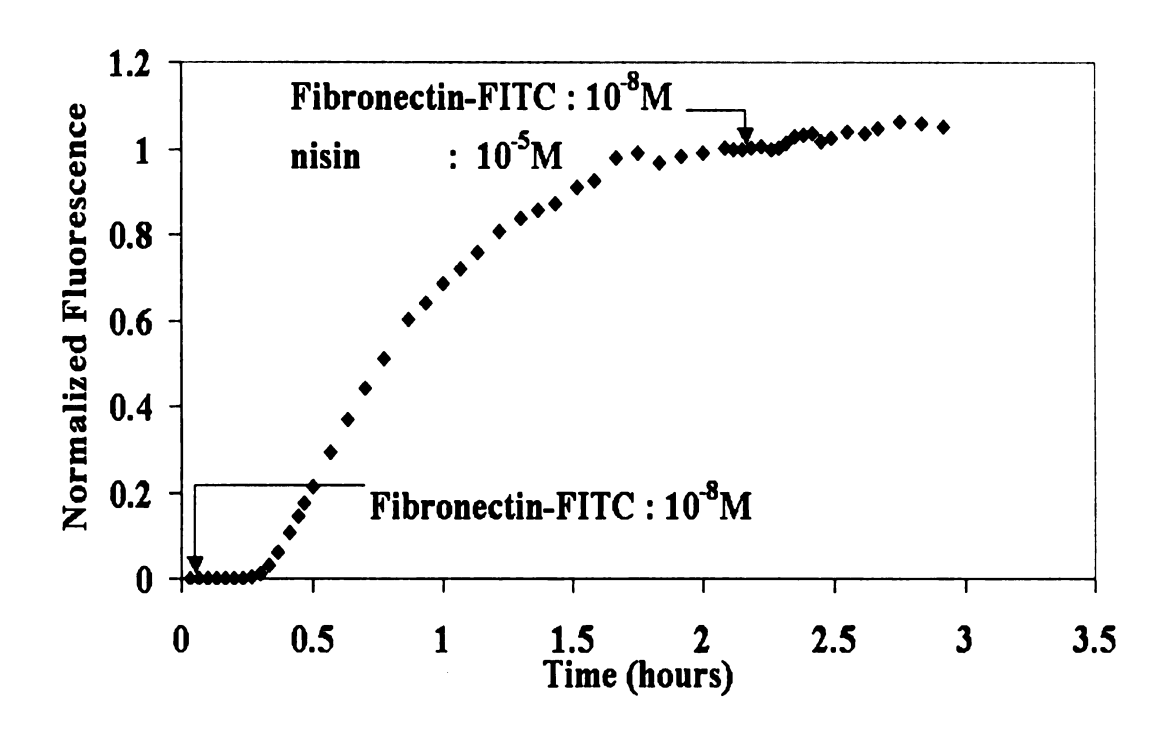


Figure 2-16. Interaction between Fibronectin (at a lower concentration) and nisin.

Following pseudo-equilibrium adsorption of fibronectin-FITC (at a lower concentration of 10⁻⁸M), a mixture of fibronectin-FITC (10⁻⁸M) and nisin (10⁻⁵M) was introduced. While this apparently resulted in increased fluorescence emission intensity, the increase was not significant. All solutions were introduced at a shear rate of 0.43 s⁻¹.

3 DEVELOPMENT OF A PROTOCOL FOR SIMULTANEOUS OPTICAL AND ELECTROCHEMICAL CHARACTERIZATION OF BIOMACROMOLECULES IN TIR GEOMETRY

3.1 ABSTRACT

We describe the development of a flow cell to enable simultaneous optical and electrochemical characterization of biomimetic interfaces. The goal was to expand the capabilities of the TIRFM apparatus so we can critically interrogate biomimetic systems that exhibit both optical and electrochemical responses to specific or non-specific interactions. Modifications were made to our existing optical flow cell to incorporate the ability to conduct cyclic voltammetry (CV) measurements using a three-electrode set-up. The top and bottom slides in our optical flow cell were replaced with indium tin oxide (ITO)-coated glass slides. The transparency of ITO allows us to conduct optical experiments, while its conductivity makes it possible to conduct electrochemical measurements on the same sample.

The feasibility of the simultaneous-optical electrochemical set-up was tested using the dye resorufin. On potential scans towards increasing negative voltages (400mV to -400mV), the fluorescent resorufin was reversibly reduced to non-fluorescent dihydroresorufin, coincident with a decrease in fluorescence emission. Similarly, upon scanning towards increasing positive voltages (-400mV to 400mV), the dihydroresorufin was reversibly oxidized to resorufin, resulting in increased fluorescence emission. The same relationship between fluorescence emission and potential was observed in all

subsequent cycles, confirming that the optical-electrochemical set-up serves its intended function. This experimental tool can also be used to characterize independent optical and electrochemical interactions taking place in a given sample at the biomimetic interface.

3.2 INTRODUCTION

Our lab has focused on using total internal reflection fluorescence microscopy (TIRFM) as the primary tool to optically characterize bio-macromolecular interactions at liquid-liquid and solid-liquid interfaces. The objective of this study was to expand the capabilities of this technique to enable characterization of more complex systems such as biomimetic interfaces that can be used as biosensors. A biosensor is a device that converts specific recognition events between a receptor and a target analyte into a measurable signal. It serves as a reliable miniaturized device with the ability to perform sophisticated detection of analytes in areas such as biology, nanotechnology, environmental quality, and food technology, and in rapid diagnostic assays. To design such systems, it is necessary to accurately characterize the associated biomacromolecular interactions at the biomimetic interfaces.

In the first part of this thesis, we concentrated on understanding fundamental protein interactions between nisin and selected proteins at the oil-water interface. In this section, we will outline the development of an experimental set-up that enables simultaneous use of two important characterization techniques: TIRFM and cyclic voltammetry (CV). Electrochemical/amperometric biosensors provide continuous and accurate measurements of the concentration of analytes in an electrical format. The need

for sensitivity, specificity, speed and accuracy of measurements has triggered interest in developing electrochemical sensors as diagnostic tools in the food and pharmaceutical industries (Prodromidis 2002).

The ability to simultaneously track biomacromolecular interactions as well as electron-transfer reactions in-situ represents a very powerful tool for analyses of complex biological systems, and would aid in the development and characterization of biosensors. TIRFM has proven to be well-suited for optical interrogation of interfacial biomolecular interactions. We believe the ability to also conduct electrochemical experiments with the same apparatus would help us identify independent events taking place in these complex systems. In cases where a single species produces both electrochemical and optical signals upon interaction, we will be able to obtain corroborative evidence of that event.

3.2.1 Optical characterization

3.2.1.1 Total Internal Reflection Fluorescence Microscopy (TIRFM)

A brief introduction to TIRFM was presented in Chapter 2, and will not be repeated here. The only additional information is that the evanescent wave for the experiments in this section was configured to a penetration depth of about 75nm. We achieved total internal reflection (TIR) at an interface between an indium tin oxide (ITO)-coated glass slide and the sample solution in the flow cell. The transparency of ITO allows us to conduct optical experiments, while its conductive surface allows for its use as an electrode for electrochemical measurements.

3.2.2 Electrochemical characterization

3.2.2.1 Cyclic voltammetry (CV)

CV is a useful and versatile technique used to study electroactive species. Its ease of use enables application in various fields of electrochemistry, inorganic chemistry, organic chemistry, and biochemistry (Kissinger and Heineman 1983). It can be used to conduct mechanistic as well as kinetic studies of redox behavior of a biological or a chemical compound over a wide potential range. There have been numerous studies of biosensors utilizing CV to monitor various enzyme-catalyzed redox reactions. Common enzymes used for biosensors include alcohol dehydrogenase (Mullor et al. 1996; Rao et al. 1999), lactate dehydrogenase (Chaubey et al. 2000), glucose oxidase (Motta and Guadalupe 1994; Willner et al. 1997; Wang et al. 1998), cytochrome c oxidase (Li et al. 1996) and horseradish peroxidase (Ferri et al. 1998; Munteanu et al. 2003). CV has also been used to study DNA-mediated electron transfer (Napier et al. 1997; Palecek et al. 1998; Kelley et al. 1999; Armistead and Thorp 2000).

A CV measurement involves cycling the potential of an electrode in solution, and measuring the resulting current (Kissinger and Heineman 1983; Bard and Faulkner; Kissinger and Heineman 1984). The electrode is the surface/interface where the biological reaction takes place. In our set-up, we use a three-electrode configuration comprising a working electrode, a counter (or auxiliary) electrode and a reference electrode. This configuration is more advantageous than the traditional two-electrode set-up. The traditional configuration does not allow for precise control of the external

applied potential (which is required in cyclic voltammetry measurements), because of potential (ohmic) drop due to solution resistance. Better control of the external applied potential is achieved by controlling the potential of the working electrode with respect to the reference electrode. Polarization of the counter electrode, which completes the current-measuring circuit, is required for cyclic voltammetry. This is not available in the two-electrode set-up (Bard and Faulkner 2000; Bioanalytical Systems 2005; Carnes and Wilkins 2005). The function of each electrode in the three-electrode system is briefly described below (Bard and Faulkner 2000).

The working electrode (WE) is the test electrode where the reaction that generates the oxidation or reduction takes place. This is the only electrode where the reaction occurs. Many different working electrodes can be used, such as glassy carbon, boron-doped diamond, gold, and indium tin oxide. These working electrodes can be further tailored or modified, based on the requirements of the desired application. For example, to study reactions catalyzed by enzymes embedded in a bilayer lipid membrane (BLM), the enzyme incorporated into either a supported or tethered BLM can be deposited on the working electrode, and the solution in contact with the modified electrode can contain the analyte of interest.

The counter electrode acts as a source or sink for electrons, so that the current can be passed through the external circuit of the cell. An ideal counter/auxiliary electrode is one which does not produce any substances by electrolysis, because these products can reach the working electrode and interfere with its function.

The reference electrode is one whose potential stays constant, so that it can be used as a standard against all measured potentials in the three-electrode cell (Faulkner 1983; Kissinger and Heineman 1983; Mabbott 1983; Van Benschoten et al. 1983; Bard and Faulkner 2000; Kissinger and Heineman 1984). The reference electrode must, therefore, have the property of ideal nonpolarizability. Some common reference electrodes are the saturated calomel electrode (SCE) and the silver/silver chloride electrode (Ag/AgCl).

In a CV experiment, the potential is maintained between the working and reference electrode, while the current is measured between the working and the counter electrode. The potential applied between the working and the reference electrode is considered the excitation signal. The potential in our experiments is a linear scan that exhibits a triangular waveform. The potential is swept between two values (called the switching potentials). Following the sweep in one direction, the scan direction is reversed and the potential is scanned back to the original starting value. The parameters of interest are the initial and final potentials, the scan direction, the scan rate, and the number of scans, all of which can be set by the operator. Usually, a window is chosen to include the potential at which the analyte of interest is oxidized and reduced. The current generated at the working electrode as a result of cycling the potential is recorded, and a cyclic voltammogram is generated. The CV obtained is thus a plot of current versus potential.

The current produced depends on two steps in the overall process: the movement

of electroactive material to the surface and the electron transfer reaction. The exponential dependence of the electron transfer rate constant on the potential is given by

$$k_f = k^0 \exp\left(\frac{-\alpha nF}{RT} \left(E - E^{0'}\right)\right) \tag{3.1}$$

where k^o is the standard homogenous electron-transfer rate constant, n is the number of electrons transferred, R is the universal gas constant, T is the absolute temperature in Kelvin, and α is the transfer coefficient.

A typical cyclic voltammogram is shown in Figure 3-1. The dependence of the current on the electrochemical reaction during a CV experiment will be explained in detail in section 3.3.3 for the ferricyanide system. Some of the important parameters of interest in a cyclic voltammogram are the anodic peak current (i_{pa}), the cathodic peak current (i_{pc}), the anodic peak potential (E_{pa}), and the cathodic peak potential (E_{pc}) (Figure 3-1). The peak current obtained in a reversible electrochemical process is directly proportional to the concentration of the analyte and is given by the Randles-Sevich equation below:

$$i_p = 2.69 \times 10^5 \, AC \sqrt{n^3 Dv} \tag{3.2}$$

where i_p is the peak current (in amperes), n is the electron stoichiometry, A is the electrode area (cm²), D is the diffusion coefficient (cm²/sec), C is the concentration (mol/cm³) and v is the scan rate (V/sec).

For a reversible system, the applied external potential controls the ratio of the oxidized to the reduced species at the electrode surface, according to the Nernst equation:

$$E = E^{0'} + 2.303 \left(\frac{RT}{nF}\right) \log \frac{[O]}{[R]}$$
(3.3)

where E is the external applied potential, F is the Faraday constant, and [O] and [R] are the concentrations of the oxidized and reduced species, respectively. The Nernst equation is valid only at equilibrium.

An electrochemically reversible couple is one in which both the species (oxidized and reduced) rapidly exchange electrons with the working electrode. The formal reduction potential (E°) for a reversible couple is given by

$$E^{O'} = \frac{E_{pa} + E_{pc}}{2} \tag{3.4}$$

where E_{pa} is the peak potential at the anode and E_{pc} is the peak potential at the cathode.

The number of electrons (n) cycled in the electrode reaction can be calculated from the separation of the cathodic and the anodic peak potential, and is given by

$$\Delta E_p = E_{pa} - E_{pc} \cong \frac{0.059}{n} \tag{3.5}$$

Thus, an ideal reversible one-electron transfer process should have a peak separation of 59mV.

Slow reaction kinetics leads to slow electron transfer. This is an indication of an irreversible reaction, and results in increased peak separation (between the cathodic and the anodic peaks). If the peak separation is such that the anodic and the cathodic peaks do not overlap on the potential axis, then the system is classified as irreversible. Usually, reactions will be irreversible if chemical bonds break or if there is a loss of substituents in solution (Mabbott 1983).

The concentration of the reactant in the bulk solution can be determined once we know the peak current. However, CV is not ideally suited for that task; techniques such as differential pulse voltammetry are better equipped for these types of measurements. CV is best used to analyze homogeneous chemical reactions that are coupled to the electron transfer process (Mabbott 1983), because it gives qualitative information about electron transfer processes. One can quickly determine the formal potential, the number of electrons transferred in the process, and the anodic and the cathodic peak potentials using CV.

3.3 EXPERIMENTAL SET-UP

3.3.1 TIRFM flow cell

The flow cell used for our TIRFM studies was developed by a previous graduate student. A detailed description can be found in the literature (Gajraj and Ofoli 2000a). Briefly, the flow cell was formed from two glass microscope slides separated by a 900µm aluminum spacer. An oval channel (2.34 inch x 0.73 inch) cut into the aluminum spacer

formed the flow channel. Teflon tubes (TTF-130-10M, Valco Instruments Co, Inc., Houston, TX) inserted into two holes drilled in the bottom slide allowed for the simultaneous infusion and withdrawal of solution into and out of the flow cell (Figure 3-2), using a Harvard apparatus infusion/withdrawal syringe pump (Model 551382, Harvard Apparatus, South Natick, MA).

3.3.2 Modifications to TIRFM set-up to conduct optical and electrochemical experiments (first generation)

To conduct both optical and electrochemical studies in the TIRFM apparatus, we made several modifications to our flow cell. The top glass slide was replaced by an indium tin oxide (ITO)-coated glass microscope slide (CG-41IN-S107, Delta Technologies Ltd., Stillwater, MN). Since the aluminum spacer used to form the flow channel in the TIRFM flow cell is conductive, it was replaced with a rubber gasket of about 800µm thickness.

We also modified our flow cell to accommodate the three-electrode set-up described earlier. To incorporate the working and the counter electrodes on the ITO slide, we adopted a design similar to that described by Asanov et al. (Asanov et al. 1998). The top ITO slide was divided into three conductive bands insulated from each other by etching the ITO layer in between the bands, using a strong acid such as 12M HCl. The bands required to be conductive were masked with photoresist during the etching process. Removal of the ITO coating in the etched bands was confirmed by ensuring a very high resistance across any pair of conductive bands. The central region was used as the

working electrode (Figure 3-3b). The area of the working electrode could be controlled by the size of the central region. Either of the other two bands could be used as the auxiliary/counter electrode. Thin electrical wires attached to the ITO surface with conductive epoxy (CW2400 Part A and B, Chemtronics, Kennesaw, GA) provided electrical contact. The epoxy was allowed to cure for 15 minutes in an oven at 75°C. This was done to ensure that the wires remained firmly attached to the electrode surface, because weak contacts lead to increased resistance.

A silver/silver chloride (Ag/AgCl) reference electrode (Bioanalytical Systems Inc. (BASi), MF-2078, West Lafayette, IN) was used for these measurements. The reference electrode was placed in the beaker into which the exit solution emptied. The electrical contact between the reference electrode and the working electrode was maintained as long as there was solution in the flow cell, the exit tube, and the exit beaker in which the reference electrode was placed. Potassium ferricyanide (K₃Fe(CN)₆) was used as a test electroactive species to evaluate how the electrochemical cell functioned.

3.3.2.1 Materials and Methods: Ferricyanide Experiments

Potassium ferricyanide (K₃Fe(CN)₆) was purchased from Mallinckrodt Laboratory Chemicals (Phillipsburg, NJ). Potassium nitrate (KNO₃) was obtained from the J T Baker Chemical Company (Phillipsburg, NJ). A 10mM aqueous solution of K₃Fe(CN)₆ in 0.1 M KNO₃ was used as the working solution.

The flow cell was assembled with a rubber spacer sandwiched between the top

ITO coated slide (housing the working and the counter electrode) and a glass bottom slide. The prism was optically coupled to the top ITO-coated slide using an immersion oil of refractive index 1.51 (Type A, 16482, Cargille Laboratories, Cedar Grove, NJ). The whole assembly was tightened down with four screws. The potassium ferricyanide solution was infused into the flow cell at a flow rate of 0.36 ml/min, and a BASi CV-50W Voltammetric Analyzer (Bioanalytical Systems, BASi, West Lafayette, IN) served as the potentiostat for the experiments. The leads from the WE, AE and the RE were connected to the potentiostat. Prior to the start of each experiment, the flow cell was visually inspected to make sure there were no air bubbles or leaks. The software program obtained with the CV-50W voltammetric analyzer (CV-50W) was used. The parameters used to acquire the cyclic voltammogram for the ferricyanide system are given in Table 3-1.

3.3.3 Results and Discussion: Ferricyanide Experiments

The current versus voltage curve obtained with the 10mM potassium ferricyanide test solution in the modified flow cell is shown in Figure 3-4. This result was compared to the cyclic voltammogram obtained in a conventional set-up with all three electrodes placed together in the same beaker (Figure 3-5). The parameters used for the scans were the same in both cases. In the conventional set-up, a platinum working electrode (MF-2013, Bioanalytical Systems (BASi), West Lafayette, IN), a platinum counter electrode, and an Ag/AgCl reference electrode (catalog # MF-2078, Bioanalytical Systems Inc. (BASi), West Lafayette, IN) were used.

The CV scan started at 700 mV in the direction of decreasing voltages, at a rate of 100mV/sec. When the potential was sufficiently negative to reduce Fe(III), a cathodic current was generated due to the electrode reaction given below:

$$Fe^{III}(CN)_6^{3-} + e^- \to Fe^{II}(CN)_6^{4-}$$
 (3.6)

The cathodic current increased rapidly until the concentration of $Fe^{III}(CN)_6^{3-}$ at the electrode surface diminished substantially, causing the current to peak (point "a" in Figure 3-5). The current decayed as the solution surrounding the electrode was depleted of $Fe^{III}(CN)_6^{3-}$ due to its electrolytic conversion to $Fe^{II}(CN)_6^{4-}$. The scan direction was reversed at 0 mV, and a backward scan was initiated. The potential was still sufficiently negative to reduce $Fe^{III}(CN)_6^{3-}$, so the cathodic current continued, even though the potential was now being scanned in the direction of increasing voltages. Oxidation of the $Fe^{II}(CN)_6^{4-}$ accumulated near the electrode started when the electrode became a strong oxidant:

$$Fe^{II}(CN)_6^{4-} \to Fe^{III}(CN)_6^{3-} + e^{-}$$
 (3.7)

This resulted in production of the anodic current, which increased until the concentration of FeII(CN)₆⁴⁻ diminished, causing the current to peak (point "b" in Figure 3-5). The current then decayed as the solution surrounding the electrode was depleted of Fe^{II}(CN)₆⁴. The first cycle was completed when the potential reached 700mV. This cycle was repeated three times.

To assess the working of our modified flow cell, the two voltammograms have been combined in Figure 3-6 for ease of comparison. The following observations can be made:

- TIRFM-CV set-up (about 500μA) was approximately 50 times higher than that obtained in the conventional set-up (about 10μA). This is simply because the electrode area was much higher in the flow cell than in the conventional set-up (as discussed earlier, current is directly proportional to electrode area).
- The maximum cathodic current in the traditional set-up was obtained at 218mV while the anodic current peaked at 292mV. The difference in potential between the anodic and cathodic peaks was about 74mV. As discussed earlier, a difference of about 59mV would have indicated a completely reversible system. In comparison, the maximum cathodic current (peak) in the TIRFM apparatus was obtained at 194mV, with the anodic current peak at 309mV under constant flow conditions. Under stopped flow conditions, the maximum cathodic current was obtained at 190mV with an anodic current peak at 314mV. The difference in peak potentials was 115mV for the experiment conducted under continuous flow conditions, and 124mV for the stopped flow experiment. The greater departure from the truly reversible case may be due to a number of factors, including increased solution resistance, slow electron transfer, wires not providing good electrical contact, undetected air gaps/bubbles, leaks in the flow cell, or the

placement of the reference electrode far away from the working electrode. These factors are addressed below.

3.3.4 Problems with first generation optical – electrochemical set-up and resulting modifications (second generation experimental set-up)

A common problem in most CV experiments is ohmic potential drop (or IR drop) due to solution resistance. IR drop can cause decreased current magnitudes, increased peak separation and shift in peak potential. The majority of the IR drop generally occurs along the electrode surface, rather than normal to the electrode surface (Kissinger and Heineman 1984), because the current between the working electrode and the auxiliary electrode passes along the channel and adjacent to the electrode. As a consequence of this, the potential is not uniform between all points on the face of the electrode surface and the solution. This problem can be overcome by placing the auxiliary electrode right across the working electrode, so the charge travels perpendicularly between the two electrodes. In this case, the potential will be uniform throughout the electrode surface and the uncompensated IR drop will be small.

With this consideration in mind, we modified the design of our first generation flow cell as follows: instead of having the working and the counter electrode next to each other on one slide, we placed them right across from each other. This was achieved by using the top ITO-coated glass slide as the working electrode, and the bottom slide (also an ITO-coated glass slide) as the auxiliary electrode (Figure 3-7b). Ohmic potential drop can also be decreased by using a high concentration of supporting or fully dissociated

electrolyte, thereby increasing the conductivity of the solution and decreasing the resistance. Therefore, in all experiments a high concentration of supporting electrolyte (100mM) was used.

The first generation system was subject to an additional problem of uncompensated IR drop or solution resistance, because the reference electrode had been placed far away from the working electrode. Placing the working and reference electrodes in close proximity minimizes the voltage errors resulting from ohmic loss (Mabbott 1983). To achieve this, we modified the set-up to incorporate the reference electrode as close to the working electrode as our existing flow cell layout would permit. A "no leak" reference electrode (EE009, ESA, Cypress Systems, Lawrence, KS) was purchased and inserted into a flangeless ferrule (P342, Upchurch Scientific, Oak Harbor, WA) fitted in a T-joint (P-712, Upchurch Scientific, Oak Harbor, WA). Teflon tubes were connected to the remaining two ends of the T-joint. One end of the teflon tube was connected to the inlet syringe, while the other end was flanged to stay in the bottom slide of the flow cell. To prevent formation of air gaps/bubbles in the tube, the flow cell was filled with solution at the beginning of each experiment, prior to insertion of the reference electrode into the T-joint (Figure 3-7).

Air gaps in the tubes caused a disruption/break in electrical contact between the reference electrode and the solution in the flow cell. By conducting control experiments in the flow cell and in the conventional three-electrode set-up, we determined that when the reference electrode was not in contact with the solution in the flow cell (due to air

gaps or bubbles), it resulted in blackening of the ITO counter electrode (due to cathodic polarization). This blackening damaged the ITO coating, resulting in either a decrease or a loss of conductivity of the ITO layer. To ensure that the reference electrode always stayed in contact with the solution, the opening in the T-joint was expanded.

Initially, wires epoxyed to the electrode were used to provide electrical contacts. However, when the flow cell was assembled and tightened with the wires in place, we noticed air gaps and some leakage of solution from the flow cell. Leakage of solution and air gaps increased solution resistance and, in some instances, resulted in blackening of the ITO electrode (cathodic polarization). To minimize these problems, we replaced the wires with copper foils. We noticed that wetting of the copper foil during experiments always resulted in leaching of the copper into the solution. Aluminum foils were, therefore, used instead to provide electrical contact. All these modifications resulted in the second generation of our optical electrochemical set-up (Figure 3-7).

3.3.4.1 Problems encountered with the second generation experimental set-up

Using aluminum foils as electrical contacts worked to prevent major leaks of solution out of our flow cell. However, at the end of a failed experiment (blackening of the electrode), we noticed that the aluminum foils and the leads were slightly wet (even though no major leaks were detected during the experiment). Wetting of the leads and the foil resulted in increased contact resistance. To prevent this problem, we tried isolating the foil by encasing it in parafilm or double-sided tape, to prevent the solution from touching the foil. This did not work, because we were limited by how much

pressure we could apply to the flow cell, since tightening the flow cell too hard most often resulted in breaking the bottom slide.

We were also limited by having to work with the existing flow cell used for TIRFM experiments. Hence, we decided to epoxy the whole assembly, connecting the top slide, bottom slide, aluminum foils and the spacer into one unit. Epoxying the flow cell assembly prevented all leaks completely. The drawback is that, at the end of an experiment, the whole set-up had to be immersed in acetone to pry the slides apart and, in some cases, the slides were rendered unusable if the epoxy could not be completely removed. We recognize that epoxying slides together is not the ideal solution, so we are in the process of designing a flow cell that would be compatible for both optical and electrochemical experiments.

3.3.4.2 Proof-of-concept of optical/electrochemical set-up

To test the simultaneous TIRFM/CV set-up, we needed to use a compound that was both electrochemically active and could be optically tracked in either of the redox states (oxidized or reduced). We had originally planned to study the redox reaction catalyzed by the enzyme secondary alcohol dehydrogenase (sADH). The cofactor for this reaction is nicotinamide adenine dinucleotide (NAD). NAD undergoes the following redox reaction to convert to NADH:

$$C_2H_5OH + NAD \Leftrightarrow CH_3CHO + NADH + H^+$$
 (3.8)

The reduced form of the cofactor NADH is fluorescent upon excitation at 340nm,

with an emission maximum at 450nm. Therefore, the conversion of NAD to NADH during the enzymatic reaction can be monitored both optically and electrochemically. Upon production of NADH, we would expect to see fluorescence emission at 450nm, coincident with the presence of a cathodic peak in the cyclic voltammogram. We characterized the reversibility of adsorption of sADH onto ITO surfaces, and NAD attachment to ITO using a boronic acid linker molecule. However, we were not able to do simultaneous optical and electrochemical characterization of this system because of the need for a UV light source, which we do not have in our laboratory at this time. This study remains as planned future work to be accomplished in our laboratory.

3.3.5 Introduction to resazurin

To assess the feasibility of our set-up, we selected a chemical dye, resazurin, which undergoes a reduction reaction to produce a form (resorufin) that is fluorescent. Resazurin (commercial name Alamar Blue) is a versatile chemical dye which is widely used in resazurin reduction assays. For example, the resazurin reduction assay has wide application in cell toxicity work to test the viability of cells (O'Brien et al. 2000; Dayeh et al. 2004; Riss and Moravec 2004). Resazurin has also been used to monitor bacterial and yeast contamination of milk (Reinheimer and Demkow 1990), to test mitochondrial function (Zhang et al. 2004), to test quality of sperm by colorimetry (Wang et al. 1998; Zrimsek et al. 2004), to probe environmental redox reactions (Tratnyek et al. 2001), and to differentiate between bacterial respiratory types (Karakashev et al. 2003). It serves as an indicator in various enzyme assays (Chapman and Zhou 1999; Maeda et al. 2001) as

well as to monitor NADH turnover (Candeias et al. 1998; Batchelor and Zhou 2002). Resorufin (produced in the resazurin reduction assay) is fluorescent and can be used as a colorimetric indicator of the progress of the reaction under study.

Resazurin undergoes a two-step electrochemical reaction. The first step is an irreversible reaction in which resazurin is converted to resorufin upon reduction (Figure 3-8a). The reduced product, resorufin, is fluorescent and thus serves as a measure of monitoring the reaction optically. The substrate resazurin is purple in color, while the product resorufin is pink in color. In the second step of the reaction, resorufin is reduced reversibly to dihydroresorufin (Figure 3-8b). While the substrate in the second reaction, resorufin, is pink and fluorescent, the dihydroresorufin is colorless and non-fluorescent. The optical properties of the dyes have been tabulated in Table 3-4. The oxidation and reduction products generated can be monitored electrochemically at the oxidation and reduction potentials listed in Table 3-3.

Thus, this reaction can be monitored both optically and electrochemically. When resorufin is generated, we should expect to see an increase in fluorescence emission coincident with a cathodic peak at about -160mV. The maximum excitation wavelength of resorufin is 571nm. Since a 571nm light source was not available, we used a 532.5 nm source for excitation. The excitation efficiency at this wavelength is about 56%. While we recognize that this efficiency is less than ideal, this source still worked well as an appropriate excitation light source.

3.3.5.1 Materials and methods: Resazurin Experiments

Resazurin (R12204) and resorufin (in kit V23110) were purchased from Molecular Probes (Eugene, OR). A 0.02mM solution of resazurin and a 0.002mM solution of resorufin were made in pH 7.4, 100mM phosphate buffer (PBS) prepared according to the protocol outlined in Chapter 2 (under Materials and methods). All solutions contained 100mM ultra pure sodium chloride (NaCl, SX0420-1, EMD Chemicals Inc., Gibbstown, NJ).

The instrumentation used for the optical experiments was similar to that in Chapter 2, except for a few minor modifications. A 32x microscope objective (440851, Achroplan, Zeiss, Thornwood, NY) was used for fluorescence emission measurements. A green laser module (DPSS 60, Beam of Light Technologies, Inc., Clackamas, Oregon) at 532nm was used as the excitation source. The filter set (45 13 66, Zeiss, Thornwood, NY) used for these experiments comprised three components:

- an excitation bandwidth filter that allows light only between 510-560nm to pass through
- a beam splitter that directs light below 580nm up into the microscope objective, and
- an emission filter that allows light above 590 nm to pass through to the photomultiplier tube.

3.3.6 Experimental details: Resazurin Experiments

A flow cell identical to the epoxyed second generation flow cell described earlier was used for these experiments. A program written in Labview was used as the data acquisition software (see Figure 5-2 in Appendix). The parameters used for the runs with resazurin as the working solution are given in Table 3-2.

3.3.7 Results and Discussion: Resazurin Experiments

A 0.02mM resazurin solution in 0.1M PBS solution was introduced into the flow cell at a flow rate of 0.36 ml/min. The reference electrode was inserted into the T-joint after the solution flowed past it, and all three electrodes were connected to the voltammetric analyzer. Once the flow cell was filled with the resazurin solution, the labview data acquisition program for collection of fluorescence emission intensities (Figure 5-2 in the appendix) and the CV-50W program for the collection of electrochemical data were started simultaneously.

The cyclic voltammogram is shown in Figure 3-9. The potential was cycled three times between 400mV and -400mV, at a scan rate of 30mV/sec. During scans towards increasing negative voltages, resazurin was reduced to resorufin at about the reduction potential for this irreversible couple (-160mV) (shown as reaction "a" in Figure 3-8). Further along the same scans, the resorufin produced was reduced to dihydroresorufin at about the reduction potential for this reversible couple (-277mV) (reaction "b" in Figure 3-8). In the reverse scan towards increasing positive voltages, the dihydroresorufin was oxidized back to resorufin at about -238mV.

The fluorescence emission data are shown in Figure 3-10. The observed increase in fluorescence emission was due to the production of resorufin by either reduction of resazurin or oxidation of dihydroresorufin. A decrease in fluorescence was a result of the reduction of resorufin to dihydroresorufin.

To illustrate how the simultaneous optical-electrochemical system functions to provide corroborative data, the fluorescence versus time and potential versus time data have been combined in one plot (Figure 3-11). The potential scan was started at 400mV towards increasing negative voltages (400mV to -400mV) at a rate of 30mV/sec. During the first scan, we observed an increase in fluorescence emission at approximately -160mV. This increase is due to the reduction of resazurin to resorufin (which is fluorescent). When the potential was scanned further towards increasing negative voltages (400mV to -400mV), the fluorescence emission dropped at about -277mV as a result of the reduction of the fluorescent product resorufin to non-fluorescent dihydroresorufin. This reaction occurred only in scans following the formation of resorufin during the first scan. When the direction was reversed to scan towards more positive voltages (-400mV to 400mV), an increase in fluorescence emission was observed at about -238mV, a result of the oxidation of non-fluorescent dihydroresorufin to fluorescent resorufin. Thus, after the first scan, observed increases in fluorescence emission could be the result of either reduction of resazurin to resorufin or oxidation of dihydroresorufin to resorufin. The data appear to confirm that our TIRFM-CV set-up works properly.

To further evaluate the system, we conducted a similar experiment with resorufin. After the flow cell was filled with 0.002mM resorufin in 0.1M PBS solution, the collection of fluorescence and CV data was started. The potential was scanned ten times to obtain CV data (Figure 3-12). The reduction of resorufin to dihydroresorufin occurred at about -277mV on scanning towards increasing negative voltages. The oxidation of dihydroresorufin back to resorufin occurred at about -238mV on scanning towards increasing positive voltages. The CV peaks are not pronounced as explained earlier.

The fluorescence emission data were collected for the same time period as the CV scans and are shown in Figure 3-13. A decrease in fluorescence was observed when resorufin was reduced to dihydroresorufin, while an increase in fluorescence emission occurred during the reverse redox reaction.

To illustrate how the simultaneous optical-electrochemical system functions to provide corroborative data, the plot of potential versus time and fluorescence emission versus time have been combined in Figure 3-14. The fluorescence emission intensity goes through cycles as the applied potential is cycled. In the first scan towards increasing negative voltages (400mV to -400mV), the fluorescence emission intensity decreased at about -277mV, as fluorescent resorufin was reduced to non-fluorescent dihydroresorufin. The same trend was observed in all subsequent potential scans towards increasing negative voltages.

As the scan direction was reversed towards increasing positive potentials, the dihydroresorufin was oxidized back to resorufin at about -238mV and an increase in

fluorescence emission was observed, due to the production of fluorescent resorufin. The same trend was observed in all subsequent scans towards increasing positive voltages. Thus the CV and fluorescence data provide confirmation of the occurrence of the same event: the production of non-fluorescent dihydroresorufin during the reduction cycle, and resorufin during the oxidation cycle. These data confirm that our modified second generation TIRFM-CV set-up works as expected, and is capable of simultaneously using two different characterization techniques on a single sample.

3.4 **CONCLUSION**

We have modified our TIRFM flow cell to incorporate cyclic voltammetry (CV), an important characterization technique for monitoring electron transfer reactions. We have tested the TIRFM-CV flow cell to demonstrate its feasibility, using fluorescent resorufin which, upon reduction, is converted reversibly to non-fluorescent dihydroresorufin. The production of the reduced product (dihydroresorufin) upon scanning towards increasing negative voltages was confirmed by an accompanying decrease in fluorescence emission. Similarly, the production of fluorescent resorufin by oxidation of dihydroresorufin upon scanning towards increased positive voltages coincided with an increase in fluorescence, as expected.

This experimental set-up provides a very powerful tool for characterization of complex biomimetic interfaces for use as biosensors. Incorporating the additional characterization technique has two advantages: it can provide corroboration of the same reaction in cases where a single species generates both an optical and an electrochemical

signal, and also enable characterization of one sample undergoing different interactions at the biomimetic interface.

3.5 FUTURE WORK

With the current flow cell design, we have to dip the slides into acetone at the end of each experiment to pry apart the slides connected by epoxy. It would be beneficial to build a leak-proof flow cell that can be easily assembled before any experiment and disassembled after every experiment, with sufficient space to put in the electrical contacts. The versatility of the modified TIRFM/CV set-up can be improved by using other transparent electrodes such as boron-doped diamond and transparent gold electrodes. In addition to TIRFM, we can use other optical techniques for characterization, such as fluorescence recovery after pattern photobleaching (FRAPP). We can also use the same flow cell with other electrochemical techniques such as time-based voltammetry and chronoamperometry.

Table 3-1. Input parameters used to obtain cyclic voltammetry measurements for the ferricyanide experiments.

High (mV)	700	
Low (mV)	0	
Initial (mV)	700	
Scan rate (mV/sec)	100	
# of scans	6	

Table 3-2. Input parameters used to obtain cyclic voltammetry measurements for the resazurin and resorufin experiments.

High (mV)	400
Low (mV)	-400
Initial (mV)	400
Scan rate (mV/sec)	30
# of scans	6 (resazurin experiments) 10 (resorufin experiments)

Table 3-3. Electrochemical properties of the dyes resazurin and resorufin (Maeda et al. 2000; Maeda et al. 2001).

Dye	Electrochemical properties		
	Oxidation potential (mV)	Reduction potential	
		(mV)	
Resazurin		-203mV*	
		(-160mV vs. Ag/AgCl)	
Resorufin/dihydroresorufin	-281mV*	-320mV*	
	(-238 mV vs. Ag/AgCl)	(-277mV vs. Ag/AgCl)	

^{*} Glassy carbon working electrode, saturated calomel reference electrode and a platinum working electrode.

Table 3-4. Optical properties of the dyes resazurin and resorufin (Maeda et al. 2000; Maeda et al. 2001).

Dye	Color	Optical Properties	
Resazurin	Purple	Not fluorescent	
Resorufin (in pH	Pink	Excitation	Emission
7.4 buffer)		maximum 563nm	Maximum 587m
Dihydroresorufin	Colorless	Not fluorescent	

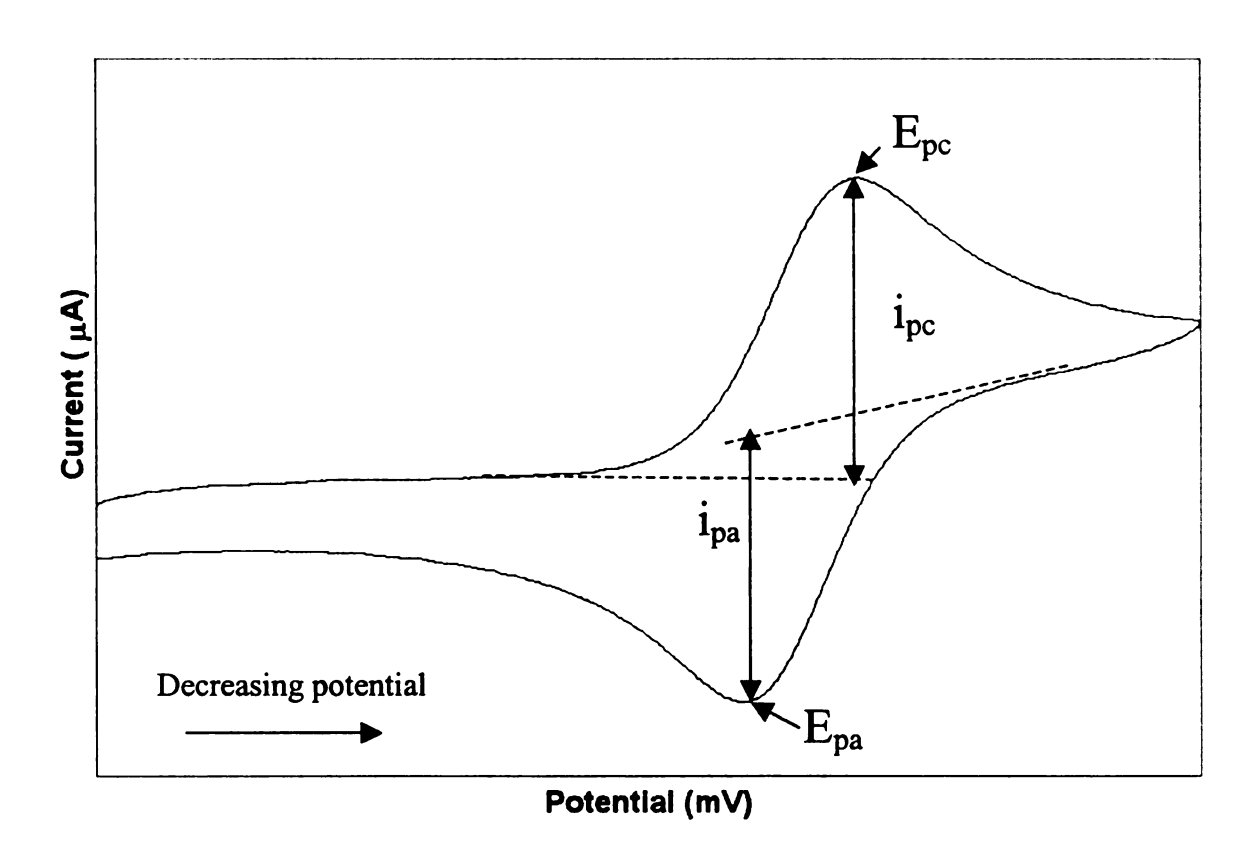


Figure 3-1. A typical cyclic voltammogram.

A cyclic voltammogram is a plot of current versus potential. The applied potential is the excitation signal and the current produced is the response signal. The parameters of interest in a voltammogram are the anodic peak current (i_{pa}) , the cathodic peak current (i_{pc}) , the anodic peak potential (E_{pa}) and the cathodic peak potential (E_{pc}) .

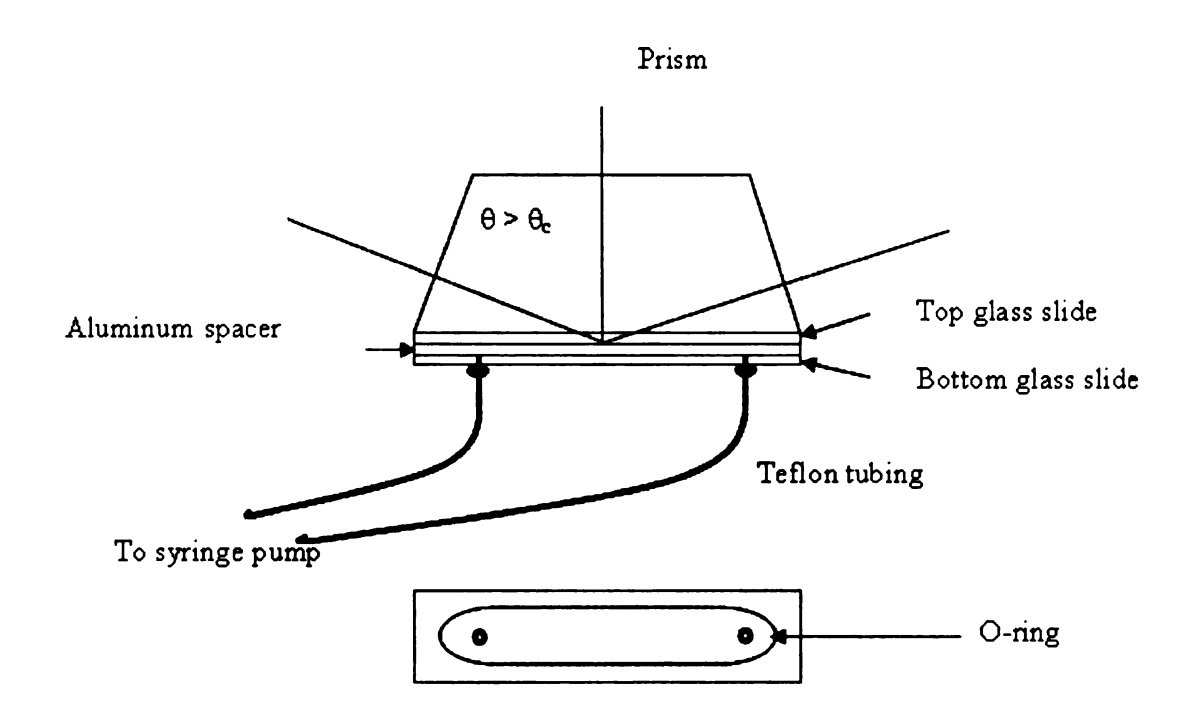


Figure 3-2. Diagram of flow cell used for TIRFM characterization experiments. It is made up of two glass microscope slides separated by a 900µm thick aluminum

spacer. An oval channel cut into the aluminum spacer and lined with a rubber o-ring forms the flow channel. Teflon tubes inserted into holes drilled into the bottom slide were used to infuse and withdraw solutions into and out of the flow cell.

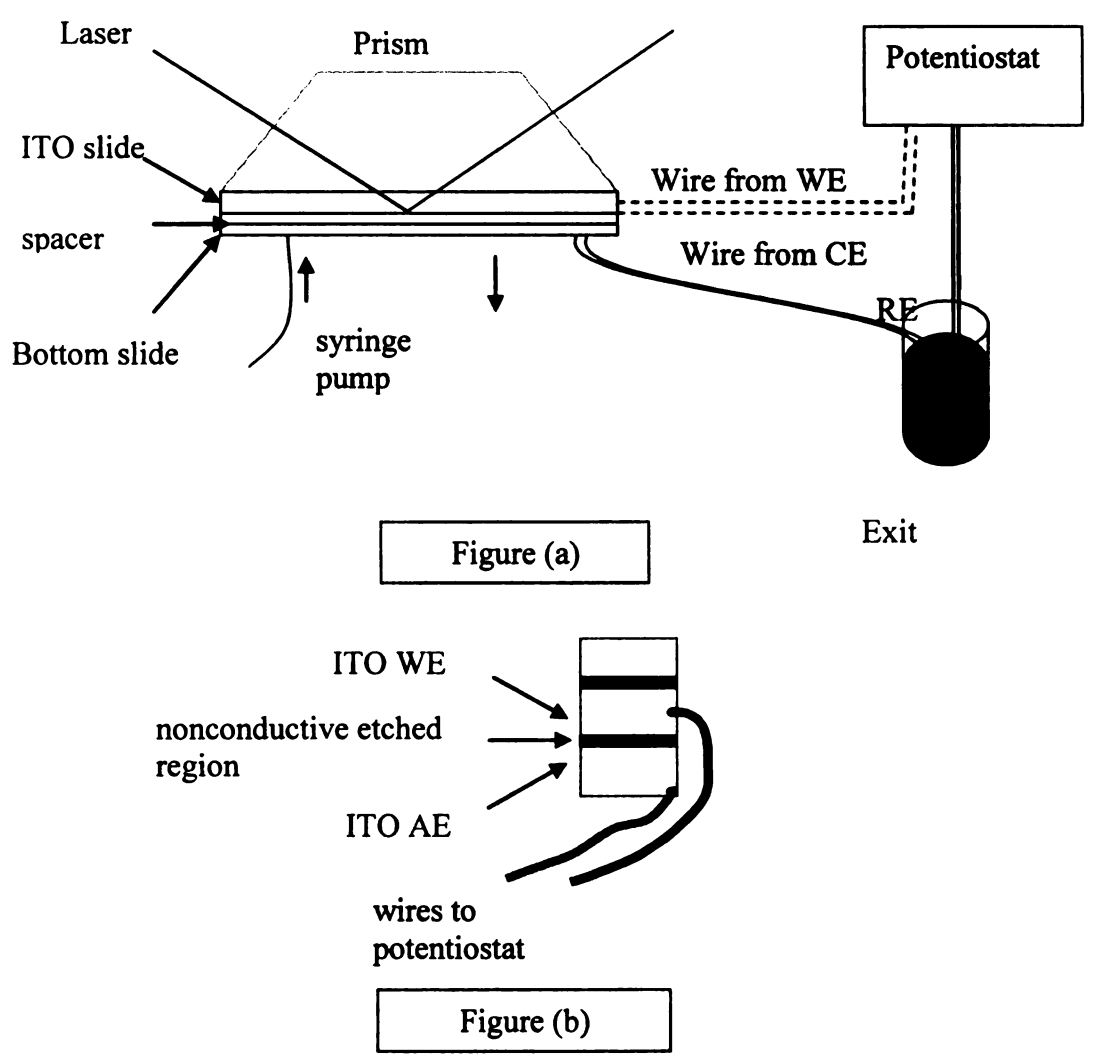


Figure 3-3. Diagram of flow cell for optical and electrochemical experiments (first generation design).

The top slide in figure (b) is an ITO-coated glass slide. The ITO electrode was etched into three conductive bands insulated from each other. One of the bands served as the working electrode (WE), while either of the other two bands served as the auxiliary/counter electrode (AE). Wires epoxyed to the conductive areas established electrical contact. The bottom slide was a glass microscope slide. An oval cut into a rubber spacer served as the flow channel. The reference electrode (RE) was placed in the exit beaker.

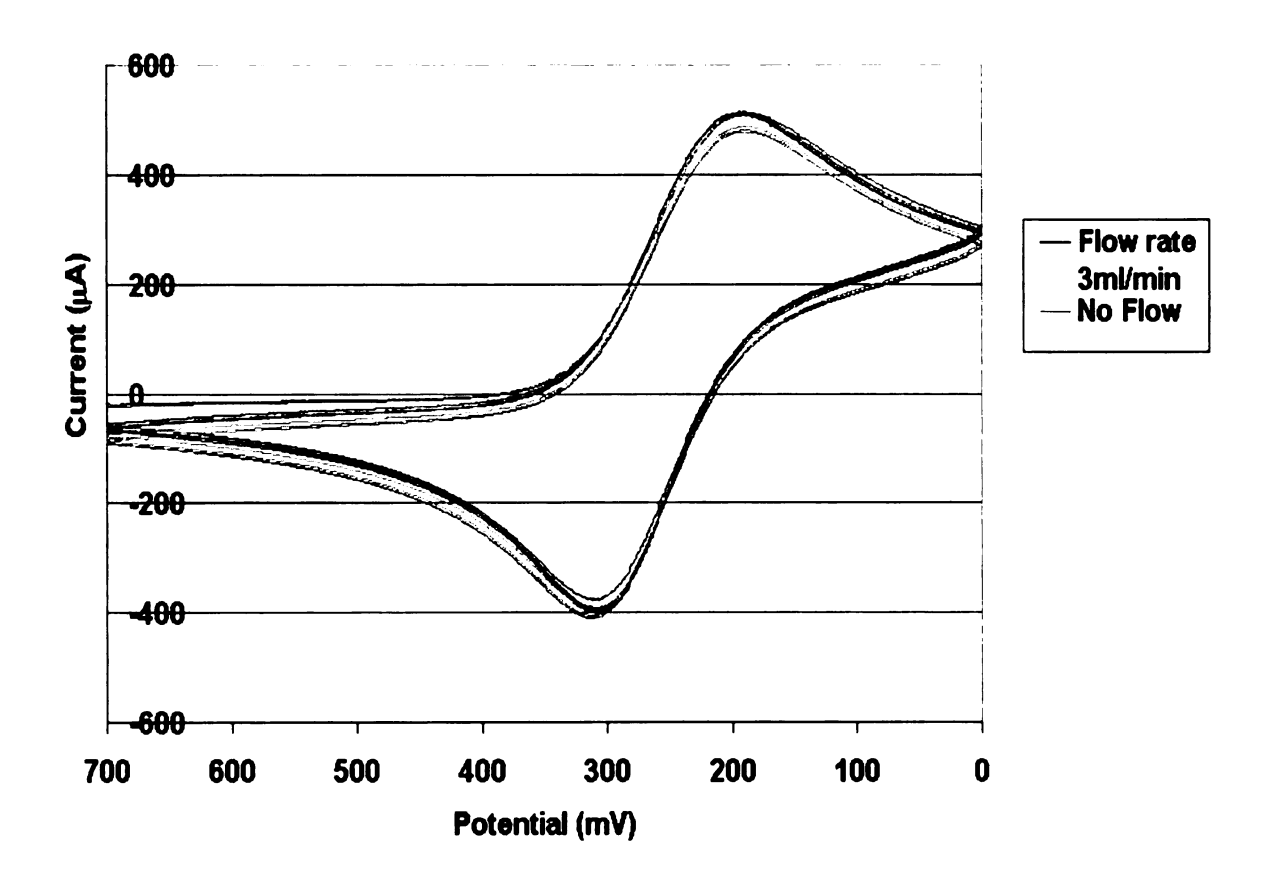


Figure 3-4. Cyclic Voltammogram obtained in the first generation TIRFM-CV flow cell.

The working solution was 10mM potassium ferricyanide in 0.1M potassium nitrate. The solution was introduced into the flow cell at a rate of 3 ml/min. The scan rate for CV was 100 mV/sec. The curve in pink was obtained under stopped flow conditions.

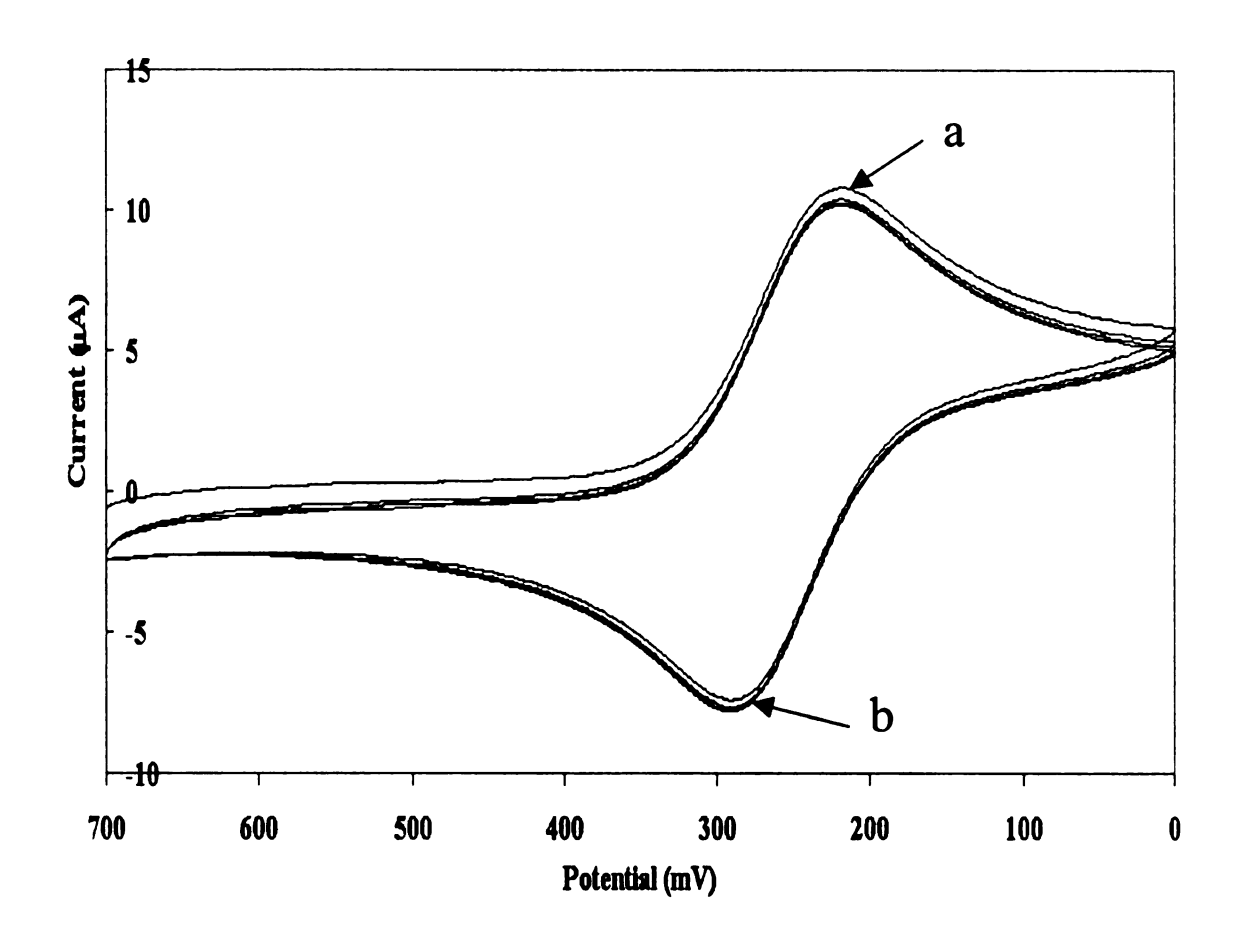
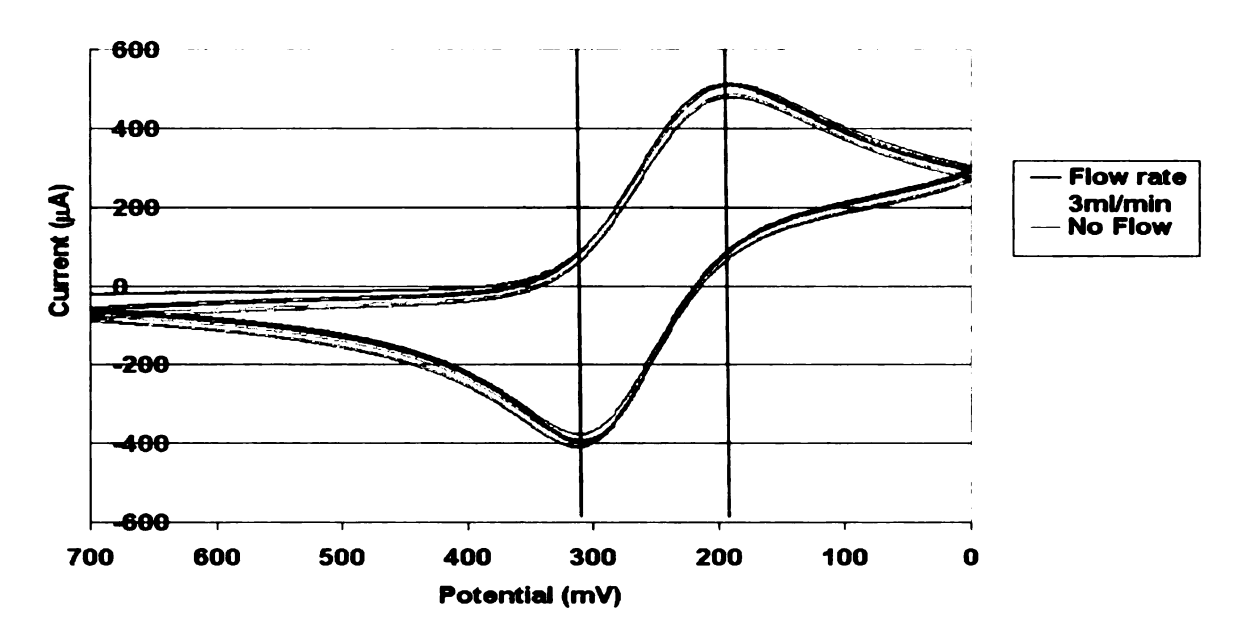
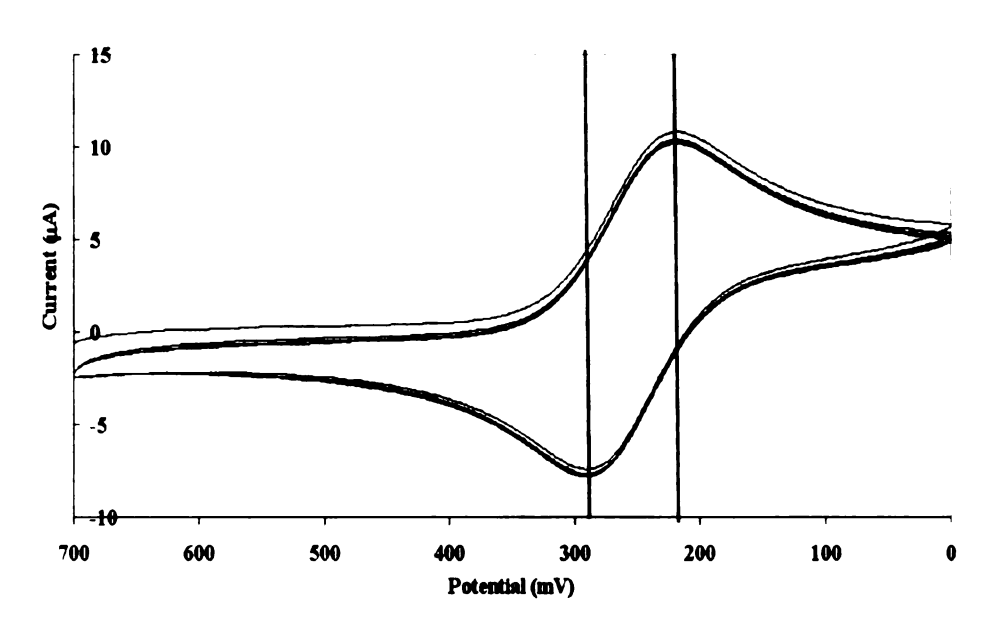


Figure 3-5. Cyclic voltammogram obtained in a conventional three-electrode set-up for comparison.

Potassium ferricyanide (10mM) in 0.1M potassium nitrate was the working solution for these experiments. A platinum working electrode, a platinum counter electrode and an Ag/AgCl reference electrode were used. All three electrodes were placed in the same solution in close proximity to each other.

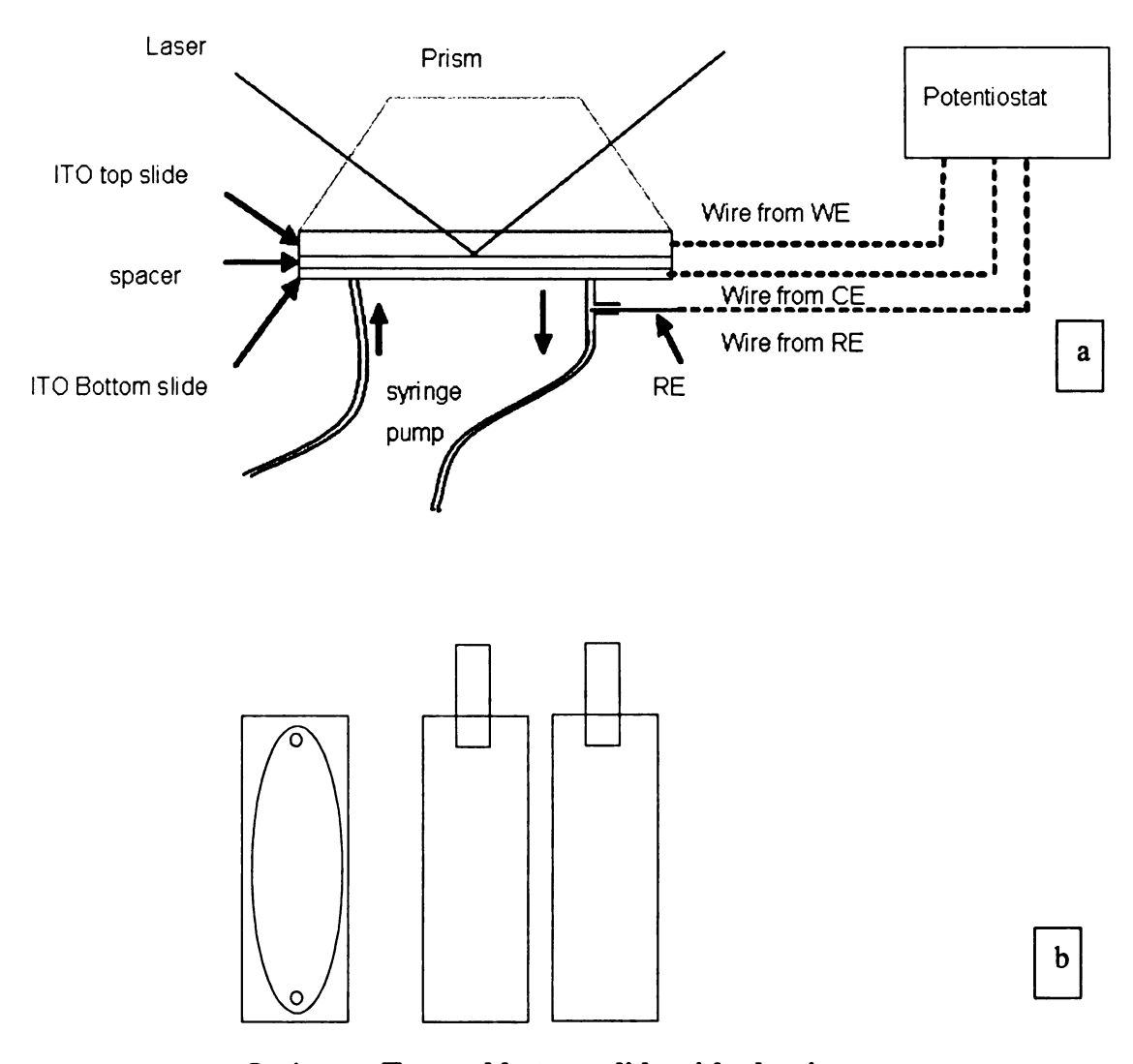


a) CV obtained in TIRFM-CV flow cell



b) CV obtained in the traditional set-up

Figure 3-6. Comparison of cyclic voltammograms obtained in our modified first generation TIRFM-CV set-up, and in a conventional three-electrode set-up. Detailed descriptions of these figures have been provided in Figure 3-4 and Figure 3-5.



O-ring Top and bottom slide with aluminum foil for provided electrical contact

Figure 3-7. Diagram of second generation optical – electrochemical flow cell. The first generation flow cell was modified to change the positions of the working electrode (WE) and the auxiliary electrode (AE). The top and the bottom ITO-coated glass slides were used as the WE and the AE respectively. Aluminum foils attached to the ITO provided electrical contact. The RE was placed closer to the flow cell by inserting it in a T-joint in the inlet tube.

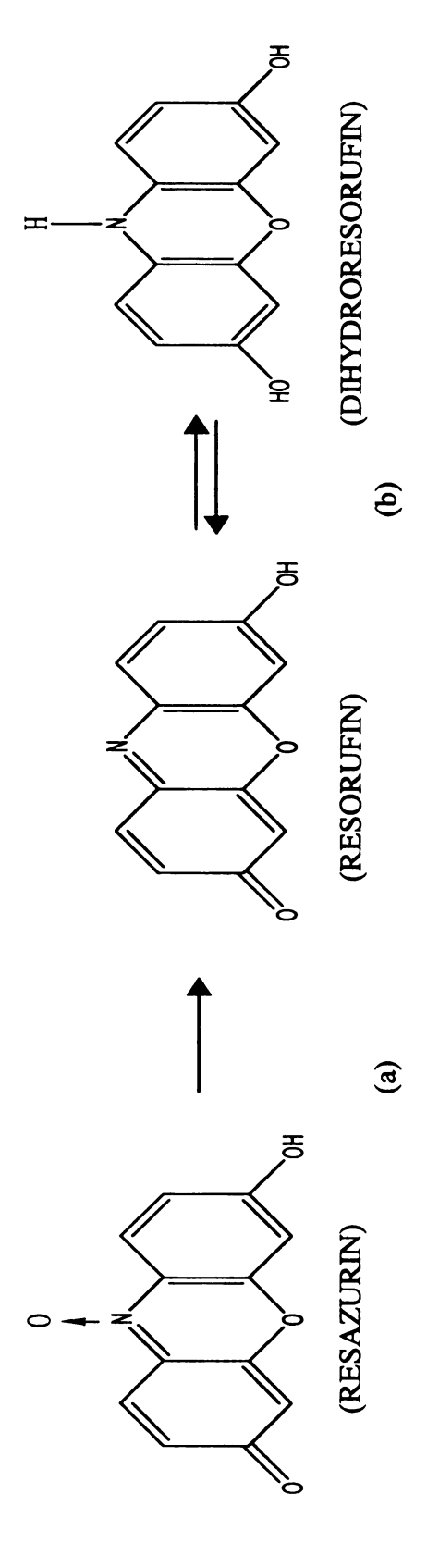


Figure 3-8. Reaction "a" is an irreversible reaction that converts resazurin to fluorescent resorufin; reaction "b" is a reversible reaction that converts resorufin to non-fluorescent dihydroresorufin.

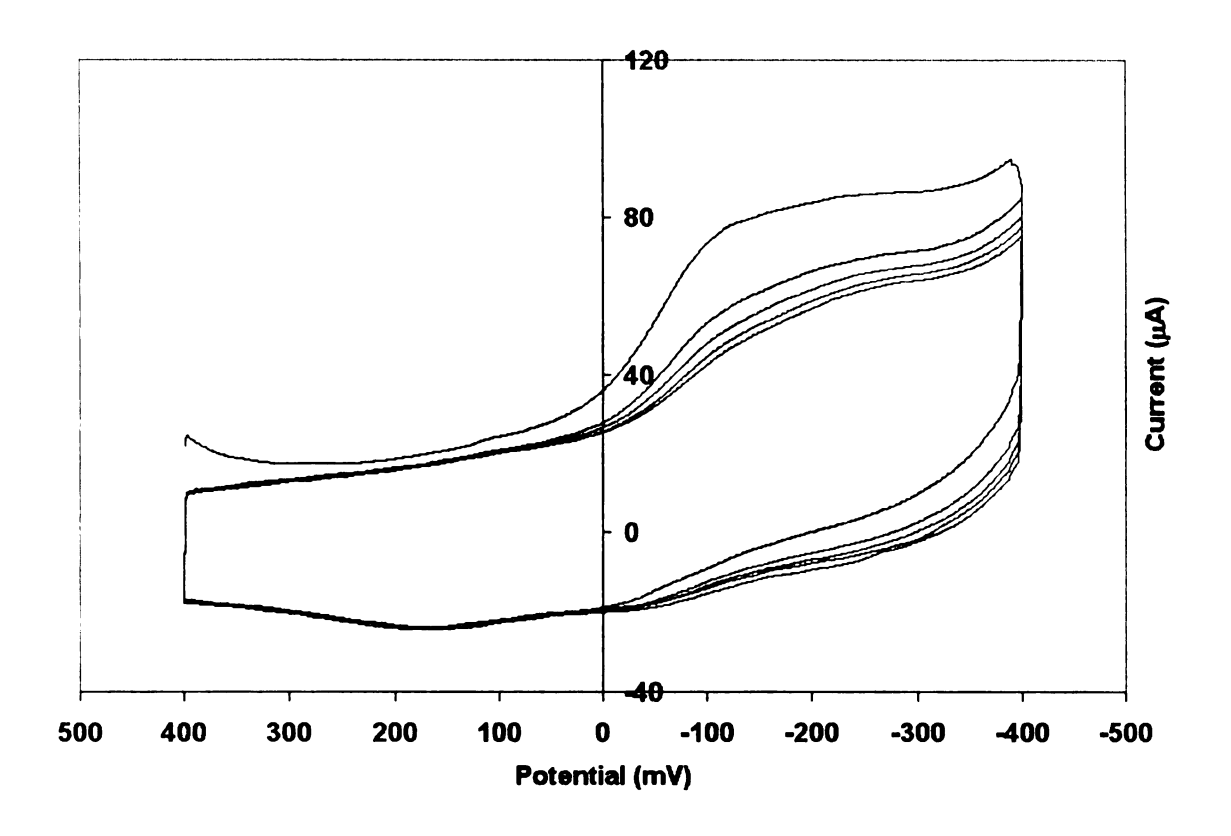


Figure 3-9. Cyclic Voltammogram of 0.02mM resazurin in PBS buffer.

The TIRFM-CV flow cell was filled with 0.02mM resazurin solution in 0.1M PBS buffer. The curve above shows the cyclic voltammogram obtained at a scan rate of 30mV/sec over three cycles. The oxidation and reduction potentials of resazurin and resorufin are listed in Table 3-3. During scans towards increasing negative voltages, resazurin was reduced to resorufin at about the reduction potential for this irreversible couple (-160mV) (shown as reaction "a" in Figure 3-8). Further along the same scans, the resorufin produced was reduced to dihydroresorufin at about the reduction potential for this reversible couple (-277mV) (reaction "b" in Figure 3-8). In the reverse scan towards increasing positive voltages, the dihydroresorufin was oxidized back to resorufin at about -238mV.

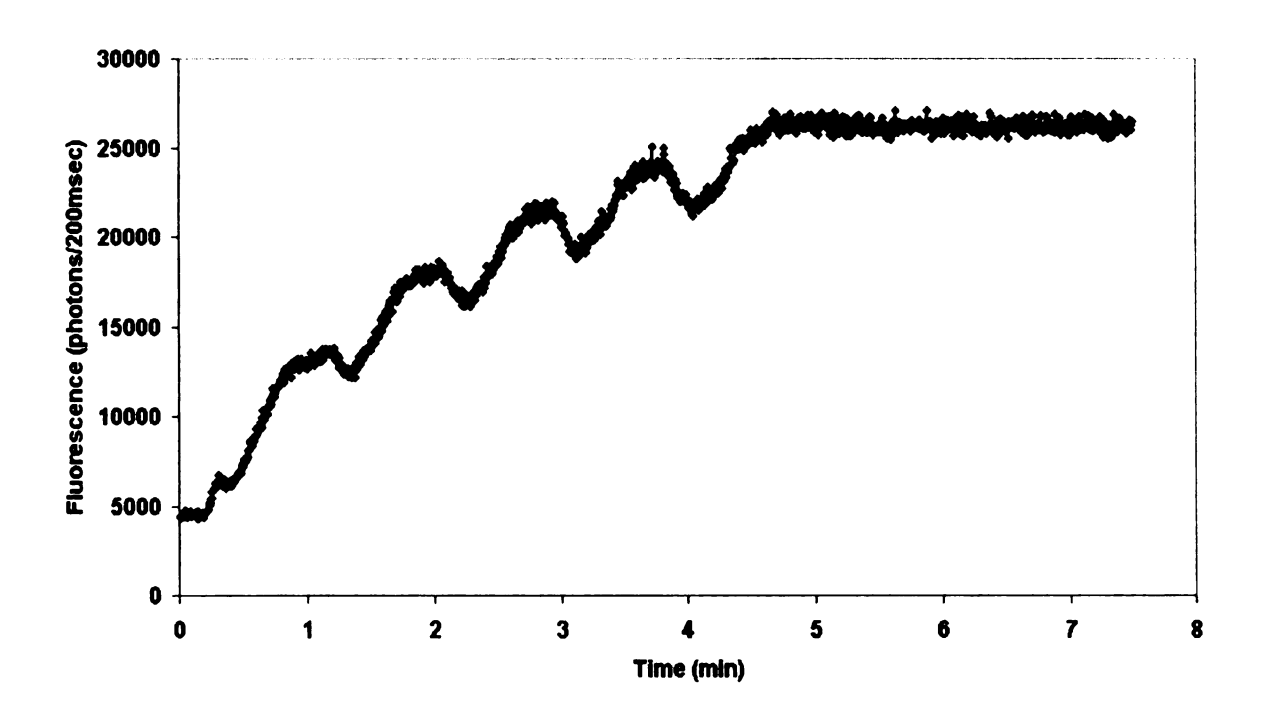


Figure 3-10. Fluorescence data obtained in the TIRFM-CV flow cell containing 0.02mM resazurin.

The working solution was 0.02mM resazurin in 0.1M PBS buffer. An increase in fluorescence emission was due to the production of resorufin, either by reduction of resazurin or by oxidation of dihydroresorufin. A decrease in fluorescence was a result of the reduction of resorufin to dihydroresorufin. The potential was cycled three times. The optical properties of the dyes are listed in Table 3-4.

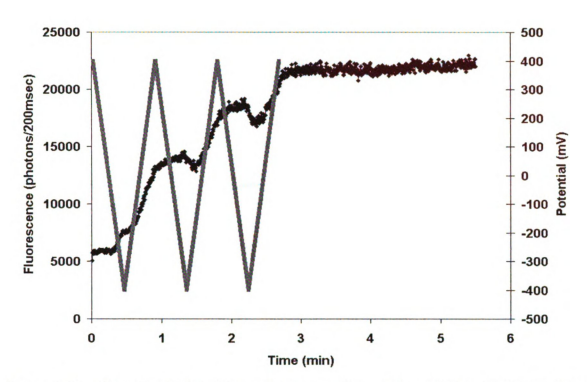


Figure 3-11. Combined plot of fluorescence vs. time and applied potential vs. time for 0.02mM resazurin.

The working solution was 0.02mM resazurin in 0.1M PBS buffer. After the flow cell was filled, fluorescence and CV data collection was started simultaneously. When the potential was scanned towards negative potentials, resazurin was reduced to resortfin at about -160mV, with an increase in fluorescence. Resorufin was further reduced to dihydroresorufin at about -277mV with a decrease in fluorescence. In the reverse scan, when the potential was scanned towards more positive potentials, the dihydroresorufin was oxidized to resorufin at about -238mV, with an increase in fluorescence. The potential was cycled three times. The electrochemical properties of the dyes are summarized in Table 3-3, while the optical properties are listed in Table 3-1.

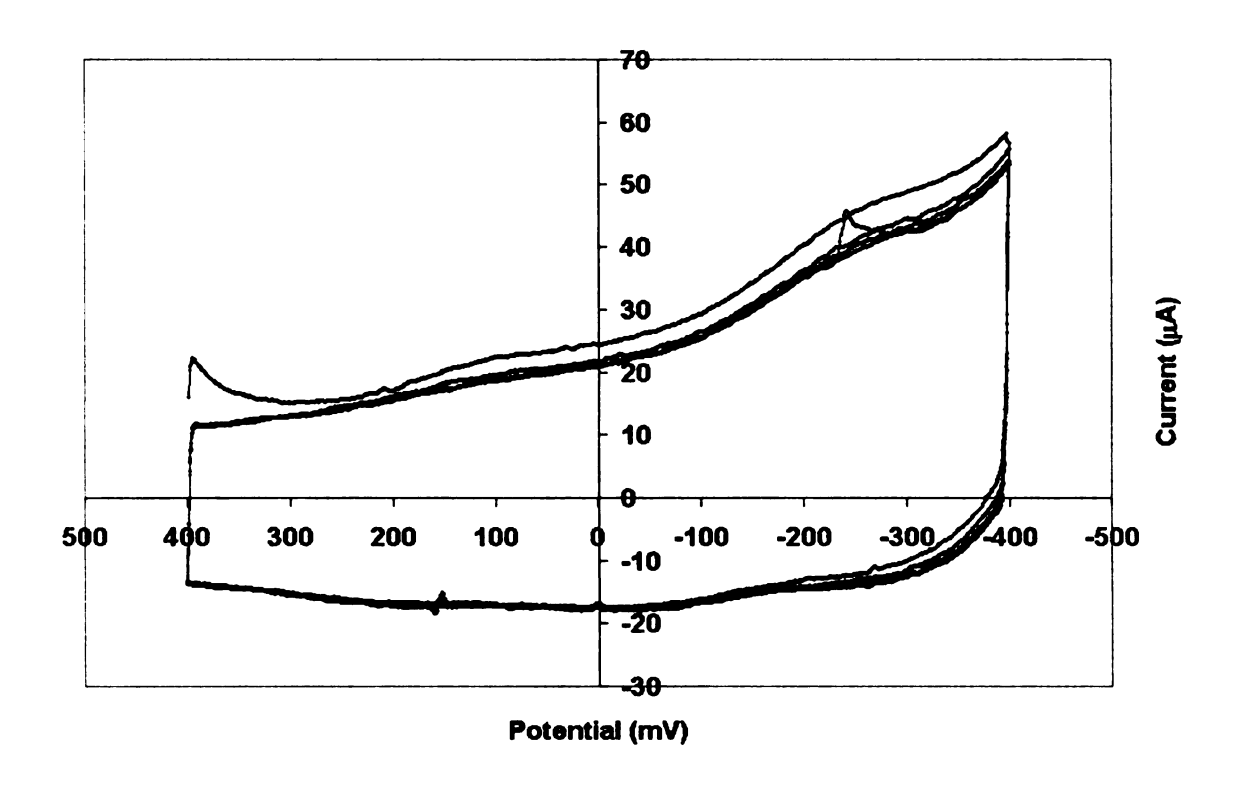


Figure 3-12. Cyclic Voltammogram of 0.002mM resorufin in PBS buffer. The TIRFM-CV flow cell was filled with 0.002mM resorufin solution in

The TIRFM-CV flow cell was filled with 0.002mM resorufin solution in 0.1M PBS buffer, then fluorescence and CV data collection was started simultaneously. The curve above shows the cyclic voltammogram obtained at a scan rate of 30 mV/sec. The reduction of resorufin to dihydroresorufin occurred at about -277mV on scanning towards increasing negative voltages. The oxidation of dihydroresorufin back to resorufin at -238mV occurred on scanning towards increasing positive voltages. The CV peaks are not pronounced, as explained earlier. The potential was cycled five times. The oxidation and reduction potentials of resorufin and dihydroresorufin are listed in Table 3-3.

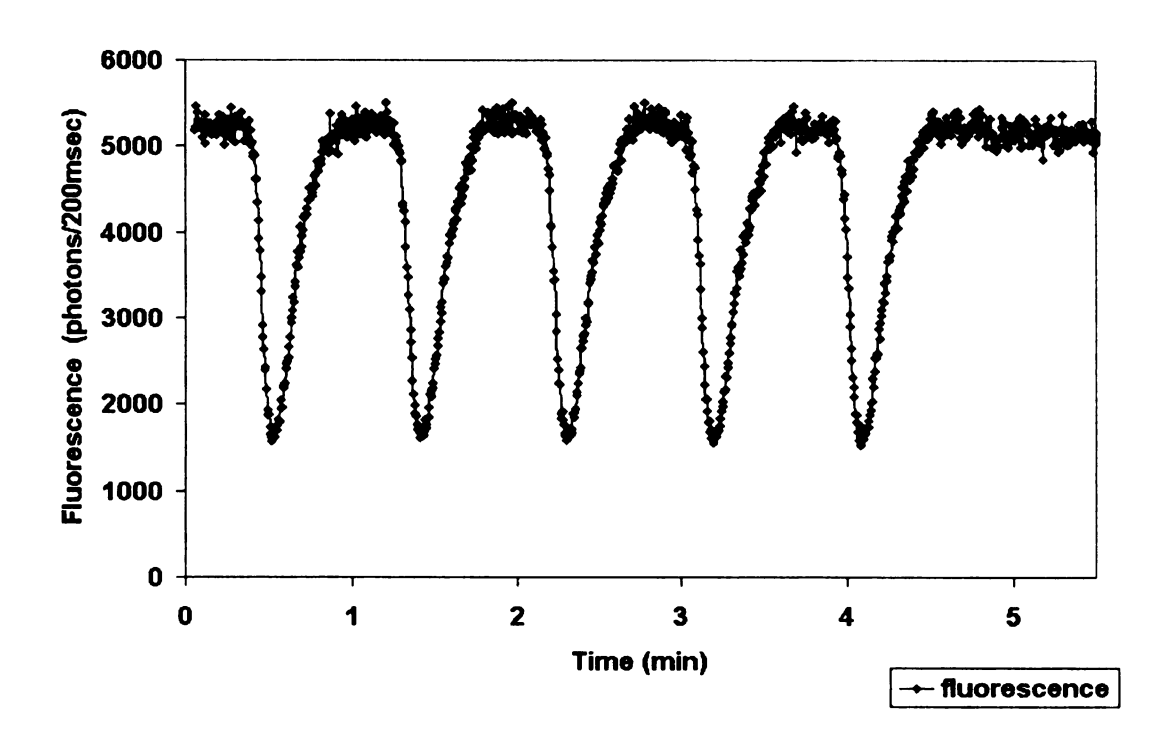


Figure 3-13. Fluorescence data obtained in the TIRFM-CV flow cell for 0.002mM resorufin.

The working solution was 0.002mM resorufin in 0.1M PBS buffer. A decrease in fluorescence was observed when resorufin was reduced to dihydroresorufin, while an increase in fluorescence resulted from the reverse redox reaction. The potential was cycled five times. The optical properties of the dyes are listed in Table 3-4.

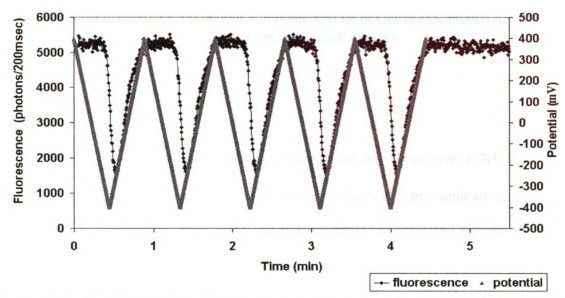


Figure 3-14. Combined plot of fluorescence versus time and applied potential versus time for 0.002mM resorufin.

The working solution was 0.002mM resorufin in 0.1M PBS buffer. After the flow cell was filled, the fluorescence and CV data collection was started simultaneously. When the potential was scanned towards negative potentials, resorufin was reduced to dihydroresorufin at about -277mV, with a decrease in fluorescence emission. In the reverse scan, the dihydroresorufin was oxidized to resorufin at about -238mV, with an increase in fluorescence. The potential was cycled five times. The electrochemical properties of the dyes are summarized in Table 3-3, while the optical properties are listed in Table 3-4.

4 DEVELOPMENT AND OPTICAL-ELECTROCHEMICAL CHARACTERIZATION OF A BIOSENSOR BASED ON D-FRUCTOSE DEHYDROGENASE (FDH)

4.1 ABSTRACT

We have developed and characterized a fructose dehydrogenase (FDH) biosensor, based on indirect bioelectrocatalysis to ensure electrical communication with the electrode, using coenzyme Q₆ as the mediator. FDH, a naturally membrane-bound enzyme, was incorporated into a bilayer lipid membrane (BLM) deposited on indium tin oxide (ITO), along with Q₆. The sensor was evaluated by using cyclic voltammetry (CV) to monitor the change in anodic current upon addition of D-fructose to the sample cell. However, this FDH biosensor exhibited poor sensitivity, because electron tunneling through the BLM was very low.

To improve electron tunneling, the carbon chain length characteristic of lipid bilayers was shortened. Octyltrimethoxysilane was used to form an 8-carbon monolayer on ITO, and liposomes containing FDH and Q₆ were deposited to form the outer leaflet of a biomimetic layer. This sensor demonstrated a clear dependence of the anodic current on D-fructose concentration, with a linear dependence over D-fructose concentrations of 0.056mM to 1.98mM and a plateau at higher D-fructose concentrations, as expected for an enzymatic sensor. Since the biomimetic interface was formed on an (ITO)-coated glass slide, we were also able to characterize the bilayer optically using fluorescence

recovery after pattern photobleaching (FRAPP). The diffusion coefficient of the upper leaflet of the biomimetic layer was $4.4 \times 10^{-10} \text{ cm}^2/\text{sec} \pm 0.7 \times 10^{-10} \text{ cm}^2/\text{sec}$, with a membrane fluidity of 0.59 ± 0.099 .

4.2 INTRODUCTION

In the previous chapter of this thesis, we demonstrated a protocol for simultaneous optical and electrochemical characterization, using the chemical dye resorufin as a test molecule. Both optical and electrochemical measurements provided corroborative evidence of the reversible conversion of fluorescent resorufin to non-fluorescent dihydroresorufin upon reduction. Besides providing confirmation of the same event, the experimental set-up can also be used to monitor independent events occurring within the same sample. In this chapter, we present details of work on developing a biosensor based on D-fructose dehydrogenase (FDH), and its characterization by the combined optical-electrochemical protocol.

Biosensors serve as reliable miniaturized analytical devices for the detection of various analytes with high sensitivity. They have applications in numerous fields such as environmental monitoring, food technology and medical diagnostics. In this study, FDH was immobilized in two different membrane-mimicking environments: a bilayer lipid membrane (BLM) and a biomimetic layer. Fluorescence recovery after pattern photobleaching (FRAPP) was used to characterize the two systems, and cyclic voltammetry (CV) was used to monitor the electrochemical redox reaction catalyzed by

FDH.

4.3 DEVELOPMENT OF AN FDH-BASED SENSOR

4.3.1 Introduction to FDH

FDH (EC 1.1.99.11) is isolated from *Gluoconobacter Industrius*, and is a membrane-bound quinoprotein that was first discovered by Yamada and coworkers (Yamada et al. 1966). It is a 140kDa pyrroloquinone quinone (PQQ)-containing oxidoreductase. PQQ is the cofactor associated with the enzyme FDH and remains permanently bound to it. Amayema and coworkers first purified and characterized the catalytic and molecular properties of FDH (Ameyama et al. 1981; Ameyama et al. 1981).

FDH catalyzes the conversion of D-fructose to 5-keto-D-fructose. Upon enzymatic oxidation of D-fructose, the prosthetic group in the enzyme (PQQ) is reduced to PQQH₂, according to the following scheme:

D-Fructose + FDH-PQQ
$$\rightarrow$$
 5-keto-D-fructose + FDH-PQQH2 (4.1)

Amayema and coworkers recognized that FDH exhibited substrate specificity, i.e. it catalyzed the conversion of the monosaccharide D-fructose only, but no other forms of sugar (Ameyama et al. 1981; Ameyama et al. 1981). Thus, an analytical assay based on FDH would be useful for the quantitative determination of D-fructose. Fructose, being sweeter than glucose and sucrose, is frequently used as a diabetic sweetener. It is also widely present in fruits, vegetables, honey and soft drinks. Fructose also serves as an

indicator of the ripening process in fruits (Paredes et al. 1997). It is also present in the seminal fluid, where its concentration is an indicator of seminal vesicle size and secretory capacity. Thus, the ability to precisely determine fructose concentrations is of great and general importance.

Numerous FDH-based amperometric biosensors have been developed to date. These sensors exhibit a unique response, based on the different environments the FDH is incorporated into. Examples of FDH-based sensors include FDH incorporated into conducting polypyrrole matrices (Begum et al. 1993), immobilization in self-assembled monolayers or membrane mimetic layers on gold (Kinnear and Monbouquette 1993; Kinnear and Monbouquette 1993; Kinnear and Monbouquette 1997; Darder et al. 2000; Campuzano et al. 2003; Campuzano et al. 2004), incorporation in carbon paste matrices (Parellada et al. 1996; Paredes et al. 1997), immobilization in cellulose acetate membranes (Tkac et al. 2001), and free FDH adsorbed on gold, platinum and glassy carbon electrodes (Khan et al. 1991).

In this study, we present an FDH-based biosensor immobilized in a biomimetic interface assembled on ITO. We exploited the transparency of the ITO film, along with its conductive property, to conduct both optical and electrochemical characterization of the sensor.

Quinoproteins are especially advantageous for use in biosensing elements, because they do not undergo auto-oxidation. This is because the cofactor is tightly bound to the enzyme, and oxygen does not compete for its reoxidation (Khan et al. 1991;

Paredes et al. 1997). Reports in the published literature suggest that FDH has a hydrophobic and a membrane-lipid-interacting structure, and is thus an intrinsic membrane protein (Ameyama et al. 1981; Ameyama et al. 1981). A membrane bound enzyme typically requires a hydrophobic environment for optimal activity and stability of the enzyme. Studies also report that the enzymatic activity is higher when FDH is bound to a membrane than when it is free in solution (Kato et al. 2003).

Besides mimicking its natural environment, the presence of a lipid bilayer prevents easily oxidized electroactive interferents such as ascorbic acid (typically present in fruits, etc.) from reaching the electrode surface. Erroneous signal generation due to electroactive interferents is thus eliminated. The lipid bilayer also causes a reduction in background noise, resulting in increased sensitivity. Studies have shown that incorporation of enzymes into such interfaces creates systems that exhibit greater reproducibility and robustness (Campuzano et al. 2003).

4.3.2 Theory

A common problem in the construction of enzyme-based amperometric biosensors is the achievement of direct electron transfer between the enzyme and the electrode. This can be a problem with enzyme-based sensors, because the prosthetic group in most enzymes is located deep within the enzyme and, as a result, is not available for efficient electron transfer. The prosthetic center, in most cases, also undergoes irreversible electrochemical reaction when present by itself. High overpotentials are required for the redox processes in these prosthetic groups (Begum et al. 1993). Ideally,

amperometric biosensors operating at less extreme potentials need to be developed, to reduce the effect of interfering reactions caused by easily oxidizable components at high potentials.

To address the problems listed above, "indirect bioelectrocatalysis" has become a commonly used method to achieve efficient electron transfer. In indirect bioelectrocatalysis, a mediator is added to act as the electron acceptor and to shuttle electrons from the enzyme to the electrode. Thus, after the completion of the enzymatic reaction given by Equation (4.1), the PQQH₂ from the enzymatic reaction is reoxidized electrochemically with the aid of the redox mediator, coenzyme Q₆. The current produced as a result is directly proportional to D-fructose concentration (Paredes et al. 1997). Coenzyme Q₆ is known to be a relatively stable mediator that can be regenerated at an electrode (Kinnear and Monbouquette 1993; Kinnear and Monbouquette 1993). The electrochemical reaction occurring in the presence of the coenzyme is given by

$$FDH(PQQH_2) \rightarrow FDH(PQQ) + 2H^+ + 2e^-$$
 (4.2)

Electron transfer between the prosthetic group (PQQ) and the coenzyme is catalyzed at less extreme potentials. The oxidation of the reduced form of the enzyme (PQQH₂) takes place at about 400mV (versus Ag/AgCl). Coenzyme Q₆, required for the FDH biosensor, is typically incorporated into the liposomes used to form the lipid bilayer. Incorporation results in immobilization of the coenzyme, preventing the mediator from diffusing away from the electrode into the bulk solution (Begum et al.

1993). This is important, because diffusion of the mediator into the bulk solution causes a loss in functionality of the biosensor (Kinnear and Monbouquette 1997).

4.3.3 Introduction to FRAPP

Fluorescence photobleaching recovery (FPR) and fluorescence recovery after pattern photobleaching (FRAPP) are both effective techniques used to measure apparent diffusion coefficients. However, diffusion of lipids and proteins in BLMs is characterized by non-ideal behavior, and cannot be well-characterized as ideal self-diffusion. In addition, the spatial profile of the excitation source in FPR can deviate from the ideal Gaussian shape as the beam passes through a series of optical components before becoming a focused spot. Since the form of the fluorescence recovery data depends critically on the beam shape, FPR cannot be used to measure non-ideal diffusion in lipid bilayers (Starr and Thompson 2002).

In the case of FRAPP, developed by Smith and McConnell in 1978 (Smith and McConnell 1978), the spatial profile of the excitation intensity is known. Thus FRAPP is commonly used to measure the lateral diffusion of fluorescent phospholipid probes in either natural lipid bilayers or in biomimetic layers. The redistribution of fluorescence emission after photobleaching is monitored in a pattern of well-characterized periodic stripes, which yields information about the motion of the fluorophores.

A mathematical model that takes diffusion non-idealities into account was developed by Starr and Thompson (Starr and Thompson 2002). In this model, the system

is characterized as being composed of a number of discrete fluorophore populations, with each population exhibiting ideal diffusion with specific diffusion coefficients. The time-dependent fluorescence emission of a two-dimensional sample containing fluorophores that undergo ideal diffusion is given by

$$F(t) = Q \int_{-\infty}^{\infty} \int_{-\infty}^{\infty} I(x, y)C(x, y, t) dx dy$$
 (4.3)

where F(t) is the time-dependent fluorescence, Q is a proportionality constant, I(x,y) is the monitoring beam intensity, and C(x,y,t) is the density of unbleached fluorophores at position (x,y) at time (t). For the specific case of the FRAPP set-up where a Gaussian laser beam is intersected by a ronchi ruling in the back image plane of a microscope, the intensity is given by

$$I(x,y) = \frac{I_0}{2} \exp\left[-\frac{2(x^2 + y^2)}{s^2}\right] \times \left[1 + \sum_{n \text{ odd}} C_n \cos(nkx)\right]$$
(4.4)

where I_0 is the beam intensity at the origin, s is the $1/e^2$ -radius of the expanded beam, k is the spatial frequency of the striped pattern, and "n odd" signifies summation over all odd numbers.

The parameters k and C_n are given by

$$k = \frac{2\pi}{a} \qquad C_n = \frac{4(-1)^{(n-1)/2}}{n\pi} \tag{4.5}$$

where a is the spatial period.

For ideal diffusion, C(x,y,t) is given by

$$C(x, y, t) = \frac{1}{4\pi Dt} \int_{-\infty}^{\infty} \int_{-\infty}^{\infty} C(x', y', 0) \times \exp\left[-\frac{(x - x')^2 + (y - y')^2}{4Dt}\right] dx' dy'$$
(4.6)

where the initial density of unbleached molecules can be approximated as

$$C(x, y, 0) = Ce^{-\kappa I(x, y)}$$
 (4.7)

where C is the total fluorophore density (bleached and unbleached) and κ is a constant of proportionality that depends on the duration of the bleach pulse, absorptivity of the fluorophores, and the quantum efficiency for bleaching.

In the situation where the striped periodicity is small compared to the illuminated area, the normalized fluorescence photobleaching recovery curve for a sample containing one diffusive population of fluorophores is given by (Smith and McConnell 1978; Wright et al. 1988)

$$\phi(t) = \phi(0) + \left(\frac{m}{2}\right)\left[1 - \phi(0)\right]\left\{1 - \left(\frac{8}{\pi^2}\right)\left[\exp\left(-\frac{4\pi^2Dt}{a^2}\right) - \left(\left(\frac{1}{9}\right)\exp\left(-\frac{36\pi^2Dt}{a^2}\right)\right)\right]\right\}, t \ge 0$$

(4.8)

where $\phi(t)$ is the ratio of the postbleach fluorescence [F(t>0)] to the constant prebleach fluorescence [F(t<0)], and m is the fraction of fluorophores that are mobile.

Thus (1-m) is the fraction of immobile fluorophores; and a is the periodicity of the striped pattern which, in our experiments, was 12.5 µm. A similar model was developed by Wright and coworkers for a sample containing two mobile species (Wright et al. 1988). However, all data obtained in this work were well-described by the "single-mobile species" model; therefore, the "two-mobile species" model will not be described here.

4.4 EXPERIMENTAL SECTION

4.4.1 Materials

D-Fructose dehydrogenase (FDH, Catalog # F-5152, 400-1,200 units/mg protein) isolated from *gluconobacter industrius*, was purchased from the Sigma Chemical Company (St. Louis, MO) and used without further purification. FDH is stable between pH 3 and 5.5, with 4.5 being optimum. Thus, all solutions were used at a pH of 4.5. Sodium phosphate monobasic (Catalog # 3818-01, J.T. Baker, Phillipsburg, NJ) and sodium chloride (Catalog # S1240, Spectrum Chemical Corporation, Gardena, CA), used in the preparation of the pH 4.5 buffer, were purchased from the Sigma Chemical Company (St. Louis, MO). Egg phosphatidylcholine (Egg-PC, Catalog # 850375C) and fluorescently labeled lipid (NBD-PC, Catalog # 810130), used in the preparation of liposomes, were purchased from Avanti Polar Lipids (Alabaster, AL). Triton X-100 (Catalog # 21123), used for the solubilization of the protein, was purchased from Supelco

(Bellefonte, PA).

Indium tin oxide (ITO)-coated glass slides (Catalog # CG-41IN-S107) were purchased from Delta Technologies Ltd. (Stillwater, MN). Co-enzyme Q₆ from Saccharomyces cerevisiae (Catalog # C9504), used as the mediator in the electrochemical assays, was purchased from the Sigma Chemical Company (St. Louis, MO). Octyltrimethoxysilane (Catalog # 376221), used for the preparation of hydrophobic monolayers on ITO, was purchased from the Sigma Chemical Company (St. Louis, MO). Dialysis was carried out with a regenerated cellulose porous membrane (Spectra/Por 1, Catalog # 132655, molecular weight cutoff – 6000 to 8000) purchased from Spectrum Laboratories (Rancho Dominguez, CA). Bio-beads (Catalog # 152-8920), used for the removal of triton, were purchased from Bio-rad Laboratories (Hercules, CA). D-Fructose (catalog # F2543) was purchased from the Sigma Chemical Company (St.Louis, MO). Potassium ferricyanide (catalog # 6912), used for the colorimetric assay, was purchased from Mallinckrodt, Inc. (Paris, KY). Ferric sulfate (Catalog # I-142), used for the colorimetric assay, was purchased from Fisher Scientific (Springfield, NJ). RBS-50 detergent concentrate (catalog # 27952), used for cleaning the glass slides and the ITOcoated glass slides, were purchased from the Pierce Chemical Co. (Rockford, IL).

4.4.2 Preparation of the proteoliposome solution

FDH and the coenzyme were incorporated into liposomes using standard protocols (Meuller et al. 1997; Graneli et al. 2003; Girard et al. 2004). One ml of 20 mg/ml Egg-PC in chloroform, 1 ml of 2 mg/ml NBD-PC in chloroform and 16.67 ml of

co-enzyme Q₆ in ethanol were added to a glass test tube, and the solvent was evaporated under a nitrogen blanket. The lipid-coenzyme mixture was freeze-dried overnight under vacuum at -47°C, in a rotovac freeze drier. Sodium phosphate buffer (0.01M) containing 0.1M sodium chloride was prepared, and the pH was adjusted to 4.5 using a strong acid or base as required.

One ml of pH 4.5 buffer was added to the lipid-coenzyme mixture and the solution was vortexed and sonicated to form small unilamellar vesicles. Solubilization of the protein was achieved by adding 50 µg/ml of Triton. FDH (0.5 mg) was added to the solution, followed by mixing for 45 minutes. The detergent was removed from the solution using two different methods. One method involved three different subsequent additions of 0.5 mg/ml of biobeads to the solution, followed by removal of the biobeads by decantation after the mixing was complete. The other method dialyzed the solution (in a regenerated cellulose membrane) against phosphate buffer for about 3-4 days at 4°C, using about 6 buffer changes.

4.4.3 Adsorption of proteoliposome solution onto ITO-coated glass slides

An ITO-coated glass slide was cut into smaller pieces and sonicated for 30 minutes in RBS-50 detergent solution, followed by rinsing under distilled water and drying using nitrogen. The slide was oxygen plasma cleaned for a period of about 20 seconds immediately before each experiment. After plasma cleaning, the slide was placed in a cell holder to ensure that the working area would be reproducible. The electrode area exposed to the solution was about 0.17 cm². About 100 µl of the enzyme

solution was added to the exposed circular ITO, and the solution was allowed to adsorb for a period of about 45 minutes to one hour to ensure formation of a lipid bilayer. Following this, the cell holder was carefully immersed in a beaker containing pH 4.5 buffer solution, ensuring that the working area always stayed in contact with the solution.

4.4.4 Preparation of hydrophobic silane monolayers on ITO-coated glass slides

The silylated surfaces were prepared by deposition from aqueous alcohol, following the protocol outlined in a technical documentation obtained from Gelest, Inc.¹ A 95% ethanol and 5% water solution was prepared, and the pH was adjusted to between 4.5 and 5.5 with acetic acid. Octyltrimethoxysilane was added with stirring to yield a 2% v/v solution. Five minutes was allowed for hydrolysis and silanol formation (Figure 4-1).

The ITO-coated glass slide was plasma cleaned under oxygen for 20 seconds, followed by piranha cleaning for 30 seconds. The slide was then washed with deionized water and dried under nitrogen. It was then immersed in the silane solution and allowed to react for 30 minutes. The slide was then rinsed in ethanol and baked in an oven at 160° C for 12 hours to cure the silane layer.

4.4.5 Adsorption of proteoliposomes onto silanized ITO slides

The hydrophobicity of the silanized ITO slide was checked visually by placing a drop of water on the surface. The contact angles were observed to be in excess of 90°. The silanized slide was placed in the cell holder to ensure a reproducible circular working area of 0.17 cm². About 100 µl of the enzyme solution was added to the exposed area,

¹ "Applying a silane coupling agent", technical documentation, Gelest Inc., Morrisville, PA

and the solution was allowed to adsorb for a period of about 45 minutes to one hour to ensure formation of a monolayer of liposomes on the C₈ hydrophobic monolayer.

4.4.6 Cyclic Voltammetry Experiments

The modified electrode (either the lipid bilayer on ITO or a monolayer of liposomes formed on the C₈ silanized monolayer) was placed in the cell holder, and was immersed in deoxygenated pH 4.5 buffer. The working electrode from the potentiostat was connected to the ITO, and the platinum counter electrode and the Ag/AgCl reference electrode were placed in the buffer solution. D-fructose in varying amounts was added to the buffer solution, and cyclic voltammetry measurements were carried out at 1 mV/sec to obtain steady state data. Films were scanned at very low rates (1 mV/sec), to allow for near redox equilibrium to be established between the electrode and the redox protein. Slow scan rates also allow us to obtain midpoint potentials (Haas et al. 2001). The parameters used for the cyclic voltammetry scans are given in Table 4-1.

4.4.7 Set-up for FRAPP Experiments

4.4.7.1 Optical set-up for FRAPP experiments

A diagram of the optical set-up used for the FRAPP experiments is shown in Figure 4-2. The laser beam from the argon ion laser was expanded using a 5x beam expander (NT55-577, Edmund Industrial Optics, Barrington, NJ). The expanded beam was then passed through a pair of optical flats. The first flat was used to split the beam into two lines of different intensities – a high intensity beam used for photobleaching

(200-500 mW) and a low intensity beam used for monitoring the interfacial dynamics (3-4 μW). The second optical flat was placed after the shutter, and exactly recombined the two beams. The combined beam was then directed through a set of mirrors into the epiport at the back of an inverted microscope (Axiovert, 135M, Carl Zeiss Inc., Thornwood, NY). The beam passed through a 50 line per inch ronchi ruling (NT56-592, Edmund Optics, Barrington, NJ) placed in the back image plane of the microscope, and through a filter cube which directed the light into a microscope objective (32x, 440851, LD Acrophlan, Carl Zeiss Inc., Thornwood, NY) placed right below the stage housing the flow cell.

When a beam passes through a ronchi ruling placed in the back image plane of the microscope, a real image of the ronchi ruling is projected onto the sample plane. The image appears as alternating bright and dark fringes (Figure 4-3) when viewed through the eyepiece of the objective or by a CCD camera (VE-1000, DAGE-MTI, Michigan City, IN). Prior to the start of an experiment, bands were marked out on an ITO-coated slide using a fluorescent marker. The position of the laser beam (adjusted using the mirrors) and the position of the microscope objective were adjusted such that the fringes (created using the fluorescent bands) came into sharp focus and filled the viewing area. This approximately located the point of focus of the objective.

Beam alignment was further ensured by using the CCD camera to confirm that the bright fringes formed by the photobleaching beam overlapped the faint fringes formed by the monitoring beam. After the experiment was started, the position of the objective was

readjusted minutely to relocate the fringes, because the position could have changed as a result of minor variations in slides or a change in position induced by the presence of a monolayer/bilayer adsorbed on the slide.

After allowing 45 minutes for the formation of the lipid bilayer (steps outlined in section 4.1.8), the illuminated area was subjected to a brief 400ms flash of the high intensity photobleaching beam. The photomultiplier tube (R4632, Hamamatsu, Bridgewater, NJ) was blocked with a shutter during the bleaching period to protect it. Fluorescence recovery data at the end of the bleaching process were collected from a much smaller area than had been bleached (Figure 4-3). This was done to ensure that the fluorescence recovery is only from unbleached fluorophores in the fringes, and not from unbleached fluorophores in areas outside the fringes. The photon counting electronics and the data acquisition software are the same as described earlier in Chapter 2.

4.4.7.2 Experimental cell used for FRAPP experiments to study FDH system

A new cell had to be designed to characterize the properties of the biomimetic layer, because of the small working volume of FDH-liposome solution (only 1 ml of working solution). The small volumes did not allow for flow experiments to be conducted in the modified second generation flow cell described earlier (Chapter 3).

The new cell consisted of a box 2 inch high, 1 inch wide, and 1 inch deep, constructed with a silanized ITO slide as the bottom surface. The walls of the box/cell were made of microscope glass slides. The box was assembled using epoxy. In

electrochemical experiments, the bottom ITO slide served as the working electrode, and the counter and the reference electrodes were placed directly in the cell.

4.4.7.3 Preparation of biomimetic layer for FRAPP experiments

After preparation of the octylsilane monolayer on the ITO bottom slide, the cell was assembled. Then, 60-100 µl of the FDH-liposome solution was placed onto the bottom silanized ITO surface of the cell, and the solution was allowed to adsorb for about 45 minutes. Loosely adsorbed FDH-liposomes were removed by rinsing with about 10 ml of buffer solution. The cell was then placed on a stage on top of the objective of our inverted microscope (Axiovert 135M, Call Zeiss Inc., Thornwood, NY).

4.5 RESULTS AND DISCUSSION

The goal of this work was to construct a bilayer lipid membrane (BLM)-based FDH sensor, using indirect bioelectrocatalysis. Indirect bioelectrocatalysis requires close contact between the enzyme, the mediator and the electrode for efficient electrical communication (Ciucu and Ciucu 2002). To achieve this close contact, the correct ratio of the enzyme, lipid and mediator must be used. Numerous trials were conducted to determine the ratio of lipid:enzyme:coenzyme that would make a functional amperometric biosensor. BLMs consisting of varying coenzyme:lipid:enzyme ratios were formed on ITO-coated slides, and the catalytic response of the sensor upon addition of D-fructose was measured electrochemically (amperometrically). In cases where the electrochemical assay exhibited no catalytic activity in the presence of D-fructose, a

colorimetric assay was conducted to determine if the FDH was active.

Activity of FDH was determined using a colorimetric assay in the presence of potassium ferricyanide. The reaction catalyzed in the assay is given by

D-Fructose +
$$2K_3Fe(CN)_6 \rightarrow 5$$
-keto-D-Fructose + $2K_4Fe(CN)_6$ (4.9)
 $2K_4Fe(CN)_6 + Fe_2(SO_4)_3 \rightarrow PrussianBlue + 3K_2SO_4$

The production of Prussian Blue can be monitored and measured at 660nm by spectrophotometry (Toyobo; Sigma 1994), allowing the activity of FDH to be calculated in terms of units, where one "unit" is defined as the amount that causes the oxidation of one micromole of D-fructose per minute (Toyobo; Ameyama et al. 1981; Ameyama et al. 1981; Sigma 1994).

For all the different ratios of lipid:enzyme:coenzyme used, the colorimetric assay outlined in Equation (4.9) always confirmed the production of Prussian blue, proving that the enzyme was incorporated in an active conformation in the BLM and was able to oxidize D-fructose to 5-keto-D-fructose. While the colorimetric assay always indicated that the enzyme was active, the electrochemical assay did not exhibit any appreciable catalytic activity upon addition of D-fructose.

One of the major problems in these experiments was the need to use low concentrations of the enzyme because of its high cost. Sensors containing lower quantities of enzyme incorporated into liposomes did not exhibit any catalytic activity upon addition of D-fructose in the CV experiments, even though a positive colorimetric assay indicated that the enzyme was active. Hence, we concluded that electron transfer to the electrode was being inhibited. We speculated that the probability of the enzyme not being in close contact with the coenzyme is enhanced when the enzyme concentration is low, resulting in lack of electrical contact.

Similarly, using the correct amount of mediator is also necessary. Studies have shown that a scarcity or excess of the co-enzyme resulted in the absence of a fully functional amperometric sensor. Having the mediator in low concentrations affected the biosensor response, since it was limited by enzyme-mediator kinetics (Li et al. 1996; Wang et al. 1998; Miao et al. 2001; Yu et al. 2003; Wang et al. 2005). Similarly, having the mediator at higher concentrations than required affected the biosensor response, since it was limited by enzyme-substrate kinetics. Using a very high mediator concentration could result in a high background signal, and thus the signal from the coenzyme could overwhelm the signal due to the presence of D-fructose. This behavior is typical of mediator-based sensors.

The concentration of liposome was also changed to determine the level high enough to form a BLM while also allowing for efficient electrical contact between the FDH, coenzyme and the electrode. Too high a liposome concentration may increase the probability of the enzyme being far away from the cofactor. We decided to use 1 mg/ml of liposomes, based on experiments conducted in our laboratory using FRAPP that showed formation of lipid bilayers at this concentration on various substrates (Vaidya

2005).

Proteoliposomes containing the coenzyme Q_6 in the ratio outlined in Section 4.4.2 were prepared. A lipid bilayer was formed on a freshly cleaned ITO slide, using the procedure outlined in Section 4.4.3. The solution was purged with nitrogen, and a nitrogen blanket was maintained during the experiment. The amperometric biosensor was tested by monitoring the catalytic activity exhibited upon addition of D-fructose. Addition of a substrate to the redox system promotes multiple turnovers of the enzyme, and a steady state transfer of electrons through the enzyme to and from the electrode.

A background CV measurement was obtained using the parameters listed in Table 4-1. Redox waves of the coenzyme in buffer, similar to that observed by Kinnear and Monbouquette (Kinnear and Monbouquette 1997), were visible in the background scan, with a decrease in current in each successive cycle. At the end of the background scan, varying amounts of D-fructose were added to the solution, followed by mixing of the solution by gentle pipetting. The response obtained for the BLM-based FDH sensor is shown in Figure 4-4. An increase in catalytic current (compared to the background) was observed upon addition of D-fructose. For easier viewing, the region between 400mV and 800mV has been expanded in Figure 4-5.

On scanning towards positive voltages beyond the redox potential of the coenzyme, the anodic current increased with increasing D-fructose concentration in our BLM-based FDH sensor, due to oxidation of D-fructose. However, the increase in anodic current appears to be a relatively weak function of D-fructose concentration. To assess

the strength of this dependence, we added D-fructose-free buffer to the solution, and observed a corresponding decrease in current. Upon addition of 10mM D-fructose, a 19% net increase in current was observed (at 800mV) compared to the background. These results appear to indicate that the BLM-based FDH biosensor is functional, albeit one that functions at very low sensitivity.

While the results indicate that we have a functional biosensor, it does not display the ideal behavior typical of enzyme-based sensors. This could be due to the fact that we did not achieve steady state during our measurements. However, we believe it is more likely that these results are an indication that electron transfer is not efficient and may, perhaps, even be inhibited as explained below.

One of the causes of inefficient electron transfer in BLMs is that electron tunneling through a lipid bilayer of high resistance may be very slow or negligibly small (Bard and Faulkner 2000). There is an exponential decrease in the rate of electron tunneling with distance, which may explain why electron tunneling through a BLM is slow. There is also a possibility that some of the electron transfer that we observe occurs because the BLMs are not highly insulating. A BLM is typically on the order of about 3-5 nm in thickness. To decrease the electron tunneling distance, we could use one of two approaches. We could form a self-assembled monolayer of a shorter carbon chain (6-10 carbons) on the ITO surface, following which the upper leaflet could be formed using lipids. Or we could use custom-synthesized lipids with shorter carbon chains, which would in effect decrease the electron tunneling distance upon formation of the bilayer.

We decided to form a self-assembled monolayer on ITO.

4.5.1 Incorporation of FDH in a biomimetic layer

Octyltrimethoxysilane was used as the linker molecule to form a self-assembled monolayer on ITO. The electron tunneling distance was decreased by using an 8 carbon chain in place of the 18-carbon lipid chain which forms the lower leaflet of the lipid bilayer. The silanization protocol outlined in Section 4.4.4 was used to form the hydrophobic C₈ monolayer on the ITO-coated glass slide. The biomimetic layer containing the FDH and the coenzyme was formed on the C₈ monolayer, using the procedure outlined in Section 4.4.5.

4.5.1.1 Optical characterization

FRAPP experiments were conducted to confirm bilayer formation and to characterize the properties of the biomimetic bilayer. The upper leaflet was formed with liposomes that contained about 2% fluorescent lipids (NBD-PC), so the fluidity of the upper leaflet could be characterized using FRAPP. FRAPP data were collected at multiple spots using the procedure outlined in Section 4.4.7.1. Figure 4-10 shows a typical FRAPP curve with the solid line representing the fit to the data, using the "single mobile species" model given in Equation (4.8). The results of the FRAPP experiments have been summarized in Table 4-2. The average diffusion coefficient was 4.4 x 10^{-10} cm²/sec \pm 0.7 x 10^{-10} cm²/sec, while the mobility of the membrane was determined to be 0.59 \pm 0.099. Similar diffusion coefficients have been observed for lipid bilayers formed on poly(diallyldimethylammonium chloride)/11-mercaptoundecanoic acid (PDAD/MUA)

(Zhang et al. 2000; Vaidya 2005)and on poly(dimethyldiallylammonium chloride) (PDAC) layers (Zhang et al. 2000; Vaidya 2005).

4.5.1.2 Electrochemical characterization

After formation of the biomimetic layer, the solution was purged with nitrogen and a nitrogen blanket was maintained during the experiment. A background CV scan was collected with the parameters listed in Section 4.4.6. After the background scan was completed, D-fructose in varying amounts was added to the solution. The CV measurements were recorded after each addition, following gentle mixing of the solution.

Upon addition of D-fructose, a stable catalytic current (or current density) was observed when scanning towards positive voltages past 400mV (Figure 4-6), due to oxidation of D-fructose and turnover of the coenzyme. The curve has been expanded for better visibility in Figure 4-7, to illustrate the dependence of the catalytic current on D-fructose concentration. Clearly, the biosensor is sensitive to D-fructose concentration. The dependence of current density on D-fructose concentration at 800mV is shown in Figure 4-8, and may be used as a calibration curve. The response of the sensor was checked at 800mV, since the current attained steady state beyond this point. We obtained a linear dependence of the catalytic current on D-fructose concentration at D-fructose concentrations between 0.056mM and 1.98mM, with a correlation coefficient of 0.9813 R² (Figure 4-9). We observed a 351% increase in current at 800mV compared to the background scan upon addition of 10mM of D-fructose. This increase is highly significant, in comparison to the 19% increase in current observed in the case of the

BLM-based FDH sensor described earlier. As expected, the current approaches a plateau at higher D-fructose concentrations, indicating saturation of the enzyme. This is a typical behavior of enzyme-based biosensors. The sensitivity of this biosensor (0.1891µA/cm²mM) is two orders of magnitude lower than others reported in the literature. For example Kinnear and coworkers (Kinnear and Monbouquette 1993) reported a sensitivity of 15µA/cm²mM, using 300µl of 1 mg/ml FDH. We speculate that the difference in sensitivity is a result of using much lower amounts of the enzyme (100µl of 0.5 mg/ml FDH) in the current experiments.

4.6 CONCLUSIONS

We have developed an FDH-based biosensor that catalyzes the conversion of D-fructose to 5-keto-D-fructose. Using ITO as the substrate gave us the ability to characterize the biosensor both optically and electrochemically. FRAPP was used to characterize the properties of the biomimetic layer, while CV was used to monitor the catalytic response to increasing D-fructose concentration. The FDH and coenzyme Q_6 were immobilized in a biomimetic layer on a silanized ITO slide. We observed a 351% increase in current at 800mV upon addition of 10mM of D-fructose, compared to the background. The catalytic current was proportional to the concentration of D-fructose with the current approaching a plateau at higher fructose concentrations. The calibration curve was linear over D-fructose concentrations between 0.056mM to 1.98mM. The diffusion coefficient of the upper leaflet of the biomimetic layer was 0.044 x 10^{-8} cm²/sec \pm 0.007 x 10^{-8} cm²/sec. The mobility of the membrane was 0.59 ± 0.099 .

4.7 FUTURE WORK

We believe that using higher concentrations of FDH would help us develop a FDH-based biosensor with higher sensitivity. We speculate that controlling the orientation of the prosthetic group, such that the reaction center is close to the electrode would also increase the efficiency of electron transfer. This could be achieved by controlling the orientation of the enzyme using short chain sulfides or promoter molecules that bind and/or align to orient the enzyme, to facilitate electron transfer using electrostatic interactions (Darder et al. 2000).

Further tests such as response to ascorbic acid, stability of the sensor, and response time upon addition of D-fructose could be conducted to further characterize the biosensor. The biosensor could in addition be tested in a real sensing application, for example to detect D-fructose in fruit juice.

The versatility of this optical and electrochemical setup allows us to expand its application to study many other enzyme-based biosensors and other biological systems. This experimental ability to conduct simultaneous optical and electrochemical measurements is being exploited, to explore the ability to tailor the properties of lipid bilayers. Specifically, ongoing work to study the effect of electric fields on BLMs is being investigated. This would be of enormous importance in any application where a BLM is used, because it would allow us to improve membrane quality (by tailoring its mobility).

Table 4-1. Input parameters used to conduct cyclic voltammetry measurements for the D-Fructose dehydrogenase system.

High (mV)	800	
Low (mV)	-400	
Initial (mV)	-400	
Scan rate (mV/sec)	1	
# of cycles	1	

Table 4-2. Summary of regression values obtained by fitting experimental FRAPP data to the single species model [Equation (4.8) (Wright et al. 1988; Starr and Thompson 2002).

Run #	Diffusion coefficient (D *10 ¹⁰) cm ² /sec	Mobile fraction m	f_0
1	4.35	0.487	0.241
2	3.72	. 0.684	0.350
3	5.09	0.594	0.266
average	4.39	0.588	

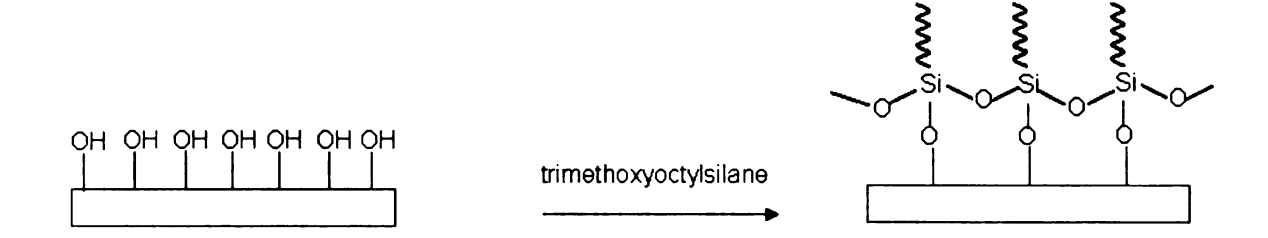


Figure 4-1. Surface chemistry used to form an 8-carbon monolayer on ITO-coated glass surface using trimethoxyoctylsilane as the linker molecule

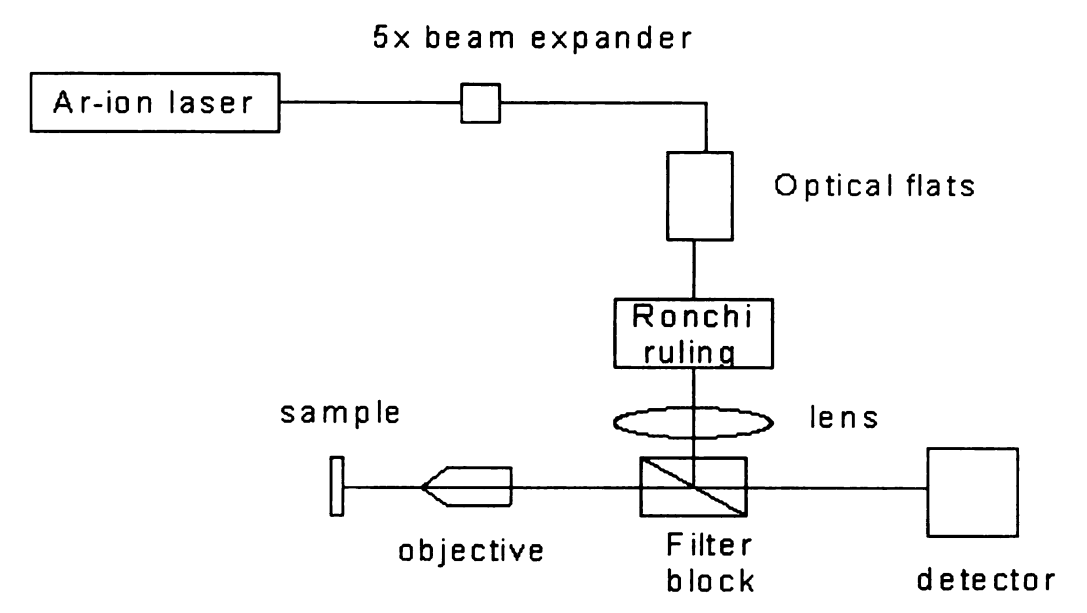


Figure 4-2. Experimental set-up for fluorescence recovery after pattern photobleaching (FRAPP) experiments in the epi-illumination mode.





(a) Photobleached area

(b) Interrogated area

Figure 4-3. Fringe pattern in illuminated region obtained by using 100 lines per inch ronchi ruling. b) The observation area is restricted by placing an aperture in the camera/PMT image plane, to ensure that fluorescence recovery is restricted to fluorophores in the fringes.

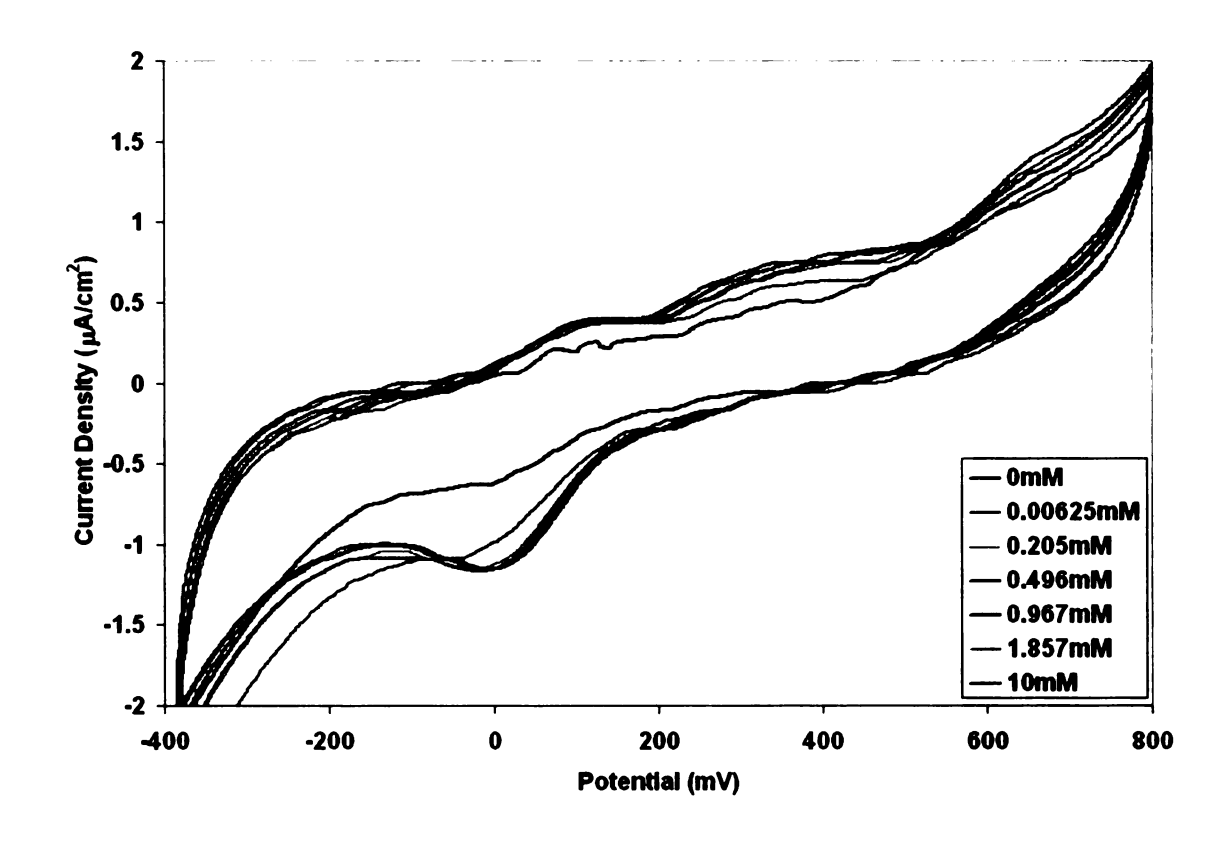


Figure 4-4. CV curves obtained for a BLM-based FDH sensor.

A lipid bilayer containing FDH and the coenzyme was formed on ITO-coated glass and the slide was then placed in a pH 4.5 sodium phosphate buffer solution. The working area was 0.17 cm². Response of the biosensor was monitored after addition of D-fructose in varying amounts, using a scan rate of 1 mV/sec.

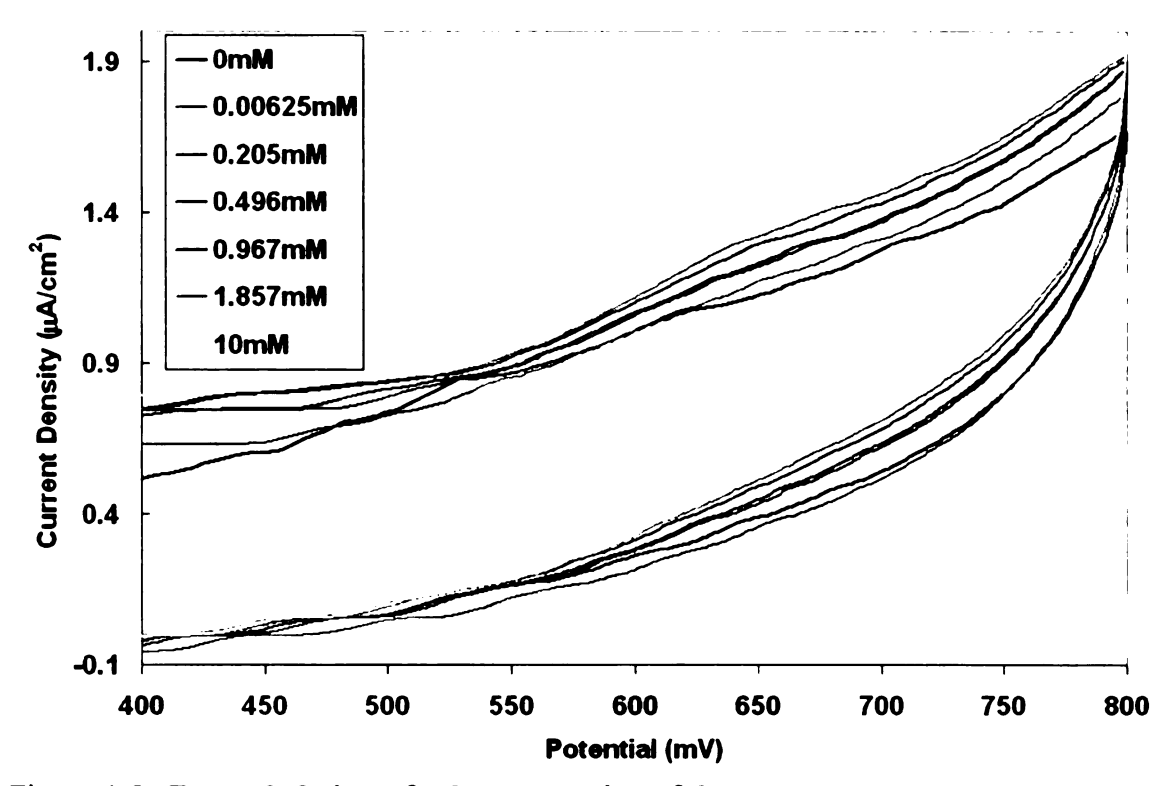


Figure 4-5. Expanded view of relevant portion of data.

Figure 4-4 has been expanded between 400mV and 800mV for better visibility. There appears to be a dependence of the current density on D-fructose concentration.

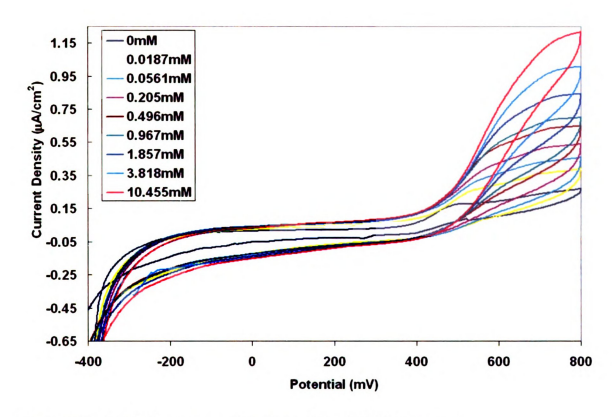


Figure 4-6. Catalytic response of an immobilized FDH biosensor. A biomimetic layer containing FDH and the coenzyme was formed on the ITO-coated glass and the slide was placed in a pH 4.5 sodium phosphate buffer solution. The working area was 0.17 cm². Response of the biosensor was monitored after addition of D-fructose in varying amounts, using a scan rate of 1 mV/sec.

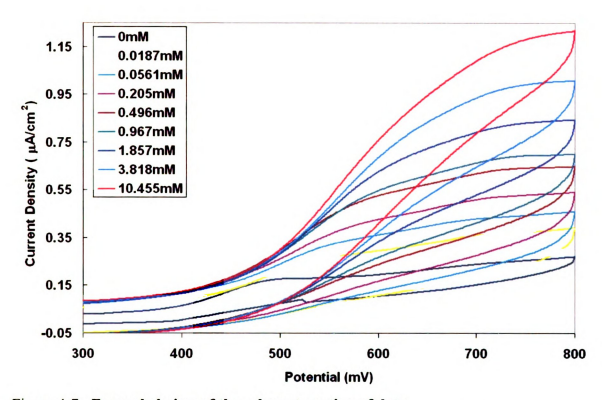


Figure 4-7. Expanded view of the relevant portion of data.

Figure 4-6 has been expanded between 300mV and 800mV to more clearly show the dependence of catalytic current on D-fructose concentration.

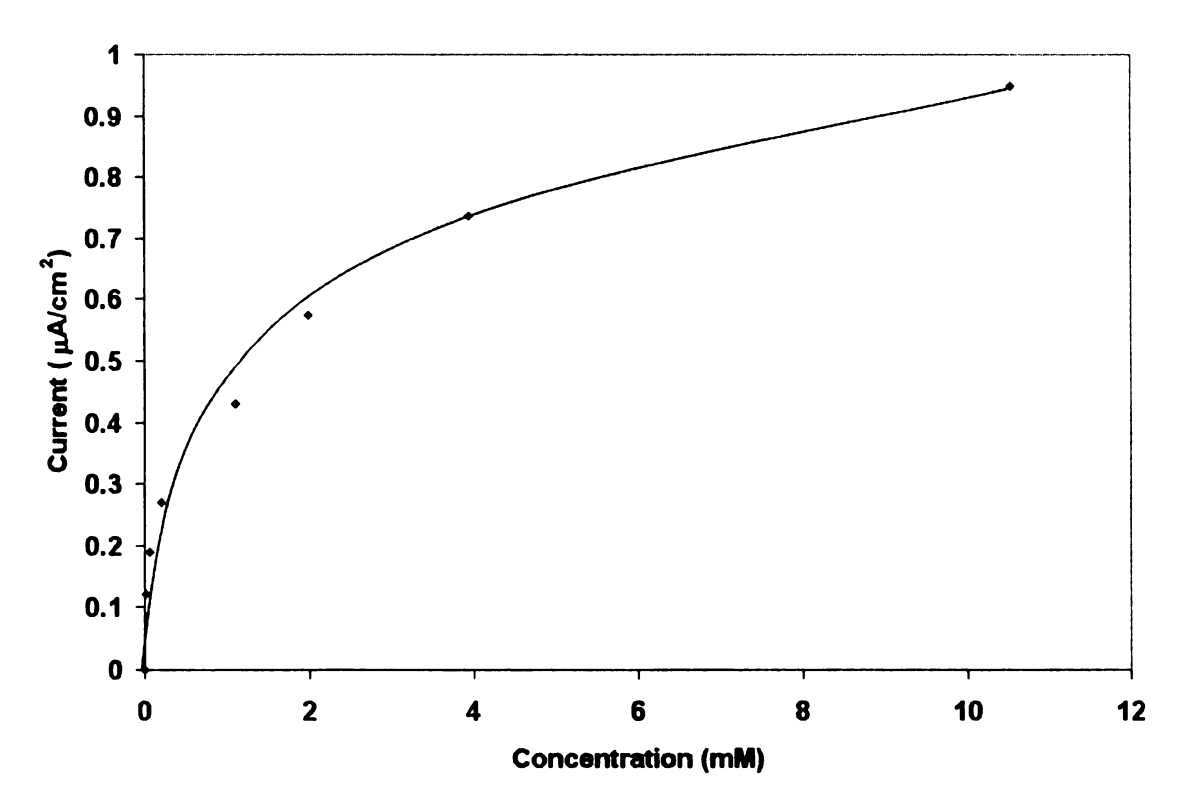


Figure 4-8. Calibration curve of current density versus D-fructose concentration. From the catalytic response of the immobilized FDH biosensor, a plot of anodic current versus D-fructose concentration was generated at 800mV, which was chosen to plot the calibration curve because the current reached steady state at this potential.

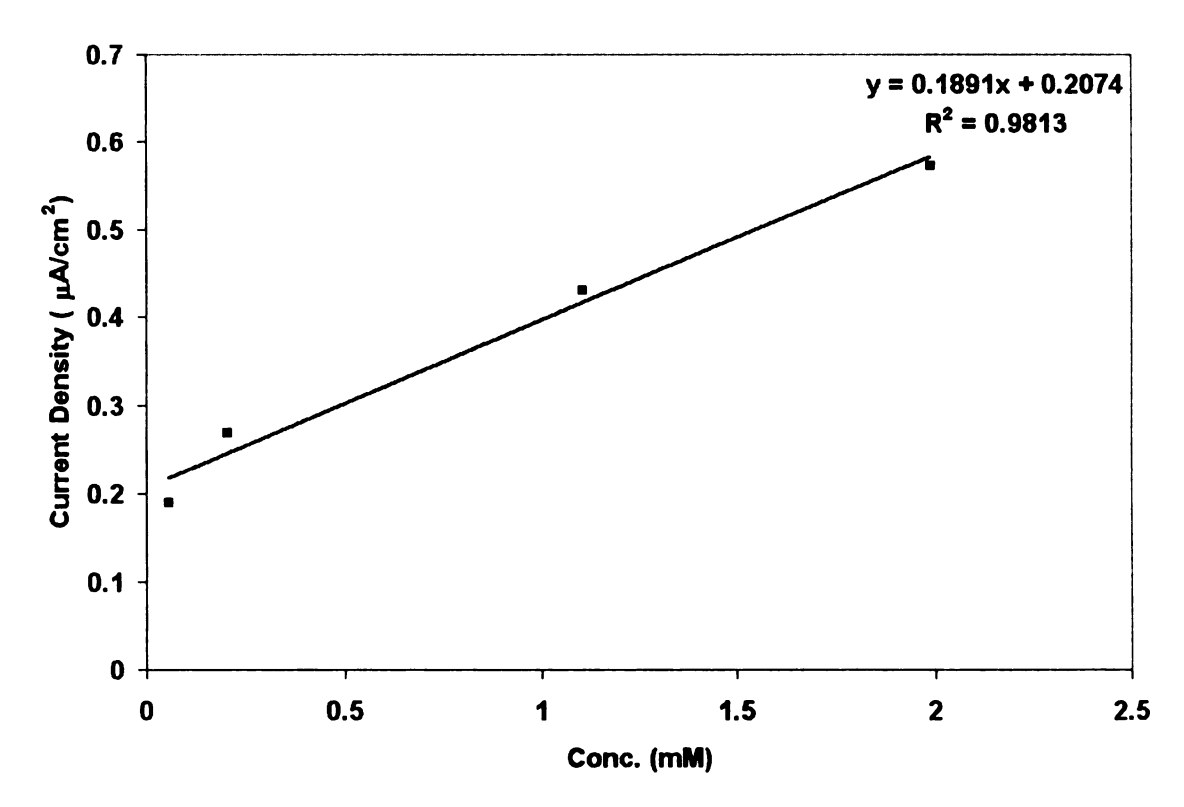
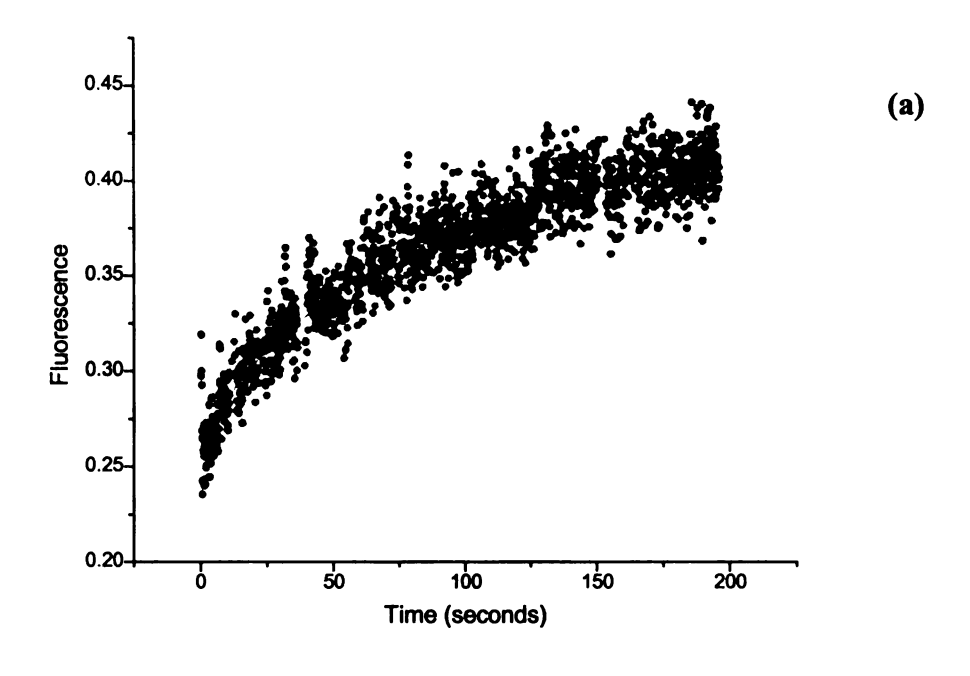


Figure 4-9. Linear part of calibration curve at 800mV. The biosensor showed a linear relationship between the catalytic current and D-fructose concentration from 0.056mM to 1.98mM.



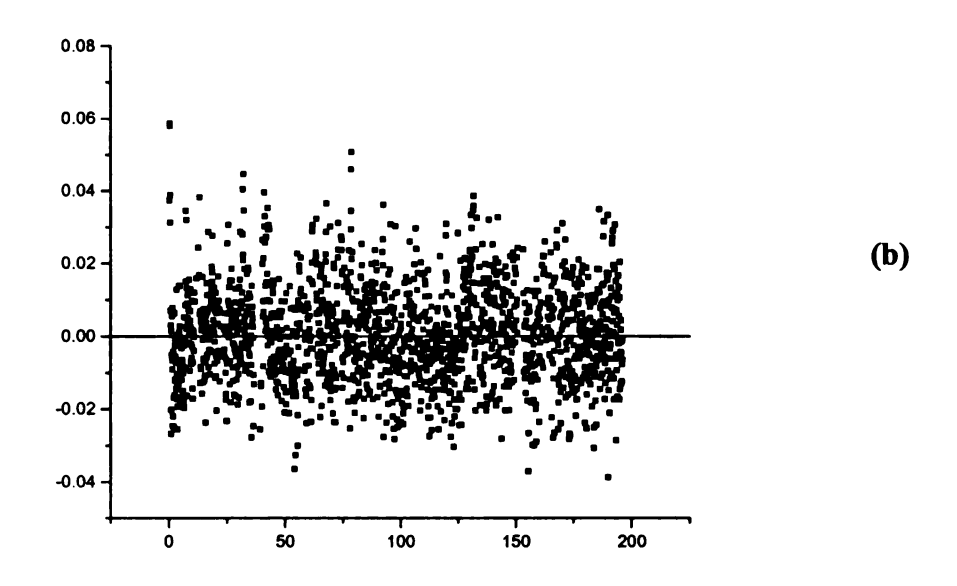


Figure 4-10. (a) Typical FRAPP curve obtained with FDH and the coenzyme immobilized in the biomimetic layer. The solid line represents fit to the data, using a model that describes a population containing a single mobile and immobile fraction (Smith and McConnell 1978; Wright et al. 1988; Starr and Thompson 2002). (b) Plot of residual versus time showing excellent goodness of fit.

5 APPENDICES

5.1 APPENDIX A:

5.1.1 MATLAB program used for filtering analog measurements to remove dark current measurements obtained during the phases when the chopper blocked the laser beam.

```
function p = test(data)
delete 'r:\colloid-surface-science\output.txt'
max val = 0;
min val = data(1,1);
for i=1:length(data)
  if (data(i,1)>max val)
  max val=data(i,1);
  end
  if (data(i,1)<min val)
  min_val=data(i,1);
  end
end
threshold = (0.72) * (max val-min val) + min val;
counter=1;
finaldata(1, 1) = 0;
finaldata(1, 2) = 0;
for i=1:length(data);
  if (data(i,1)>threshold)
  finaldata(counter, 1) = data(i,1);
  finaldata(counter, 2) = data(i,2);
   counter = counter+1;
  end
end
p=finaldata;
%mean and std. dev.%
m=mean(p,1)
average=m(1)
s=std(p,1)
```

```
stdev=s(1)

counter=1;
endgame(1, 1) = 0;
endgame(1, 2) = 0;

for i=1:length(p);
    diff=p(i,1)-average;
    absolute=abs(diff);
    if (absolute<stdev)
    endgame(counter, 1) = p(i,1);
    endgame(counter, 2) = p(i,2);
    counter = counter+1;
    end
end
save 'r:\colloid-surface-science\output.txt' endgame -ASCII;
p=endgame;</pre>
```

5.1.2 MATLAB program used for averaging data

```
c=1;
b=1;
g=size(A,1)/8;
p=floor(g)+1
while b<p
sum=0;
d=c+7;
for j=c:d
sum=sum+A(j);
end
avg(1,b)=sum/8;
c=c+8;
b=b+1;
end;
n=avg';
delete 'r:\colloid-surface-science\my_data.txt'
save my_data.txt n -ASCII
```

5.1.3 Labview Program for collecting fluorescence data in the analog mode.

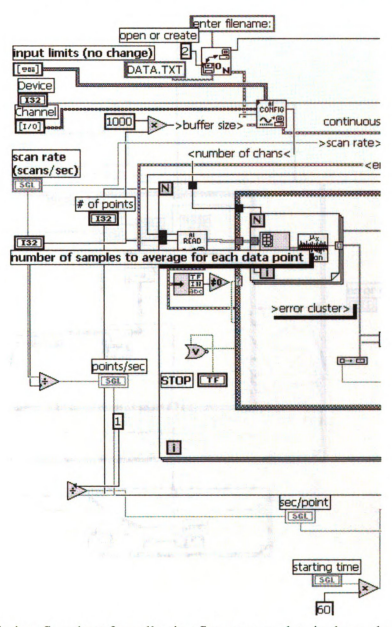


Figure 5-1. Labview flowsheet for collecting fluorescence data in the analog mode (left hand side) (Figure 5.1 continued on next page).

Labview Program for collecting fluorescence data in the analog mode.

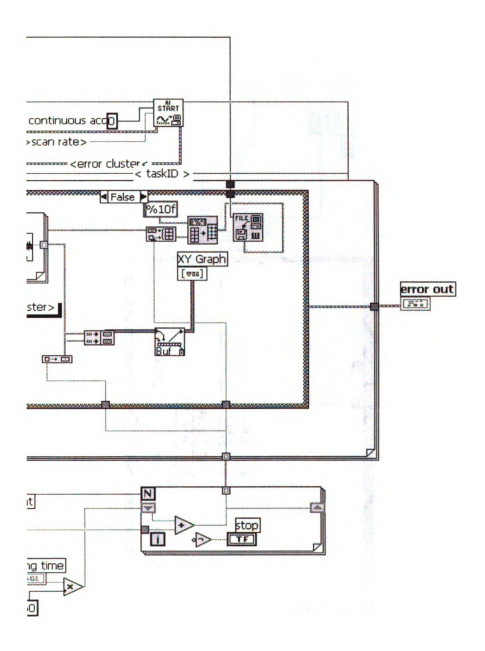


Figure 5-2contd. Labview flowsheet for collecting fluorescence data in the analog mode (Right hand side of Figure 5.1)

5.1.4 Labview Program for collecting fluorescence data in the digital (photon counting) mode.

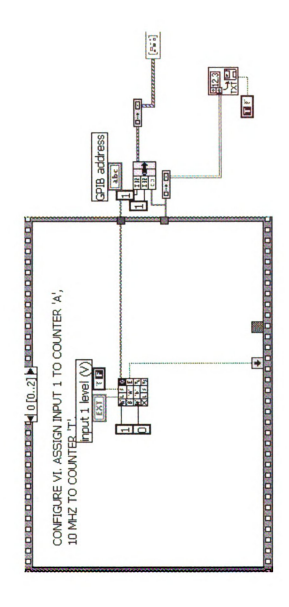


Figure 5-3. Labview flowsheet for collecting fluorescence data in the digital (photon counting) mode (Figure 5-3 continued on next two pages).

Labview Program for collecting fluorescence data in the digital (photon counting) mode.

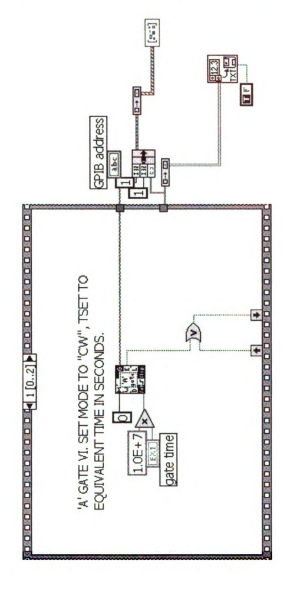


Figure 5-4contd. Labview flowsheet for collecting fluorescence data in the digital (photon counting) mode (Figure 5-3 continued on next page).

Labview Program for collecting fluorescence data in the digital (photon counting) mode.

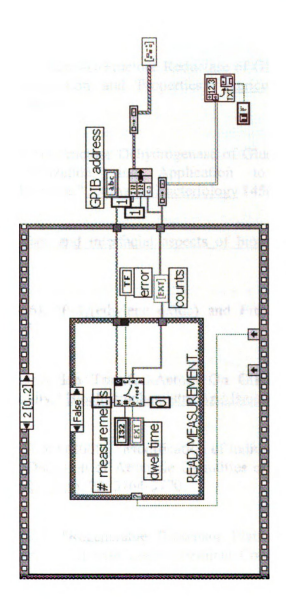


Figure 5-5contd. Labview flowsheet for collecting fluorescence data in the digital (photon counting) mode.

REFERENCES

- Abel, A. P., et al. (1996). "Fiber-optic evanescent wave biosensor for the detection of oligonucleotides." Analytical Chemistry 68(17): 2905-2912.
- Ameyama, M., et al. (1981). "5-Keto-D-Fructose Reductase of Gluconobacter-Industrius Purification, Crystallization and Properties." <u>Agricultural and Biological Chemistry</u> **45**(4): 863-869.
- Ameyama, M., et al. (1981). "D-Fructose Dehydrogenase of Gluconobacter-Industrius Purification, Characterization, and Application to Enzymatic Micro-Determination of D-Fructose." <u>Journal of Bacteriology</u> **145**(2): 814-823.
- Andrade, J. D. (1985). <u>Surface and interfacial aspects of biomedical polymers</u>. New York, Plenum Press.
- Andrade, J. D., et al. (1996). "Poly(ethylene oxide) and Protein Resistance." ADV CHEM SER 248: 51-59.
- Arai, K., et al. (1993). "Drug Ion Transfer Across On Oil-Wwater Interface And Pharmacological Activity." <u>Bioelectrochemistry And Bioenergetics</u> 31: 65-76.
- Armistead, P. M. and H. H. Thorp (2000). "Modification of Indium Tin Oxide Electrodes with Nucleic Acids: Detection of Attomole Quantities of Immobilized DNA by Electrocatalysis." <u>Anal. Chem.</u> 72: 3764-3770.
- Asanov, A. N., et al. (1998). "Regenerable Biosensor Platform: A Total Internal Reflection Fluorescence Cell with Electrochemical Control." <u>Anal. Chem.</u> 70: 1156-1163.
- Axelrod, D. (1989). "Total Internal-Reflection Fluorescence Microscopy." Methods in Cell Biology 30: 245-270.
- Axelrod, D., et al. (1983). "Total internal reflection fluorescence micrscopy." Journal of

- Microscopy 129(1): 19-28.
- Axelrod, D. H., E.H.; Fulbright, R.M. (1992). Total internal reflection fluorescence.

 <u>Topics in fluorescence spectroscopy Volume 3: Biochemical Applications Lakowicz</u>, Joseph.R.: 289-335.
- Bani-Jaber, A., et al. (2000). "Efficacy of the antimicrobial peptide nisin in emulsifying oil in water." <u>Journal of Food Science</u> 65(3): 502-506.
- Barak, L. S., et al. (1997). "A beta-arrestin green fluorescent protein biosensor for detecting G protein-coupled receptor activation." <u>Journal of Biological Chemistry</u> **272**(44): 27497-27500.
- Bard, A. J. and L. R. Faulkner (2000). <u>Electrochemical Methods Fundamentals and Applications</u>, John Wiley & Sons.
- Baselt, D. R., et al. (1998). "A biosensor based on magnetoresistance technology." <u>Biosensors & Bioelectronics</u> 13(7-8): 731-739.
- Batchelor, R. H. and M. Zhou (2002). "A Resorufin-Based Fluorescent Assay for Quantifying NADH." <u>Analytical Biochemistry</u> **305**: 118–119.
- Begum, A., et al. (1993). "New Electrocatalytic Biomolecular Interface for Fabricating a Fructose Dehydrogenase-Based Sensing System." Analytica Chimica Acta 280(1): 31-36.
- Bioanalytical Systems (2005). http://www.bioanalytical.com/products/ec/faqele.html#Three.
- Bower, C. K., et al. (2001). "Lantibiotics as surface active agents for biomedical applications." Colloids and Surfaces B- Biointerfaces 22(4): 259-265.
- Bower, C. K. M., J.; Daeschel, M. A. (1995). "Suppression of Listeria-Monocytogenes Colonization Following Adsorption of Nisin onto Silica Surfaces." <u>Applied and Environmental Microbiology</u> 61(3): 992-997.
- Breukink, E. and B. de Kruijff (1999). "The lantibiotic nisin, a special case or not?"

- Biochimica Et Biophysica Acta-Biomembranes 1462(1-2): 223-234.
- Breukink, E., et al. (1998). "The orientation of nisin in membranes." <u>Biochemistry</u> 37(22): 8153-8162.
- Breukink, E., et al. (1999). "Use of the cell wall precursor lipid II by a pore-forming peptide antibiotic." Science 286(5448): 2361-2364.
- Brinkley, M. (1992). "A Brief survey of methods for preparing protein conjugates with dyes, haptens, and cross-linking reagents." Bioconjugate Chem. 3: 2-13.
- Campuzano, S., et al. (2003). "An integrated electrochemical fructose biosensor based on tetrathiafulvalene-modified self-assembled monolayers on gold electrodes."

 <u>Analytical and Bioanalytical Chemistry</u> 377(4): 600-607.
- Campuzano, S., et al. (2004). "An integrated bienzyme glucose oxidase-fructose dehydrogenase-tetrathiafulvalene-3-mercaptopropionic acid-gold electrode for the simultaneous determination of glucose and fructose." <u>Bioelectrochemistry</u> 63(1-2): 199-206.
- Candeias, L. P., et al. (1998). "The catalysed NADH reduction of resazurin to resorufin."

 Journal of the Chemical Society-Perkin Transactions 2(11): 2333-2334.
- Carnes, E. and E. Wilkins (2005). "The Development of A New, Rapid, Amperometric Immunosensor for the Detection of Low Concentrations of Bacteria Part I: Design of the Detection System and Applications." <u>American Journal of Applied Sciences</u> 2(3): 597-606.
- Castillo, J., et al. (2004). "Biosensors for life quality Design, development and applications." <u>Sensors and Actuators B-Chemical</u> **102**(2): 179-194.
- Chapman, J. and M. Zhou (1999). "Microplate-based fluorometric methods for the enzymatic determination of l-glutamate: application in measuring l-glutamate in food samples." Analytica Chimica Acta 402: 47-52.
- Chaubey, A., et al. (2000). "Immobilization of lactate dehydrogenase on electrochemically prepared polypyrrole-polyvinylsulphonate composite films for

- application to lactate biosensors." <u>Electrochimica Acta</u> 46(5): 723-729.
- Chaubey, A. and B. D. Malhotra (2002). "Mediated biosensors." Biosensors & Bioelectronics 17(6-7): 441-456.
- Ciucu, A. and C. Ciucu (2002). "Organic Phase Amperometric Biosensor for Detection of Pesticides." Roum. Biotechnol. Lett. 7(2): 667-676.
- Cush, R., et al. (1993). "The Resonant Mirror a Novel Optical Biosensor for Direct Sensing of Biomolecular Interactions .1. Principle of Operation and Associated Instrumentation." <u>Biosensors & Bioelectronics</u> 8(7-8): 347-353.
- Daly, S. M., et al. (2003). "Coverage-dependent orientation of lysozyme adsorbed on silica." <u>Langmuir</u> 19(9): 3848-3857.
- Darder, M., et al. (2000). "Biosensors based on membrane-bound enzymes immobilized in a 5-(octyldithio)-2-nitrobenzoic acid layer on gold electrodes." <u>Analytical</u> Chemistry **72**(16): 3784-3792.
- Davis, K. A. and T. R. Leary (1989). "Continuous Liquid-Phase Piezoelectric Biosensor for Kinetic Immunoassays." <u>Analytical Chemistry</u> 61(11): 1227-1230.
- Dayeh, V. R., et al. (2004). "Evaluating the toxicity of Triton X-100 to protozoan, fish, and mammalian cells using fluorescent dyes as indicators of cell viability." Ecotoxicology and Environmental Safety 57: 375-382.
- DiazGarcia, M. E. and M. J. ValenciaGonzalez (1995). "Enzyme catalysis in organic solvents: A promising field for optical biosensing." Talanta 42(11): 1763-1773.
- Dickinson, E. (1977). Proteins at Liquid Interfaces. <u>Introduction to Food Colloids</u>, Oxford University Press. **Chapter 6:** 140-173.
- Dickinson, E. (1994). "Protein-Stabilized Emulsions." <u>Journal of Food Engineering</u> **22**(1-4): 59-74.
- Dickinson, E. (1998). "Proteins at interfaces and in emulsions Stability, rheology and interactions." <u>Journal of the Chemical Society-Faraday Transactions</u> **94**(12):

- Dickinson, E., et al. (1993). "A neutron reflectivity study of the adsorption of .beta.-casein at fluid interfaces." Langmuir 9: 242-248.
- Dzyadevych, S. V., et al. (2002). "Assessment of the toxicity of methyl parathion and its photodegradation products in water samples using conductometric enzyme biosensors." Analytica Chimica Acta 459(1): 33-41.
- Enserink, M. (1999). "Microbiology Promising antibiotic candidate identified." <u>Science</u> **286**(5448): 2245-+.
- Fang, F. and I. Szleifer (2001). "kinetics and thermodyanmics of Protein Adsorption: A Generalized Molecular Theoretical Approach." <u>Biophysical Journal</u> 80: 2568-2589.
- Faulkner, L. R. (1983). "Understanding Electrochemistry: Some Distinctive Concepts." Journal of Chemical Education 60: 262-264.
- Ferri, T., et al. (1998). "Direct electrochemistry of membrane-entrapped horseradish peroxidase. Part II: Amperometric detection of hydrogen peroxide."

 <u>Bioelectrochemistry And Bioenergetics</u> 45(2): 221-226.
- Gajraj, A. (1999). A TIRF technique for investigating macromolecular adsorption and interactions at the liquid-liquid interface. <u>Chemical Engineering</u>. East Lansing, Michigan State University: 1-153.
- Gajraj, A. and R. Y. Ofoli (2000a). "Quantitative technique for investigating macromolecular adsorption and interactions at the liquid-liquid interface." <u>Langmuir</u> 16(9): 4279-4285.
- Gajraj, A. and R. Y. Ofoli (2000b). "Effect of extrinsic fluorescent labels on diffusion and adsorption kinetics of proteins at the liquid-liquid interface." <u>Langmuir</u> 16(21): 8085-8094.
- Gerard, M., et al. (2002). "Application of conducting polymers to biosensors." Biosensors

- & Bioelectronics 17(5): 345-359.
- Giffard, C. J., et al. (1996). "Interaction of nisin with planar lipid bilayers monitored by fluorescence recovery after photobleaching." J. Membrane Biol. 151: 293-300.
- Girard, P., et al. (2004). "A new method for the reconstitution of membrane proteins into giant unilamellar vesicles." <u>Biophysical Journal</u> **2004**: 419-429.
- Graham, D. E. and M. C. Phillips (1979). "Proteins at Liquid Interfaces. 3. Molecular-structures of adsorbed films." <u>Journal of Colloid and Interface Science</u> **70**(3): 427-439.
- Graneli, A., et al. (2003). "Formation of supported lipid bilayer membranes on SiO₂ from proteoliposomes containing transmembrane proteins." <u>Langmuir</u> 19: 842-850.
- Haas, A. S., et al. (2001). "Cytochrome c and cytochrome c oxidase: Monolayer assemblies and catalysis." <u>Journal of Physical Chemistry B</u> 105(45): 11351-11362.
- Hunter, J. R., et al. (1991). "Beta-casein adsorption at the air-water interface." <u>Journal of Colloid and Interface Science</u> **142**(2): 429-446.
- Hurst, A. (1981). Nisin. <u>Advances in Applied Microbiology</u>, Academic Press. 27: 85-123.
- Hynes, R. O. (1992). "Integrins Versatility, Modulation, and Signaling in Cell-Adhesion." Cell 69(1): 11-25.
- Ivnitski, D., et al. (1999). "Biosensors for detection of pathogenic bacteria." <u>Biosensors & Bioelectronics</u> 14(7): 599-624.
- Jeon, S. I. and J. D. Andrade (1991). "Protein-Surface Interactions in the Presence of Polyethylene Oxide." <u>Journal of Colloid and Interface Science</u> **142**(1): 159-166.
- Karakashev, D., et al. (2003). "A simple and rapid test for differentiation of aerobic from anaerobic bacteria." World Journal of Microbiology & Biotechnology 19: 233-

- Karlsson, R. and A. Falt (1997). "Experimental design for kinetic analysis of proteinprotein interactions with surface plasmon resonance biosensors." <u>Journal of Immunological Methods</u> **200**(1-2): 121-133.
- Kato, K., et al. (2003). "Enzymatic activity and stability of D-fructose dehydrogenase and sarcosine dehydrogenase immobilized onto giant vesicles." <u>Biotechnology and Bioengineering</u> **84**(4): 415-423.
- Kelley, S. O., et al. (1999). "Long-Range Electron Transfer through DNA Films." Angew. Chem. Int. Ed. 38(7): 941-945.
- Khan, G. F., et al. (1991). "Electrochemical-Behavior of Monolayer Quinoprotein Adsorbed on the Electrode Surface." <u>Journal of Electroanalytical Chemistry</u> 315(1-2): 263-273.
- Kinnear, K. T. and H. G. Monbouquette (1993). "Direct Electron-Transfer to Escherichia-Coli Fumarate Reductase in Self-Assembled Alkanethiol Monolayers on Gold Electrodes." <u>Langmuir</u> 9(9): 2255-2257.
- Kinnear, K. T. and H. G. Monbouquette (1993). "Micelle-Supported Electroenzymology Succinate Dehydrogenation by Escherichia-Coli Fumarate Reductase in Decylubiquinone and Octyl Glucoside Micelles." <u>Biotechnology and Bioengineering</u> 42(1): 140-144.
- Kinnear, K. T. and H. G. Monbouquette (1997). "An amperometric fructose biosensor based on fructose dehydrogenase immobilized in a membrane mimetic layer on gold." <u>Analytical Chemistry</u> **69**(9): 1771-1775.
- Kissinger, P. T. and W. R. Heineman (1983). "Cyclic Voltammetry." <u>Journal of Chemical Education</u> **60**(9): 702-706.
- Kissinger, P. T. and W. R. Heineman (1984). <u>Laboratory Techniques in Electroanalytical</u>
 <u>Chemistry</u>, Marcel Dekker Inc.
- Lakamraju, M., et al. (1996). "Nisin adsorption and exchange with selected milk proteins

- at silanized silica surfaces." <u>Journal of Colloid and Interface Science</u> 178(2): 495-504.
- Lee, W. K., et al. (2000). "Interfacial tension kinetics of nisin and beta-casein at an oil-water interface." Korean Journal of Chemical Engineering 17(2): 179-183.
- Li, J., et al. (1996). "Silica sol-gel immobilized amperometric biosensor for hydrogen peroxide." Analytica Chimica Acta 335(1-2): 137-145.
- Li, J. H., et al. (1996). "Direct electron transfer to cytochrome c oxidase in self-assembled monolayers on gold electrodes." <u>Journal of Electroanalytical</u> Chemistry **416**(1-2): 97-104.
- Lin, V. S. Y., et al. (1997). "A porous silicon-based optical interferometric biosensor." Science 278(5339): 840-843.
- Mabbott, G. A. (1983). "An Introduction to Cyclic Voltammetry." <u>Journal of Chemical Education</u> **60**(9): 697-701.
- Maeda, H., et al. (2000). "Resorufin as an electron acceptor in glucose oxidase-catalyzed oxidation of glucose." Chemical & Pharmaceutical Bulletin 48(7): 897-902.
- Maeda, H., et al. (2001). "Resazurin as an electron acceptor in glucose oxidase-catalyzed oxidation of glucose." Chemical & Pharmaceutical Bulletin 49(5): 622-625.
- Mehrvar, M. and M. Abdi (2004). "Recent developments, characteristics, and potential applications of electrochemical biosensors." <u>Analytical Sciences</u> **20**(8): 1113-1126.
- Mehrvar, M., et al. (2000). "Fiber-optic biosensors Trends and advances." <u>Analytical Sciences</u> 16(7): 677-692.
- Meuller, J., et al. (1997). "Properties of a cysteine-free proton-pumping nicotinamide nucleotide transhydrogenase." <u>Biochemical Journal</u> **324**: 681-687.
- Miao, Y., et al. (2001). "Amperometric Glucose Biosensor Based on Immobilization of Glucose Oxidase in Chitosan Matrix Cross-Linked with Glutaraldehyde."

- Electroanalysis 13(4): 347-349.
- Motta, N. and A. R. Guadalupe (1994). "Activated Carbon Paste Electrodes for Biosensors." Anal. Chem. 66: 566-571.
- Mullor, S. G., et al. (1996). "Alcohol biosensor based on alcohol dehydrogenase and Meldola Blue immobilized into a carbon paste electrode." Talanta 43(5): 779-784.
- Munteanu, F., et al. (2003). "Electrochemical and catalytic investigation of carbon paste modified with Toluidine Blue O covalently immobilised on silica gel." Analytica Chimica Acta 476: 43-54.
- Muramatsu, H., et al. (1987). "Piezoelectric Crystal Biosensor Modified with Protein-a for Determination of Immunoglobulins." <u>Analytical Chemistry</u> **59**(23): 2760-2763.
- Napier, M. E., et al. (1997). "Probing Biomolecule Recognition with Electron Transfer: Electrochemical Sensors for DNA Hybridization." <u>Bioconjugate Chem.</u> 8: 906-913.
- O'Brien, J., et al. (2000). "Investigation of the Alamar Blue (resazurin) fluorescent dye for the assessment of mammalian cell cytotoxicity." <u>Eur. J. Biochem.</u> 267: 5421-5426.
- Palecek, E., et al. (1998). "Electrochemical biosensors for DNA hybridization and DNA damage." <u>Biosensors & Bioelectronics</u> 13(6): 621-628.
- Paredes, P. A., et al. (1997). "Amperometric mediated carbon paste biosensor based on D-fructose dehydrogenase for the determination of fructose in food analysis." <u>Biosensors & Bioelectronics</u> 12(12): 1233-1243.
- Parellada, J., et al. (1996). "Amperometric flow injection determination of fructose in honey with a carbon paste sensor based on fructose dehydrogenase." <u>Analytica Chimica Acta</u> 330(1): 71-77.
- Prodromidis, M. I., Karayannis, M.I. (2002). "Enzyme Based Amperometric Biosensors

- for Food Analysis." Electroanalysis 14(4): 241-261.
- Raiteri, R., et al. (2001). "Micromechanical cantilever-based biosensors." Sensors and Actuators B-Chemical 79(2-3): 115-126.
- Ramanathan, K. and B. Danielsson (2001). "Principles and applications of thermal biosensors." Biosensors & Bioelectronics 16(6): 417-423.
- Rao, T. N., et al. (1999). "Electrochemical Oxidation of NADH at Highly Boron-Doped Diamond Electrodes." Anal. Chem. 71: 2506-2511.
- Reinheimer, J. A. and M. R. Demkow (1990). "Comparison of rapid tests for assessing UHT milk sterility." J Dairy Res. 57(2): 239-243.
- Riss, T. L. and R. A. Moravec (2004). "Use of Multiple Assay Endpoints to Investigate the Effects of Incubation Time, Dose of Toxin, and Plating Density in Cell-Based Cytotoxicity Assays." ASSAY and Drug Development Technologies 2(1): 51-62.
- Robeson, J. L. and R. D. Tilton (1996). "Spontaneous reconfiguration of adsorbed lysozyme layers observed by total internal reflection fluorescence with a pH-sensitive fluorophore." <u>Langmuir</u> 12(25): 6104-6113.
- Russev, S. C., et al. (2000). "Beta-casein adsorption kinetics on air-water and oil-water interfaces studied by ellipsometry." <u>COLLOIDS AND SURFACES B-BIOINTERFACES</u> 19(1): 89-100.
- Saini, S., et al. (1991). "Organic-Phase Enzyme Electrodes." Analytica Chimica Acta 249(1): 1-15.
- Sanocki, V. A. (2004). Cell culture at the liquid-liquid interface: effects of fluorocarbon layer thickness on cell growth. <u>Chemical Engineering & Materials Science</u>. East Lansing, Michigan State University.
- Sigma, A. (1994). Enzymatic assay of D-fructose dehydrogenase, Sigma Aldrich.
- Smith, B. A. and H. M. McConnell (1978). "Determination of Molecular-Motion in Membranes Using Periodic Pattern Photobleaching." <u>Proceedings of the National</u>

- Academy of Sciences of the United States of America 75(6): 2759-2763.
- Starr, T. E. and N. L. Thompson (2002). "Fluorescence pattern photobleaching recovery for samples with multi-component diffusion." <u>Biophysical Chemistry</u> 97(1): 29-44.
- Thompson, N. L., et al. (1981). "Measuring surface dynamics of biomolecules by total internal reflection fluorescence with photobleaching recovery or correlation spectroscopy." <u>Biophysical Journal</u> 33: 435-454.
- Tkac, J., et al. (2001). "Fructose biosensor based on D-fructose dehydrogenase immobilised on a ferrocene-embedded cellulose acetate membrane." <u>Analytica Chimica Acta</u> 439(1): 39-46.
- Toyobo, E. D-Fructose Dehydrogenase.
- Tratnyek, P. G., et al. (2001). "Visualizing Redox Chemistry: Probing Environmental Oxidation-Reduction Reactions with Indicator Dyes." Chem. Educator 6: 172-179.
- Tupy, M. J., et al. (1998). "Total internal reflection fluorescence spectrometer to study dynamic adsorption phenomena at liquid/liquid interfaces." <u>Industrial & Engineering Chemistry Research</u> 37(8): 3159-3168.
- Vaidya, S. and R. Y. Ofoli (2005). "Adsorption and Interaction of Fibronectin and Human Serum Albumin at the Liquid-Liquid Interface." <u>Langmuir</u> 21(13): 5852 5858.
- Vaidya, S. S. (2005). Adsorption and Interactions of Biomacromolecules at Fluid-Like Interfaces. <u>Chemical Engineering & Materials Science</u>. East Lansing, Michigan State University.
- Van Benschoten, J. J., et al. (1983). "Cyclic Voltammetry Experiment." <u>Journal of Chemical Education</u> **60**(9): 772-776.
- Van heusden, H. E., et al. (2002). "Lipid II Induces a Transmembrane Orientation of the

- Pore-Forming Peptide Lantibiotic Nisin." Biochemistry 41: 12171-12178.
- Van Kraaij, C., et al. (1998). "Pore formation by nisin involves translocation of its C-terminal part across the membrane." <u>Biochemistry</u> 37(46): 16033-16040.
- Volkov, A. G. (1998). "Redox reactions at liquid hydrocarbon/water interfaces: Biophysical aspects." Electrochimica Acta 44: 139-153.
- Wagner, M. L. and L. K. Tamm (2000). "Tethered polymer-supported planar lipid bilayers for reconstitution of integral membrane proteins: Silane-polyethyleneglycol-lipid as a cushion and covalent linker." <u>Biophysical Journal</u> 79(3): 1400-1414.
- Wang, B., et al. (1998). "Amperometric Glucose Biosensor Based on Sol-Gel Organic-Inorganic Hybrid Material." <u>Anal. Chem.</u> 70: 3170-3174.
- Wang, H., et al. (2005). "A Biosensor Based on Immobilization of Horseradish Peroxidase in Chitosan Matrix Cross-linked with Glyoxal for Amperometric Determination of Hydrogen Peroxide." Sensors 5: 266-276.
- Wang, S., et al. (1998). "Resazurin reduction assay for ram sperm metabolic activity measured by spectrophotometry." <u>Proceedings of the Society for Experimental</u> Biology and Medicine **217**: 197-202.
- Wertz, C. F. and M. M. Santore (1999). "Adsorption and relaxation kinetics of albumin and fibrinogen on hydrophobic surfaces: Single-species and competitive behavior." <u>Langmuir</u> 15(26): 8884-8894.
- Wertz, C. F. and M. M. Santore (2001). "Effect of surface hydrophobicity on adsorption and relaxation kinetics of albumin and fibrinogen: Single-species and competitive behavior." <u>Langmuir</u> 17(10): 3006-3016.
- Wertz, C. F. and M. M. Santore (2002). "Adsorption and reorientation kinetics of lysozyme on hydrophobic surfaces." <u>Langmuir</u> 18(4): 1190-1199.
- Wertz, C. F. and M. M. Santore (2002). "Fibrinogen adsorption on hydrophilic and hydrophobic surfaces: Geometrical and energetic aspects of interfacial

- relaxations." Langmuir 18(3): 706-715.
- Willner, I., et al. (1997). "Assembly of functionalized monolayers of redox proteins on electrode surfaces: Novel bioelectronic and optobioelectronic systems." Biosensors & Bioelectronics 12(4): 337-356.
- Wright, L. L., et al. (1988). "Inhomogeneous Translational Diffusion of Monoclonal-Antibodies on Phospholipid Langmuir-Blodgett Films." <u>Biophysical Journal</u> 54(3): 463-470.
- Yamada, Y., et al. (1966). "A New Enzyme D-Fructose Dehydrogenase." Agric. Biol. Chem. 30: 95-96.
- Yu, J., et al. (2003). "Glucose sensor for flow injection analysis of serum glucose based on immobilization of glucose oxidase in titania sol-gel membrane." <u>Biosensors & Bioelectronics</u> 19: 401-409.
- Yuan, Y., et al. (2003). "Mobility of adsorbed proteins studied by fluorescence recovery after photobleaching." Langmuir 19: 3705-3711.
- Zhang, H. X., et al. (2004). "Assay of mitochondrial functions by resazurin in vitro." Acta Pharmacol Sin 25(3): 385-389.
- Zhang, L. Q., et al. (2000). "Phosphatidylserine/cholesteral bilayers supported on a polycation/alkylthiol layer pair." <u>Journal of Colloid and Interface Science</u> **228**(1): 82-89.
- Zrimsek, P., et al. (2004). "Spectrophotometric application of resazurin reduction assay to evaluate boar semen quality." <u>International journal of andrology</u> 27: 57–62.

MICHIGAN STATE UNIVERSITY LIBRARIES
3 1293 02736 4334